

**PHENOMENOLOGY OF NEUTRINO PORTAL
DARK MATTER AND SUPERSYMMETRY**

by

Barmak Shams Es Haghi

B.S. in Electrical Engineering, Tehran Polytechnic, 2009

M.Sc. in Physics, Sharif University of Technology, 2012

Submitted to the Graduate Faculty of
the Kenneth P. Dietrich School of Arts and Sciences in partial
fulfillment

of the requirements for the degree of

Doctor of Philosophy

University of Pittsburgh

2019

UNIVERSITY OF PITTSBURGH
KENNETH P. DIETRICH SCHOOL OF ARTS AND SCIENCES

This dissertation was presented

by

Barmak Shams Es Haghi

It was defended on

May 14th 2019

and approved by

Brian Batell, Professor, University of Pittsburgh

Steven Dytman, Professor, University of Pittsburgh

Tao Han, Professor, University of Pittsburgh

Matthew Walker, Professor, Carnegie Mellon University

Andrew Zentner, Professor, University of Pittsburgh

Dissertation Advisors: Brian Batell, Professor, University of Pittsburgh,

Tao Han, Professor, University of Pittsburgh

PHENOMENOLOGY OF NEUTRINO PORTAL DARK MATTER AND SUPERSYMMETRY

Barmak Shams Es Haghi, PhD

University of Pittsburgh, 2019

In this thesis we investigate the neutrino portal dark matter which tries to explain non-baryonic dark matter and the neutrino masses at the same time. Bearing in mind that natural theories like the Minimal Supersymmetric Standard Model also provide a WIMP type candidate for dark matter, we also calculate the sensitivities of the High Luminosity (HL) and High Energy (HE) upgrades of the Large Hadron Collider to strong supersymmetry signals. Firstly, we study the feasibility of the indirect detection of dark matter in a simple model using the neutrino portal. We derive the existing constraints on this scenario from Planck cosmic microwave background measurements, Fermi dwarf spheroidal galaxies and Galactic Center gamma-rays observations, and AMS-02 antiprotons observations. Secondly, by modifying our simple model, we analyze the scenario in which a thermal dark matter annihilating to standard model neutrinos via the neutrino portal. We derive existing constraints and future projections from direct detection experiments, colliders, rare meson and tau decays, electroweak precision tests, and small scale structure observations. Finally, we evaluate the sensitivities of the High Luminosity (HL) and High Energy (HE) upgrades of the LHC to gluinos and stops, decaying through the simplified topologies. Our HL-LHC analyses improve on existing experimental projections by optimizing the acceptance of kinematic variables.

TABLE OF CONTENTS

PREFACE	xv
1.0 INTRODUCTION	1
1.1 Quest for New Physics at TeV Scale	1
1.1.1 The Standard Model	2
1.1.2 Limitations of the Standard Model	5
1.2 Neutrino Mass	7
1.2.1 Mixing, oscillation, Neutrino Mass	7
1.2.2 Dirac and Majorana masses	8
1.3 Supersymmetry	11
2.0 DARK MATTER	20
2.1 Early Universe in a Nutshell	20
2.1.1 Homogeneous Isotropic Universe	20
2.1.2 Thermal History of the Early Universe	22
2.2 Evidence for Dark Matter	26
2.3 Particle Dark Matter Candidates	28
2.4 Dark Matter Detection	32
2.4.1 Direct Detection	32
2.4.1.1 Spin-Independent and Spin-Dependent Interactions	33
2.4.2 Indirect Detection	35
2.4.2.1 Gamma Rays	36
2.4.2.2 Antiproton	37
2.4.2.3 Neutrino	37

2.4.3	Collider Searches	38
3.0	INDIRECT DETECTION OF NEUTRINO PORTAL DARK MATTER	39
3.1	Introduction	39
3.2	Neutrino Portal Dark Matter	41
3.3	Indirect Detection Constraints and Prospects	45
3.3.1	Cosmic Microwave Background	47
3.3.2	Gamma rays from the galactic center	50
3.3.3	Gamma rays from dwarf spheroidal galaxies	55
3.3.4	Antiprotons	58
3.3.5	Summary of limits and future prospects	61
3.4	Galactic Center gamma ray excess interpretation	66
3.5	Beyond the minimal scenario	69
3.5.1	Large neutrino Yukawa coupling	69
3.5.2	Higgs portal coupling	71
3.6	Summary and Outlook	72
4.0	THERMAL DARK MATTER THROUGH THE DIRAC NEUTRINO PORTAL	74
4.1	Introduction	74
4.2	Framework	77
4.2.1	Model	77
4.2.2	Cosmology	80
4.2.3	Decays of new states	85
4.3	Sterile Neutrino Constraints	86
4.3.1	μ, τ decays	86
4.3.2	Rare meson decays	87
4.3.3	Three body decays	87
4.3.4	Neutrino oscillations	88
4.3.5	Invisible Higgs and Z decays	88
4.3.6	LHC searches	89
4.4	Dark Matter Phenomenology	90

4.4.1	Direct Detection	90
4.4.2	DM structure	93
4.5	Summary and Outlook	94
5.0	SUSY SIGNALS FROM QCD PRODUCTION AT THE UPGRADED LHC	97
5.1	Introduction and Methodology	97
5.2	Gluinos	99
5.2.1	$\tilde{g} \rightarrow q\bar{q}\tilde{\chi}^0$	101
5.2.2	$\tilde{g} \rightarrow t\bar{t}\tilde{\chi}^0$	102
5.3	Stops	106
5.4	Discussion and Conclusions	110
6.0	CONCLUSIONS	112
	APPENDIX A. BOOSTED SPECTRUM FOR MASSLESS PARTICLES	115
A.1	Boosting the spectrum of a massless particle	115
A.1.1	Generalization to a Continuous Energy Spectrum	117
	APPENDIX B. BOOSTED SPECTRUM FOR MASSIVE PARTICLES	118
B.1	Boosting the spectrum of a massive particle	118
B.1.1	Generalization to a Continuous Energy Spectrum	121
	BIBLIOGRAPHY	124

LIST OF TABLES

1	Chiral supermultiplets in the Minimal Supersymmetric Standard Model . . .	15
2	Gauge supermultiplets in the Minimal Supersymmetric Standard Model . . .	16
3	Cut flow for the two gluino benchmark points in Eq. (5.3) at HL-LHC. At each step, the cross section remaining after the indicated cut is shown in fb. The baseline cuts are identical for both points as stated in the text.	103
4	Cut flow for the two stop benchmark points in Eq. (5.5) at HL-LHC. At each step, the cross section remaining after the indicated cut is shown in fb. The baseline cuts are identical for both points.	107

LIST OF FIGURES

1	Seesaw mechanism with a heavy fermion that gives the left-handed neutrino a small Majorana mass	9
2	Renormalization group evolution of the inverse gauge couplings $\alpha_a^{-1}(Q)$ in the Standard Model and the MSSM. Plots are taken from Ref. [37].	19
3	Thermal history of the early Universe.	23
4	Planck 2018 temperature power spectrum, taken from Ref. [25]	27
5	WIMP freeze-out to its final abundance	31
6	Dark matter search strategies	32
7	WIMP cross sections (normalized to a single nucleon) for spin-independent coupling versus mass, plot taken from Ref. [37]	35
8	The Feynman diagrams for the DM particle annihilation to RHN pair and the decay of N to SM particles	43
9	Continuum γ -ray, electron, and antiproton spectra $E_i^2 dN_i/dE_i$ versus E_i ($i = \gamma, e^-, \bar{p}$) for DM mass $m_\chi = 200$ GeV and RHN masses $m_N = 20$ GeV (solid), 50 GeV (dashed), 100 GeV (dotted). The RHN is assumed to couple to the electron-type lepton doublet.	48
10	Contours of the 95% C.L. upper limit on $\log_{10}(\langle\sigma v\rangle/(\text{cm}^3 \text{s}^{-1}))$ in the $m_\chi - m_N$ plane (black curves) from <i>Planck</i>	51
11	Contours of the 95% C.L. upper limit on $\log_{10}(\langle\sigma v\rangle/(\text{cm}^3 \text{s}^{-1}))$ in the $m_\chi - m_N$ plane from the Galactic Center	54
12	Contours of the 95% C.L. upper limit on $\log_{10}(\langle\sigma v\rangle/(\text{cm}^3 \text{s}^{-1}))$ in the $m_\chi - m_N$ plane (black curves) from <i>Fermi</i> observations of gamma-rays	57

13	Contours of the upper limit on $\log_{10} (\langle\sigma v\rangle/(\text{cm}^3 \text{s}^{-1}))$ in the $m_\chi - m_N$ plane (black curves) from the AMS-02	60
14	Constraints on the neutrino portal DM model in the in the $m_\chi - m_N$ plane from the CMB	62
15	Contours of the 95% C.L. projected sensetivity on $\log_{10} (\langle\sigma v\rangle/(\text{cm}^3 \text{s}^{-1}))$ in the $m_\chi - m_N$ plane (black curves) from CTA	67
16	The best-fitted gamma-ray spectrum together with the observed central values and the error bars. The data and error bars are from Ref. [62].	68
17	Interpretation of the Galactic Center gamma ray excess.	70
18	Limits and constraints on the parameter $Y = y_L^4 (\sum_i U_{i4} ^2)^2 (m_\chi/m_\phi)^4$ as a function of the DM mass m_χ	82
19	90% C.L. upper limits on the mixing angles $ U_{\ell 4} ^2$ as functions of the heavy neutrino mass m_4 in the case that the heavy neutrino decays invisibly.	91
20	The H_T distribution after all cuts except for that on the H_T are applied, at HL-LHC. In the left/right panel, the signal corresponds to the benchmark points in Eq. (5.3). The arrows indicate the final cuts on H_T for the chosen signal regions.	104
21	The expected reach of LHC upgrades in probing gluinos decaying through off-shell squarks $\tilde{g} \rightarrow q\bar{q}\tilde{\chi}_1^0$ (left panel) and $\tilde{g} \rightarrow t\bar{t}\tilde{\chi}_1^0$ (right panel), in the gluino-LSP mass plane. The plots show the gluino mass reach at the LHC for 14 (27) TeV with 3 ab^{-1} (15 ab^{-1}) of data.	104
22	The \cancel{E}_T distribution after all cuts except for that on the \cancel{E}_T are applied, at HL-LHC. In the left/right panel, the signal corresponds to the benchmark points in Eq. (5.5). The arrows indicate the final cuts on \cancel{E}_T for the chosen signal regions.	109
23	The expected reach of LHC upgrades in probing stops decaying through $\tilde{t} \rightarrow t\tilde{\chi}_1^0$ in the stop-LSP mass plane. The plot shows the stop mass reach at 14 (27) TeV with 3 ab^{-1} (15 ab^{-1}) of data. The shaded region indicates the current observed limits from the LHC.	109

LIST OF EQUATIONS

1.1	2
1.2	2
1.3	3
1.4	3
1.5	3
1.6	4
1.7	4
1.8	4
1.9	4
1.10	4
1.11	4
1.12	9
1.13	9
1.14	9
1.15	10
1.16	10
1.17	10
1.18	10
1.19	10
1.20	10
1.21	11
1.22	11
1.23	12

1.24	12
1.25	13
1.26	17
1.27	17
2.1	20
2.2	20
2.3	21
2.4	21
2.5	21
2.6	21
2.7	21
2.8	29
2.9	29
2.10	30
2.11	31
2.12	33
2.13	33
2.14	33
2.15	34
2.16	34
2.17	34
2.18	36
2.19	36
2.20	37
3.1	42
3.2	42
3.3	42
3.4	43
3.5	43
3.6	44

3.7	44
3.8	44
3.9	46
3.10	47
3.11	49
3.12	49
3.13	50
3.14	52
3.15	55
3.16	55
3.17	55
3.18	56
3.19	56
3.20	59
3.21	59
3.22	59
3.23	65
3.24	65
3.25	66
3.26	71
4.1	75
4.2	78
4.3	78
4.4	79
4.5	79
4.6	79
4.7	81
4.8	81
4.9	85
4.10	85

4.11	85
4.12	87
4.13	89
4.14	90
4.15	92
4.16	92
4.17	94
5.1	101
5.2	101
5.3	102
5.4	105
5.5	108
A.1	115
A.2	115
A.3	115
A.4	115
A.5	116
A.6	116
A.7	116
A.8	116
A.9	116
A.10	116
A.11	116
A.12	117
A.13	117
A.14	117
A.15	117
A.16	117
A.17	117
B.1	118

B.2	118
B.3	119
B.4	119
B.5	119
B.6	119
B.7	119
B.8	119
B.9	120
B.10	120
B.11	120
B.12	120
B.13	120
B.14	121
B.15	121
B.16	121
B.17	121
B.18	122
B.19	122
B.20	122
B.21	122
B.22	122
B.23	123
B.24	123

PREFACE

I would like to gratefully acknowledge my debt to my Ph.D. advisor, Brian Batell who made me familiar with the dark side of the Universe! I cannot be thankful enough for his constant support and encouragement. Doing physics with Brian is fun and inspiring, he has the ability to turn a casual conversation into a stimulating physics discussion. I have always admired him for his keen talent for physics and being thorough in research.

I also want to express my gratitude and appreciation to my co-advisor, Tao Han who taught me lots of things, among them collider physics. His non-stop passion for research and his creative intuition in physics make him one of the most influential figures in my life. Without Tao's support this journey would not have been possible.

I would like to thank my collaborators, Ahmed Ismail and David McKeen from whom I have learned a lot. I would like to thank my Ph.D. committee for their constructive feedbacks.

Special thanks to the professors at PITT and CMU, who taught me physics, Ayres Freitas, Kaoru Hagiwara, Tao Han, Richard Holman, Ralph Roskies, Ira Rothstein, Eric Swanson, and Andrew Zentner. They made graduate school unforgettable. I also like to thank Arthur Kosowsky with whom I had many stimulating discussions.

I am also grateful to Junmou Chen, Hongkai Liu, Zhuoni Qian, Han Qin, Xing Wang, and Daniel Wiegand with whom I have shared office at some point. They made particle physics fun!

I should thank Amro Abdelrahim, Rudrajit Banerjee and Fernando Salviatto Zago for our long passionate physics discussions, I always learnt something new from them.

I would like to thank Yang Ma, who by asking very basic questions made me realize that there are so many things in my field that I still do not know. He made my last year at

graduate school memorable.

Special thanks to Lin Dai with whom I spent most of my time in graduate school learning physics and mathematics. Knowing him and learning from him was one of the best things that happened to me in graduate school.

I would like to thank Leyla Hirschfeld, she is the best and with her help, I was able to focus only on physics, without being worried about paperwork and bureaucracy.

Finally I would like to thank my parents for their unconditional love and support during my whole life, and my brother for always believing in me.

1.0 INTRODUCTION

This thesis is organized as follows. Chapter 1 motivates briefly the importance of physics beyond the Standard Model (SM). Chapter 2 reviews the early universe cosmology with an emphasis on dark matter (DM). Chapters 3 and 4 are devoted to the study of possible interactions between dark matter and neutrino (neutrino portal dark matter) and Chapter 5 studies the sensitivity of the high-luminosity and high-energy upgrades of the Large Hadron Collider (LHC) to signals of strongly produced supersymmetry.

1.1 QUEST FOR NEW PHYSICS AT TeV SCALE

One of the triumphs of modern science is the Standard Model of elementary particles. According to the Standard Model the matter constituents of the subatomic universe are elementary particles. These matter particles interact with each other via three fundamental forces (ignoring gravity), a consequence of the exchange of other particles associated with them. One can simply say particles talk to each other by exchanging other particles. Equipped with this physical picture, one can use Quantum Field Theory as mathematical framework to make very precise predictions. It is remarkable that nearly every experimental observable measured in particle physics laboratories over the past five decades agrees with the predictions of the Standard Model. The discovery of the Higgs boson seems to complete the Standard Model, but despite its extraordinary successes, it is known that the Standard Model cannot be the final theory of nature. Besides some theoretical issues concerning physics of higher energy scales, such as hierarchy problem or lack of gravity in the Standard Model, there are several observational facts which cannot be explained in the Standard

Model. These include neutrino masses and its nature (Majorana or Dirac), the identity of the non-baryonic dark matter, and the origin of the asymmetry of matter and antimatter. It is necessary to go beyond the Standard Model to address these mysteries. The lightness of the Higgs mass, theoretical motivations for a special type of dark matter candidate, etc. all point to the existence of new physics at the TeV scale and they motivate us to keep running Large Hadron Collider (LHC) at TeV scale with larger and larger luminosity.

1.1.1 The Standard Model

The Standard Model that describes the strong, weak, and electromagnetic interactions of elementary particles in the framework of quantum field theory is a gauge theory based on the local symmetry group $SU(3)_C \times SU(2)_L \times U(1)_Y$, where the subscripts C , L and Y denote color, weak isospin and hypercharge, respectively. The gauge structure uniquely determines the interactions between particles and force carriers with only three independent unknown coupling constants of the $SU(3)_C$, $SU(2)_L$, and $U(1)_Y$ groups, all of which must be determined from experiments. The only constraint on the number and properties of scalar bosons and fermions is that they must transform in a definite way under the symmetry group, i.e. they must belong to the representations of the symmetry group, and the fermion representations must lead to the cancellation of quantum anomalies. The scalar bosons are chosen in order to implement, in a minimal way, the Higgs mechanism for the generation of masses, whereas the number and properties of fermions are determined by experiments.

The Lagrangian of the Standard Model at the classical level includes four different parts:

$$\mathcal{L}_{\text{SM}} = \mathcal{L}_{\text{gauge}} + \mathcal{L}_{\text{fermion}} + \mathcal{L}_{\text{Higgs}} + \mathcal{L}_{\text{Yukawa}} \quad (1.1)$$

which refer respectively to the gauge, fermion, Yukawa, and Higgs sectors of the theory. After quantization, ghost and gauge-fixing terms need to be added appropriately. The gauge terms are

$$\mathcal{L}_{\text{gauge}} = -\frac{1}{4}G_{\mu\nu}^i G^{\mu\nu i} - \frac{1}{4}W_{\mu\nu}^i W^{\mu\nu i} - \frac{1}{4}B_{\mu\nu} B^{\mu\nu} \quad (1.2)$$

where the field strength tensors for $SU(3)_C$, $SU(2)_L$, and $U(1)_Y$ are respectively

$$\begin{aligned}
G_{\mu\nu}^i &= \partial_\mu G_\nu^i - \partial_\nu G_\mu^i - g_s f_{ijk} G_\mu^j G_\nu^k, \quad i, j, k = 1, \dots, 8 \\
W_{\mu\nu}^i &= \partial_\mu W_\nu^i - \partial_\nu W_\mu^i - g \epsilon_{ijk} W_\mu^j W_\nu^k, \quad i, j, k = 1, \dots, 3 \\
B_{\mu\nu} &= \partial_\mu B_\nu - \partial_\nu B_\mu
\end{aligned} \tag{1.3}$$

The fermion part of the Standard Model involve three families of quarks and leptons (written as two component left-handed Weyl spinors). Each family (with identical gauge structures) consists of

$$\begin{aligned}
L_i &= \begin{pmatrix} \nu_i \\ l_i \end{pmatrix} \sim (\mathbf{1}, \mathbf{2})_{-1}; & D_\mu L_i &= (\partial_\mu + \frac{ig}{2} \vec{\tau} \cdot \vec{W}_\mu - \frac{ig'}{2} B_\mu) L_i \\
\bar{l}_i &\sim (\mathbf{1}, \mathbf{2})_2; & D_\mu \bar{l}_i &= (\partial_\mu + ig' B_\mu) \bar{l}_i \\
Q_i &= \begin{pmatrix} u_i \\ d_i \end{pmatrix} \sim (\mathbf{3}, \mathbf{2})_{\frac{1}{3}}; & D_\mu Q_i &= (\partial_\mu + \frac{ig_s}{2} \vec{\lambda} \cdot \vec{G}_\mu + \frac{ig}{2} \vec{\tau} \cdot \vec{W}_\mu + \frac{ig'}{6} B_\mu) Q_i \\
\bar{u}_i &\sim (\bar{\mathbf{3}}, \mathbf{1})_{-\frac{4}{3}}; & D_\mu \bar{u}_i &= (\partial_\mu - \frac{ig_s}{2} \vec{\lambda}^* \cdot \vec{G}_\mu - \frac{2ig'}{3} B_\mu) \bar{u}_i \\
\bar{d}_i &\sim (\bar{\mathbf{3}}, \mathbf{1})_{\frac{2}{3}}; & D_\mu \bar{d}_i &= (\partial_\mu - \frac{ig_s}{2} \vec{\lambda}^* \cdot \vec{G}_\mu + \frac{ig'}{3} B_\mu) \bar{d}_i
\end{aligned} \tag{1.4}$$

where τ_i , $i = 1, \dots, 3$ and λ_i , $i = 1, \dots, 8$ are Pauli and Gell-Mann matrices respectively. The notation $(SU(3)_C, SU(2)_L)_Y$ denotes the color, isospin, and hypercharge assignments. The bars on the $SU(2)_L$ -singlet fields are parts of their names, and do not denote any kind of conjugation. Rather, the unbarred fields are the left-handed pieces of a Dirac spinor, while the barred fields are the names given to the conjugates of the right-handed piece of a Dirac spinor. For example, the electron 4-component Dirac field is $\begin{pmatrix} e_\alpha \\ \bar{e}^{\dagger\dot{\alpha}} \end{pmatrix}$. We follow two-spinor notation and convention in [1]. The values of the hypercharge, Y , have been adjusted so as to satisfy the Gell-Mann-Nishijima formula,

$$Q = I_3 + \frac{Y}{2} \tag{1.5}$$

The $SU(2)_L$, and $U(1)_Y$ representations are chiral, so no fermion mass terms are allowed.

The fermion part of the Standard Model therefore consists entirely of gauge-covariant kinetic energy terms

$$\mathcal{L}_{\text{fermion}} = i \sum_{i=1}^3 \left(L_i^\dagger \bar{\sigma}^\mu D_\mu L_i + \bar{l}_i^\dagger \bar{\sigma}^\mu D_\mu \bar{l}_i + Q_i^\dagger \bar{\sigma}^\mu D_\mu Q_i + \bar{u}_i^\dagger \bar{\sigma}^\mu D_\mu \bar{u}_i + \bar{d}_i^\dagger \bar{\sigma}^\mu D_\mu \bar{d}_i \right) \quad (1.6)$$

where

$$\bar{\sigma}^\mu = (I_{2 \times 2} ; -\vec{\tau}) \quad (1.7)$$

All gauge couplings respect chirality: left- and right-handed fermions evolve separately in the absence of masses, but in the real world, most fermions and some of the gauge bosons have masses. Masses can be generated dynamically, without spoiling renormalizability, through the elegant Higgs mechanism by introducing a complex scalar field

$$H = \begin{pmatrix} H^+ \\ H^0 \end{pmatrix} \sim (\mathbf{1}, \mathbf{2})_1; \quad D_\mu H = \left(\partial_\mu + \frac{ig}{2} \vec{\tau} \cdot \vec{W}_\mu + \frac{ig'}{2} B_\mu \right) H \quad (1.8)$$

The Higgs part of the Standard Model Lagrangian is

$$\mathcal{L}_{\text{Higgs}} = (D^\mu H)^\dagger D_\mu H - \mu^2 H^\dagger H - \frac{\lambda}{4} (H^\dagger H)^2 \quad (1.9)$$

Vacuum stability demands $\lambda > 0$. For $\mu^2 < 0$ there will be spontaneous symmetry breaking and the vacuum expectation value of the Higgs field will generate W and Z masses. Fermion masses are generated through Yukawa couplings to the Higgs doublet:

$$\mathcal{L}_{\text{Yukawa}} = - \sum_{i,j=1}^3 \left(y_{ij}^u \bar{u}_i \tilde{H}^\dagger Q_j + y_{ij}^d \bar{d}_i H^\dagger Q_j + y_{ij}^l \bar{l}_i H^\dagger L_j \right) + h.c. \quad (1.10)$$

where

$$\tilde{H} \equiv i\tau^2 H^* = \begin{pmatrix} H^{0*} \\ -H^- \end{pmatrix} \sim (\mathbf{1}, \mathbf{2})_{-1} \quad (1.11)$$

and y^u, y^d , and y^l are completely arbitrary 3×3 matrices which ultimately determine the

fermion masses and mixings. It is worth mentioning that in the Standard Model neutrinos are massless by construction. We will get back to the possibility of adding neutrino masses to the Standard Model in [1.2](#).

1.1.2 Limitations of the Standard Model

The Standard Model of elementary particles is a consistent renormalizable field theory that is in remarkably good agreement with all experimental facts. It successfully predicted the existence of the weak neutral current, the existence and masses of the W and Z bosons, and those of the charm quark, as necessitated by the GIM mechanism. The consistency between theory and experiment indirectly tested the radiative corrections and ideas of renormalization and allowed the successful approximate prediction of the top quark and Higgs boson masses. The discovery of Higgs boson in 2012 was the most recent astonishing triumph of this theory. Despite its extraordinary successes in describing the low energy regimes, it is widely known that the Standard Model cannot be the final theory of nature. Besides some theoretical issues concerning physics of higher energy scales, there are several observational facts which cannot be explained in the Standard Model. This thesis will try to address some of these issues and explore their possible interconnection.

Observational evidence for physics beyond the Standard Model includes non-zero neutrino masses, existence of dark matter and dark energy, strong CP problem, and baryon asymmetry in the universe. From a theoretical point of view issues such as hierarchy problem, the gauge symmetry problem, mass hierarchy of the elementary particles, flavor problem, and gravity cannot be explained by the Standard Model itself. Some of these issues are discussed in the following.

Neutrino masses: In the Standard Model neutrinos are massless as there is no right-handed neutrino (the mass term of a fermion in the Lagrangian involves both left- and right-handed quantum field). But now it is clear that neutrino flavors oscillate which can be explained quantum mechanically as the result of tiny, non-zero mass difference of mass eigenstates of neutrino. Although neutrino masses can be introduced in the Standard Model simply by adding right-handed singlet neutrinos and coupling them to the Higgs field, the

smallness of the corresponding Yukawa coupling motivates physicists to look for more natural mechanisms beyond the Standard Model to generate neutrino masses.

Existence of dark matter and dark energy: Cosmological observations including cosmic microwave background radiation (CMB), acceleration of the Universe as determined by Type Ia supernova observations, large scale distribution of galaxies and clusters, and big bang nucleosynthesis has allowed precise determinations of the cosmological parameters. The Standard Model constitutes only about 5% of the total energy budget of the Universe today. About 23% is the cold dark matter, which is a type of matter that barely talks to the Standard Model fields. The expected properties of dark matter, i.e. stability, darkness, and collisionlessness, leave us with no candidate in the Standard Model. The rest of the energy budget should be dark energy, a constant tiny energy density for the vacuum that is also not accounted for in the Standard Model.

Strong CP problem: One can use the dual field strength tensor of gluons to add an additional gauge-invariant term like $\tilde{G}G$ to the Lagrangian of The Standard Model. This term which breaks the CP symmetry would induce an electric dipole moment for the neutron. The stringent limits on this dipole makes the contribution of this additional term to the Lagrangian very small. It is a puzzling that why this contribution is so small.

Matter, antimatter asymmetry: The observed excess of baryons with respect to antibaryons is presumably due to a tiny asymmetry that could have been generated dynamically if the three Sakharov conditions are met. Yet, no known mechanism can generate sufficient matter, antimatter asymmetry in the Standard Model.

Hierarchy problem: Standard Model generates particle masses through the Higgs mechanism. Since in contrast to fermions, there is no symmetry in the Standard Model to protect Higgs mass from large quantum corrections due to high-scales physics (which could be as high as Planck scale), the actual mass of the Higgs boson, 125 GeV, is unnaturally light and it must be fine tuned in such a way that almost completely cancels the quantum corrections. The sensitivity of Higgs mass to any high energy scale in the theory is the origin of the hierarchy problem.

Gauge symmetry problem: The Standard Model symmetry group structure is a complicated direct product of three subgroups, $SU(3)_C \times SU(2)_L \times U(1)_Y$, with separate

gauge couplings. There is no explanation for why only the electroweak part is chiral and parity-violating. Similarly, the standard model incorporates but does not explain charge quantization. This is important because it allows the electrical neutrality of atoms. Charge quantization may be explained, at least in part, by the absence of anomalies or the existence of magnetic monopoles, but either of these is likely to find its origin in some kind of underlying unification.

Gravity: Gravity is not fundamentally unified with the other interactions in the standard model. General relativity is not a quantum theory, and there is no obvious way to generate one within the standard model context.

1.2 NEUTRINO MASS

This section reviews briefly the neutrino masses and how it introduces new degrees of freedom to the Standard Model.

1.2.1 Mixing, oscillation, Neutrino Mass

The charged leptons can be detected from their continuous track forming from ionized atoms as they traverse matter. On the contrary, neutrinos are directly observed through their weak interactions, e.g., charged current and neutral current scattering processes. Different neutrino flavors can only be distinguished by the flavors of their accompanying charged lepton produced in charged-current weak interactions.

Until the late 1990s, our knowledge about neutrinos was limited to the facts that there are three distinct flavors and that they are extremely light (and possibly massless). However, even at that time several experiments had reported possible anomalies in the observed interaction rates of atmospheric and solar neutrinos. The publication of the solar and atmospheric neutrino data from the Super-Kamiokande detector [2], which provided compelling evidence for the phenomenon of neutrino flavor oscillations over very large distances changed this picture entirely.

In the absence of any direct evidence for their mass, neutrinos were introduced in the Standard Model as truly massless fermions for which no gauge-invariant renormalizable mass term can be constructed. Consequently, in the Standard Model there is no mixing in the lepton sector. However, the evidences of neutrino oscillations were found in the Super-Kamiokande [2], SNO [3], KamLAND [4], and other solar [5, 6] and atmospheric [7] neutrino experiments. Observation of neutrino oscillations has opened a new window into physics beyond the Standard Model. New physics seems to have manifested itself in the form of neutrino masses and lepton mixing.

The observation of neutrino flavor oscillations arises from mixing between the flavor and mass eigenstates of neutrinos (misalignment of mass and flavor states). In other words the three neutrino states that interact with the charged leptons in weak interactions are each a different superposition of the three (propagating) neutrino states of definite mass. Neutrinos are created (and absorbed) in weak processes in their flavor eigenstates. Therefore neutrino flavor oscillations is a direct sign of neutrinos being massive particles.

As we mentioned before the gauge group structure of the Standard Model fixes only the gauge bosons of the model. The fermions and Higgs contents have to be chosen somewhat arbitrarily. In the Standard Model, these choices are made in such a way that the neutrinos are massless and the masslessness is maintained to all orders in perturbation theory. But neutrinos are massive, and so one has to incorporate neutrino mass in a realistic model of particle interactions. Thus we must seek physics beyond the Standard Model to explain observed evidences for neutrino masses. This does not necessarily mean going beyond the gauge group of the standard model, which fixes only the gauge bosons of the model. Even with the same gauge group as the standard model, one can conjecture extra fermions or Higgs bosons in the model so that the model predicts massive neutrinos. In the next section we consider models with enlarged fermion sector.

1.2.2 Dirac and Majorana masses

One can simply treat neutrino mass on exactly the same footing as the masses of other known fermions. The neutrinos are Dirac particles just like all other known fermions. To

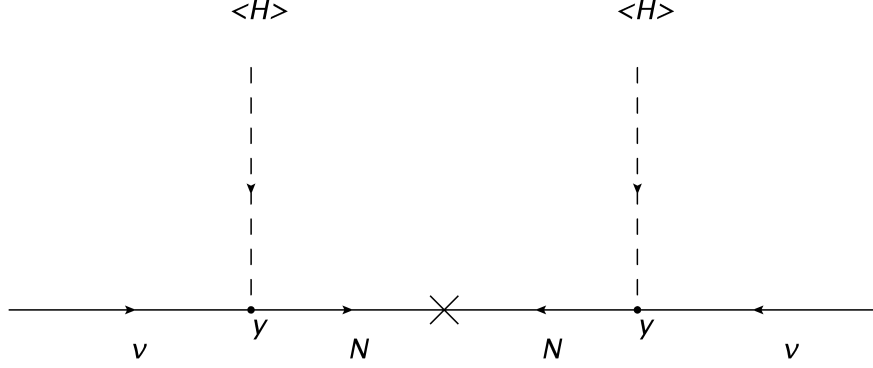


Figure 1: Seesaw mechanism with a heavy fermion that gives the left-handed neutrino a small Majorana mass

this end we need to add right-handed neutral fields N_l^\dagger corresponding to each charged lepton, l . Like the other right-handed fields, they are assumed to be $SU(2)_L$ singlets:

$$N_l \sim (\mathbf{1}, \mathbf{1})_0 \quad (1.12)$$

Then Yukawa part of the Lagrangian of the Standard Model can be upgraded as follows:

$$\mathcal{L}_{\text{Yukawa}} \supset - \sum_{i,j} y_{ij}^\nu N_{li} \tilde{H}^\dagger L_i + h.c. \quad (1.13)$$

Although this model can generate the mass of neutrino after spontaneous symmetry breaking but it cannot explain the lightness of neutrinos. Following Gell-Mann’s totalitarian principle, “Everything not forbidden is compulsory”, we can also add a bare mass term for the N field which reads

$$\mathcal{L}_N \supset - \frac{m_N}{2} (NN + N^\dagger N^\dagger) \quad (1.14)$$

After the Higgs gets a vev, as it is illustrated in Figure.1, we have the following mass terms which mix ν and N

$$\begin{aligned}
\mathcal{L} &\supset -\frac{m_N}{2}N'N' - m_D\nu'N' + h.c. \\
&= -\frac{1}{2}(\nu' N') \begin{pmatrix} 0 & m_D \\ m_D & m_N \end{pmatrix} \begin{pmatrix} \nu' \\ N' \end{pmatrix} + h.c.,
\end{aligned} \tag{1.15}$$

where $m_D \equiv yv/\sqrt{2}$ represents the Dirac mass term with $v = 246$ GeV. The prime denotes gauge eigenstates, to be distinguished from unprimed fields which will denote the mass basis.

We diagonalize the mass matrix with the following transformation:

$$\begin{pmatrix} \nu' \\ N' \end{pmatrix} = \begin{pmatrix} c_\nu & s_\nu \\ -s_\nu & c_\nu \end{pmatrix} \begin{pmatrix} \nu \\ N \end{pmatrix}, \tag{1.16}$$

where we have defined

$$c_\nu \equiv \cos \theta_\nu, \quad s_\nu \equiv \sin \theta_\nu, \quad \tan 2\theta_\nu = \frac{2m_D}{m_N} \tag{1.17}$$

the mass Lagrangian becomes

$$\begin{aligned}
\mathcal{L} &\supset -\frac{1}{2}(\nu N) \begin{pmatrix} m_1 & 0 \\ 0 & m_2 \end{pmatrix} \begin{pmatrix} \nu \\ N \end{pmatrix} + h.c. \\
&= -(m_1\nu\nu + m_2NN) + h.c.
\end{aligned} \tag{1.18}$$

where

$$m_{1,2} \equiv \frac{1}{2} \left[m_N \mp \sqrt{m_N^2 + 4m_D^2} \right] \tag{1.19}$$

Note that the minus sign for the mass of the light neutrino can be absorbed in to the definition of the fields.

It can be seen that when $m_N \ll m_D$ then the corresponding fermion masses and the mixing angle are

$$m_1 \sim \frac{m_D^2}{m_N}, \quad m_2 \sim m_N, \quad \theta \sim \frac{m_D}{m_N} \tag{1.20}$$

Eq. (1.18) shows we have a theory with two Majorana fermions which with a heavy Majorana mass term, m_N , one of them is very light and the other one is heavy. This is the essence of seesaw mechanism [8], the lightness of the neutrino can be explained by introducing a heavy scale.

1.3 SUPERSYMMETRY

As it was explained in 1.1.2, one of the theoretical issues of the Standard Model is the hierarchy problem, the sensitivity of Higgs mass to any high energy scale. In this section we introduce supersymmetry (SUSY), an elegant theoretical framework which not only resolves this problem but also has several interesting outcomes such as a candidate for the dark matter, and unification of gauge couplings.

Supersymmetry is a hypothetical symmetry between bosons and fermions. The huge quantum corrections to Higgs mass from higher energy scales in theory can be controlled by the interplay between these symmetrical fermionic and bosonic degrees of freedom. This can be shown simply by comparing quantum correction to the Higgs mass originated from a fermion and a scalar. Consider the interaction between Higgs, a Dirac fermion, f , and a complex scalar field S :

$$\mathcal{L} \supset -\lambda_f H \bar{f} f - \lambda_S |H|^2 |S|^2 \quad (1.21)$$

Then we have a correction to m_H^2 from a loop containing f

$$\delta m_{H-f}^2 = \frac{\lambda_f^2}{16\pi^2} \left[-2\Lambda^2 + 6m_f^2 \ln\left(\frac{\Lambda}{m_f}\right) \right] \quad (1.22)$$

and another correction to m_H^2 from a loop containing S

$$\delta m_{H-S}^2 = \frac{\lambda_S}{16\pi^2} \left[\Lambda^2 - 2m_S^2 \ln\left(\frac{\Lambda}{m_S}\right) \right] \quad (1.23)$$

where Λ is an ultraviolet momentum cutoff used to regulate the loop integrals. It should be interpreted as at least the energy scale at which new physics enters to alter the high-energy behavior of the theory. The hierarchy problem manifests itself in the quadratic dependence of m_{H-f}^2 and m_{H-S}^2 on the cutoff. The relative minus sign of fermionic and bosonic loops is the key factor here. If each of the fermions of the Standard Model is accompanied by two complex scalars with $\lambda_S = \lambda_f^2$, then the Λ^2 contributions will neatly cancel. This can happen through a new symmetry, symmetry relating fermions and bosons that is called supersymmetry.

It should be emphasized that if we use dimensional regularization on the loop integral instead of a momentum cutoff, then there will be no Λ^2 piece. However, even then the term proportional to m_S^2 in δm_{H-S}^2 cannot be eliminated without the tuning of a counter-term specifically for that purpose. Therefore m_H^2 is sensitive to the masses of the heaviest particles that H couples to.

A supersymmetry transformation changes a bosonic state into a fermionic state, and vice versa:

$$Q|\text{boson}\rangle = |\text{fermion}\rangle, \quad Q|\text{fermion}\rangle = |\text{boson}\rangle \quad (1.24)$$

where Q is the generator of these transformations, a fermionic operator which is a spinor under Lorentz transformations. By adding Q and Q^\dagger to the generators of the Poincare group, $\{P^\mu, J^{\mu\nu}\}$, the algebra of the supersymmetry transformations can be summarized as

$$\begin{aligned}
[P^\mu, P^\nu] &= 0 \\
[J^{\mu\nu}, P^\lambda] &= i(g^{\nu\lambda}P^\mu - g^{\mu\lambda}P^\nu) \\
[J^{\alpha\beta}, J^{\rho\sigma}] &= i(g^{\beta\rho}J^{\alpha\sigma} - g^{\alpha\rho}J^{\beta\sigma} - g^{\beta\sigma}J^{\alpha\rho} + g^{\alpha\sigma}J^{\beta\rho}) \\
[Q_\alpha, P^\mu] &= [Q_\alpha^\dagger, P^\mu] = 0 \\
[Q_\alpha, J^{\mu\nu}] &= (\sigma^{\mu\nu})_\alpha^\beta Q_\beta \\
[Q_\alpha^\dagger, J^{\mu\nu}] &= -Q_\beta^\dagger (\bar{\sigma}^{\mu\nu})^{\beta\alpha} \\
\{Q_\alpha, Q_\beta\} &= \{Q_\alpha^\dagger, Q_\beta^\dagger\} = 0 \\
\{Q_\alpha, Q_\beta^\dagger\} &= 2\sigma_{\alpha\beta}^\mu P_\mu
\end{aligned} \tag{1.25}$$

The fermionic nature of the generators of such symmetries and the highly restricted representations of them in an interacting quantum field theory are the outcomes of the Haag-Lopuszanski-Sohnius extension [9] of the Coleman-Mandula no-go theorem [10] which states that under reasonable assumptions the space-time symmetry of a field theory cannot be extended beyond the Poincare algebra except for internal symmetry generators if the generators obey commutation rules.

The single-particle states of a supersymmetric theory fall into irreducible representations of the supersymmetry algebra, called supermultiplets. Each supermultiplet includes both fermion and boson states, which are known as superpartners of each other. By using the algebra, Eq.1.25, one can easily show that the squared-mass operator, P^2 , commutes with the operators Q and Q^\dagger , and with all spacetime rotation and translation operators, so particles living in the same irreducible supermultiplet must have equal masses. The supersymmetry generators also commute with the generators of gauge transformations. Therefore particles in the same supermultiplet must also belong to the same representation of the gauge group, and so must have the same quantum numbers such as electric charges, weak isospin, and color degrees of freedom. By using the spin angular momentum and supersymmetry algebra one can show that each supermultiplet contains an equal number of fermions and bosons. The simplest supermultiplet consists of a single Weyl fermion (with two spin helicity states)

and two real scalars. The two real scalar degrees of freedom together can be interpreted as a complex scalar field. This combination of a two-component Weyl fermion and a complex scalar field is called a chiral or matter or scalar supermultiplet.

The other simple possibility for a supermultiplet contains a spin-one vector boson. By forcing the theory to be renormalizable, this must be a gauge boson that is massless, at least before the gauge symmetry is spontaneously broken. A massless spin-one boson has two helicity states, so the number of bosonic degrees of freedom is two. Its superpartner is therefore a massless Weyl fermion, with two helicity states. Since gauge bosons transform as the adjoint representation of the gauge group, their fermionic super partners, called gauginos, must also live in the adjoint representation. The adjoint representation of a gauge group is always its own conjugate, therefore the gaugino fermions must have the same gauge transformation properties for left-handed and for right-handed components. Such a combination of spinor gauginos and spin-one gauge bosons is called a gauge or vector supermultiplet.

In an extension of the Standard Model that realizes supersymmetry [11, 12, 13], each particle lives in either a chiral or gauge supermultiplet, and must have a superpartner with spin differing by one-half unit. It is worth noticing that only chiral supermultiplets can contain fermions whose left-handed parts transform differently under the gauge group than their right-handed parts. All of the Standard Model fermions (quarks and leptons) have this property, so they must be members of chiral supermultiplets. The bosonic partners of the quarks and leptons therefore must be spin-zero scalars, and not spin-one vector bosons.

The names for the spin-zero partners of the quarks and leptons are constructed by prepending an “s”, for scalar. So, generically they are called squarks and sleptons or sometimes sfermions. The left-handed and right-handed parts of the quarks and leptons each must have its own complex scalar partner. The symbols for the squarks and sleptons are the same as for the corresponding fermion, but with a tilde, ($\tilde{}$) used to denote the superpartner of a Standard Model particle.

Since Higgs scalar boson has spin zero, it must reside in a chiral supermultiplet. It turns out that just one chiral supermultiplet is not enough for Higgs. One reason for this is that if there were only one Higgs chiral supermultiplet, the electroweak gauge symmetry would suffer a gauge anomaly, and would be inconsistent as a quantum theory. This can be avoided

Name		Spin 0	Spin 1/2	$SU(3)_C \times SU(2)_L \times U(1)_Y$
squarks, quarks	Q	$(\tilde{u}_L \tilde{d}_L)$	$(u_L d_L)$	$(\mathbf{3}, \mathbf{2})_{\frac{1}{3}}$
	\bar{u}	\tilde{u}_R^*	u_R^\dagger	$(\bar{\mathbf{3}}, \mathbf{2})_{-\frac{4}{3}}$
	\bar{d}	\tilde{d}_R^*	u_R^\dagger	$(\bar{\mathbf{3}}, \mathbf{2})_{\frac{2}{3}}$
sleptons, leptons	L	$(\tilde{\nu} \tilde{e}_L)$	(νe_L)	$(\mathbf{1}, \mathbf{2})_{-1}$
	\bar{e}	\tilde{e}_R^*	e_R^\dagger	$(\mathbf{1}, \mathbf{1})_2$
Higgs, higgsinos	H_u	$(H_u^+ H_u^0)$	$(\tilde{H}_u^+ \tilde{H}_u^0)$	$(\mathbf{1}, \mathbf{2})_1$
	H_d	$(H_d^0 H_d^-)$	$(\tilde{H}_d^0 \tilde{H}_d^-)$	$(\mathbf{1}, \mathbf{2})_{-1}$

Table 1: Chiral supermultiplets in the Minimal Supersymmetric Standard Model

if there are two Higgs supermultiplets, one with each of hypercharges $Y = \pm 1/2$, so that the total contribution to the anomaly traces from the two fermionic members of the Higgs chiral supermultiplets vanishes by cancellation. The other reason for this is that because of the structure of supersymmetric theories (the holomorphy of the superpotential), only a $Y = 1/2$ Higgs chiral supermultiplet can have the Yukawa couplings necessary to give masses to up-type quarks (up, charm, top), and only a $Y = -1/2$ Higgs can have the Yukawa couplings necessary to give masses to down-type quarks (down, strange, bottom) and to the charged leptons.

All of the chiral supermultiplets of a minimal phenomenologically viable extension of the Standard Model are summarized in Table.1, classified according to their transformation properties under the Standard Model gauge group $SU(3)_C \times SU(2)_L \times U(1)_Y$.

The gauge vector bosons of the Standard Model clearly belong to gauge supermultiplets. The superpartners of the gauge and Higgs bosons are fermions, whose names are obtained by appending “ino” to the end of the corresponding Standard Model particle name, i.e. gaugino and Higgsino respectively. The $SU(3)_C$ color gauge interactions of QCD are mediated by the gluon, whose fermionic color-octet supersymmetric partner is the gluino. As mentioned before, a tilde is used to denote the supersymmetric partner of a Standard Model state. The electroweak gauge symmetry $SU(2)_L \times U(1)_Y$ is associated with spin-one gauge bosons

Name	Spin 1/2	Spin 1	$SU(3)_C \times SU(2)_L \times U(1)_Y$
gluino, gluon	\tilde{g}	g	$(\mathbf{8}, \mathbf{1})_0$
winos, W bosons	\tilde{W}	W	$(\mathbf{1}, \mathbf{3})_0$
bino, B boson	\tilde{B}	B	$(\mathbf{1}, \mathbf{1})_0$

Table 2: Gauge supermultiplets in the Minimal Supersymmetric Standard Model

$W_{1,2,3}^\mu$ and B^μ , with spin-one half superpartners $\tilde{W}_{1,2,3}^\mu$ and \tilde{B}^μ , called winos and bino. After electroweak symmetry breaking, the W_3^μ , B^μ gauge eigenstates mix to give mass eigenstates Z^μ and A^μ . The corresponding gaugino mixtures of \tilde{W}_3^μ and \tilde{B}^μ are called zino, \tilde{Z}^μ , and photino, \tilde{A}^μ . Table.2 summarizes the gauge supermultiplets of a minimal supersymmetric extension of the Standard Model.

The chiral and gauge supermultiplets in Tables. 1 and 2 make up the particle content of the Minimal Supersymmetric Standard Model (MSSM). None of the superpartners of the Standard Model particles has been discovered yet. If supersymmetry were an unbroken symmetry of nature, then there would have to be selectrons with masses exactly equal to the mass of the electron. A similar statement applies to each of the other sleptons and squarks, and there would also have to be a massless gluino and photino. Because of their masses, we would have been expected to discover them long time ago. Therefore, supersymmetry must be a broken symmetry.

The nature of supersymmetry breaking can be better understood in the light of motivation provided by the hierarchy problem. Supersymmetry needs two complex scalar fields for each Standard Model Dirac fermion, which is just what is needed to enable a cancellation of the quadratically sensitive corrections. This type of cancellation also requires that the associated dimensionless couplings should be related. The necessary relationships between couplings actually occur in unbroken supersymmetry; unbroken supersymmetry guarantees that quadratic divergences in scalar squared masses, and therefore the quadratic sensitivity to high mass scales, must vanish to all orders in perturbation theory. Now, if broken supersymmetry is still to provide a solution to the hierarchy problem even in the presence of

supersymmetry breaking, then the relationships between dimensionless couplings that hold in an unbroken supersymmetric theory must be maintained. We therefore need to consider “soft” supersymmetry breaking. This means that the effective Lagrangian of the MSSM can be written in the form

$$\mathcal{L} = \mathcal{L}_{\text{SUSY}} + \mathcal{L}_{\text{soft}} \quad (1.26)$$

where $\mathcal{L}_{\text{SUSY}}$ contains all of the gauge and Yukawa interactions and preserves supersymmetry invariance, and $\mathcal{L}_{\text{soft}}$ violates supersymmetry but includes only mass terms and coupling parameters with positive mass dimension. If the largest mass scale associated with the soft terms is denoted m_{soft} , then the additional non-supersymmetric corrections to the Higgs scalar squared mass must vanish in the $m_{\text{soft}} \rightarrow 0$ limit and they diverge logarithmically as

$$\delta m_H^2 = m_{\text{soft}}^2 \left[\frac{\lambda}{16\pi^2} \ln\left(\frac{\Lambda}{m_{\text{soft}}}\right) + \dots \right] \quad (1.27)$$

where λ represents various dimensionless couplings, and the ellipses represents terms that are independent of Λ and also higher loop corrections. Because the mass splittings between the Standard Model particles and their superpartners are originated from the parameters m_{soft} appearing in $\mathcal{L}_{\text{soft}}$, Eq.1.27 shows that the superpartner masses should not be too large. Otherwise, we would end up with the hierarchy problem again. Using $\Lambda \sim m_{\text{Pl}}$ and $\lambda \sim 1$ in Eq.1.27, one estimates that the masses of at least the lightest few superpartners, should probably not be much greater than the TeV scale, in order for the MSSM scalar potential to provide a Higgs vacuum expected vacuum resulting in $m_W, m_Z = 80.4, 91.2 \text{ GeV}$ without fine-tuned cancellations.

There are some other implications of supersymmetry which make it a very interesting theory, such as providing a dark matter candidate and unification of gauge couplings. Many supersymmetric models involve or impose a discrete R-parity symmetry [13], R_p , which requires that every allowed interaction vertex involves an even number of superpartners. This implies that the lightest superpartner (LSP) is absolutely stable, and therefore a good candidate for dark matter particle. Although Neutralinos are the most promising possibility,

sneutrinos and the gravitino are viable alternatives. But the possibility of a sneutrino making up the dark matter with a cosmologically interesting density has been largely ruled out by direct searches.

The gauge problem described in Section 1.1.2 suggests the possibility of grand unification [14, 15], in which the Standard Model gauge group, $SU(3)_C \times SU(2)_L \times U(1)_Y$, is embedded in a simple group G , with the quarks and leptons combined in the same multiplets. Grand unified theories (GUTs) predict the unification of gauge couplings at some very high energy scale [16]. The running of the couplings is determined by the particle content of the effective theory that resides below the GUT scale. However, attempts to embed the Standard Model in an unified theory such as $SU(5)$ or $SO(10)$ do not quite succeed. In particular, the three running gauge couplings (the strong QCD coupling g_s and the electroweak gauge couplings g and g') do not meet at a single point. In contrast, in the case of the MSSM with superpartner masses of order 1 TeV, the renormalization group evolution is modified above the SUSY-breaking scale. In this case, unification of gauge couplings, as illustrated in Figure 2, can be (approximately) achieved [17, 18, 19].

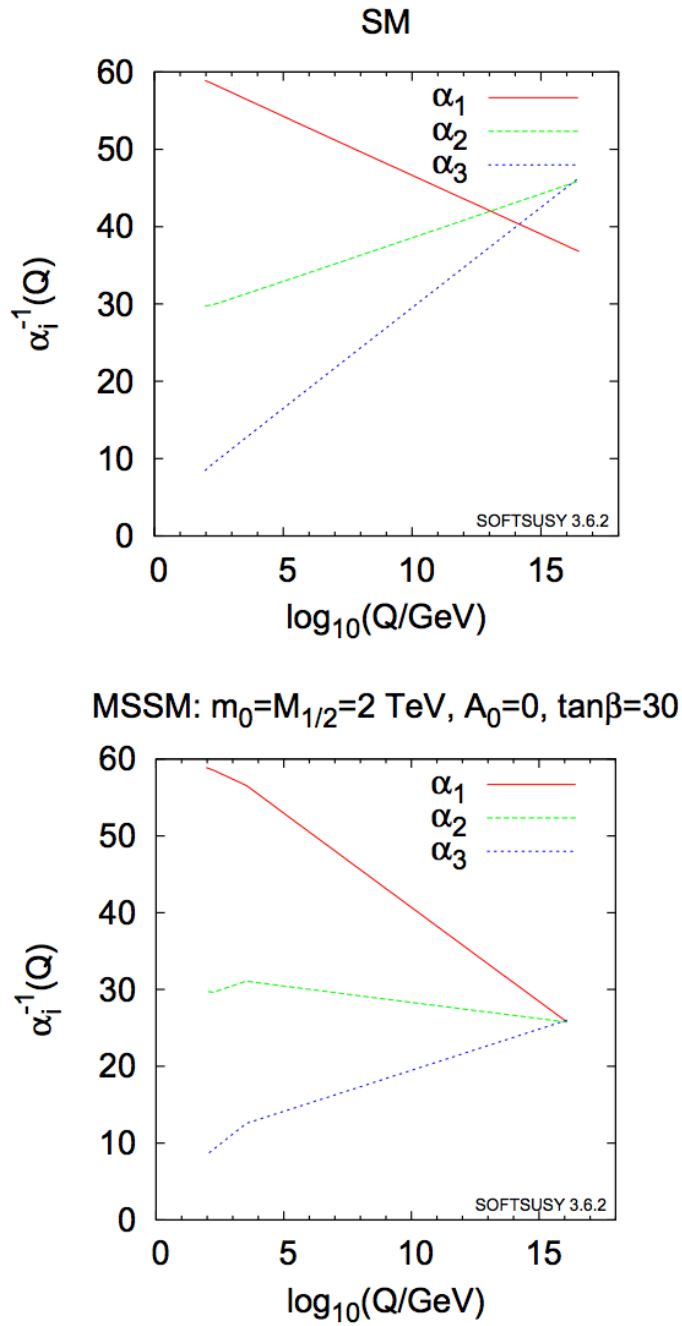


Figure 2: Renormalization group evolution of the inverse gauge couplings $\alpha_a^{-1}(Q)$ in the Standard Model and the MSSM. Plots are taken from Ref. [37].

2.0 DARK MATTER

2.1 EARLY UNIVERSE IN A NUTSHELL

2.1.1 Homogeneous Isotropic Universe

To a very good approximation, our Universe is homogeneous and isotropic at sufficiently large scales. This means that at any given moment of time, the geometry of space is the geometry of a homogeneous and isotropic manifold. This is the basis of the cosmological principle that there is no preferred direction or preferred position. The metric for a space with homogeneous and isotropic spatial sections is the maximally-symmetric metric or Friedmann-Robertson-Walker metric, which can be written as

$$ds^2 = dt^2 - a(t)^2 \left(\frac{dr^2}{1 - kr^2} + r^2 d\theta^2 + r^2 \sin^2 \theta d\phi^2 \right) \quad (2.1)$$

where (t, r, θ, ϕ) are coordinates (comoving coordinates), $a(t)$ is the cosmic scale factor and with an appropriate rescaling of the coordinates, k can be chosen to be +1, -1, or 0 for spaces of constant positive, negative, or zero spatial curvature, respectively. The dynamics of the Universe is described implicitly by the scale factor $a(t)$. To understand the evolution of the scale factor by time, one must solve the Einstein equations:

$$R_{\mu\nu} - \frac{1}{2}Rg_{\mu\nu} = 8\pi G_N T_{\mu\nu} + \Lambda g_{\mu\nu} \quad (2.2)$$

in which the Λ term is interpreted as an effective energy-momentum tensor $T_{\mu\nu}$ for the vacuum of $\Lambda g_{\mu\nu}/8\pi G_N$. For a Friedmann-Robertson-Walker universe containing a perfect

fluid with energy density ρ and pressure p , the 0-0 component of this equation gives the Friedmann's equation:

$$\left(\frac{\dot{a}}{a}\right)^2 + \frac{k}{a^2} = \frac{8\pi G_N}{3}\rho + \frac{\Lambda}{3} \quad (2.3)$$

while the $i-i$ component gives

$$2\frac{\ddot{a}}{a} + \left(\frac{\dot{a}}{a}\right)^2 + \frac{k}{a^2} = -8\pi G_N p + \Lambda \quad (2.4)$$

Equations. 2.3 and 2.4 can be accompanied by the continuity equation

$$d(\rho a^3) = -p d(a^3) \quad (2.5)$$

which is dependent on the other two. In fact, each of the three equations 2.3, 2.4 and 2.5 can be obtained combining the other two. In general, to describe the dynamics of the Universe it is convenient to choose the Friedmann equation and the continuity equation. The former provides a link between matter and geometry, while the latter closes the dynamical problem, fixing the behavior of the energy density in terms of the scale factor, once an equation of state for the cosmological fluid is assigned.

The expansion rate of the Universe is determined by the Hubble parameter, $H \equiv \dot{a}/a$. Friedmann's equation, 2.3, can be recast as

$$H^2 = H_0^2(\Omega_{m,0}a^{-3} + \Omega_{R,0}a^{-4} + \Omega_{\Lambda,0} + \Omega_{k,0}a^{-2}) \quad (2.6)$$

where

$$\Omega_i \equiv \frac{\rho}{\rho_c}, \quad \rho_k \equiv -\frac{3k}{8\pi G_N a^2}, \quad \rho_c \equiv \frac{3H^2}{8\pi G_N} \quad (2.7)$$

and the subscript 0 indicates the value of the quantity today, or $a = 1$. Eq.2.6 describes the evolution of the scale factor with time depending on the species dominating the energy

density of the universe. Current observations [25] show that we are living in a flat Universe, $k \sim 0$ which consists of $\sim 73\%$ dark energy in the form of a cosmological constant, $\sim 23\%$ of Dark Matter which behaves as non relativistic matter component but effectively does not interact with photons. The photon density only represents a small contribution $\sim 10^{-3}\%$ while the remaining $\sim 4\%$ are composed of standard baryonic matter, i.e. the astrophysical structures and objects that are observable in the universe. These are the ingredients of the Standard Cosmological Model (Λ CDM).

2.1.2 Thermal History of the Early Universe

The hot Big Bang theory describes the early Universe as a thermal bath in which all fundamental particle species are involved and are maintained at equilibrium by interactions with other species. The cosmological expansion implies that the thermodynamical parameters of the macroscopic cosmological fluid depend only on time. Therefore, one can assume that the Universe expansion happens through equilibrium states and that it is characterized by a global temperature $T(t)$, the temperature of photons, as long as non-ideal fluid effects due to out-of-equilibrium features such as dissipative mechanisms can be neglected. Indeed, the main part of the thermal history of the Universe can be well described as equilibrium phases and the cosmological fluid is well-modeled by a perfect one, even if some stages of the early evolution of the Universe are associated to phase transitions or species decays and decoupling, which require an appropriate out-of-equilibrium representation.

Here we present a brief scheme of the main events characterizing the thermal history of the Universe which has also been illustrated in Figure.3.

The Planck scale and Inflationary Epoch: The Planck scale, $M_{\text{Pl}} \sim 10^{19}$ GeV, is some upper threshold in the energy, to which we can extend our classical theory of gravity. Beyond that threshold, since quantum effects of gravity are expected to dominate, we should incorporate them to describe gravity. It is expected that these issues will be properly addressed in an as yet unknown non-perturbative string/quantum gravity theory.

The Hot Big Bang theory has its own problems. Some of them is due to the fact that this theory needs special initial conditions to describe the early and present Universe. One

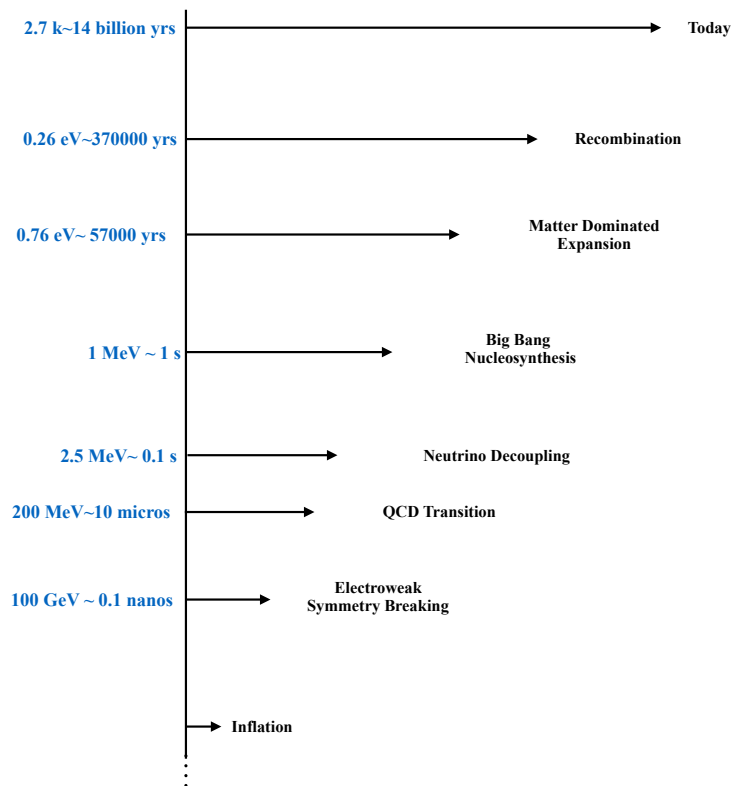


Figure 3: Thermal history of the early Universe.

of these initial conditions is the huge amount of entropy ($\sim 10^{88}$) of the Universe which is almost constant during its evolution. This and other similar problems can be rephrased qualitatively as why our Universe is so large, warm, spatially flat, homogeneous and isotropic. Inflationary theory proposes elegant solutions to resolve these problems. According to this theory, the hot cosmological epoch was preceded by the epoch of exponential expansion (inflation). During the inflationary epoch, initially small region of the Universe expanded to very large size, typically many order of magnitudes larger than the size of the part of the Universe we see today. This rapid expansion in the end explains flatness, homogeneity and isotropy of the observable part of the Universe.

Baryogenesis: The present Universe contains baryons (protons, neutrons) and practically no antibaryons. Presumably the Universe was baryon-symmetric in the beginning. The same conclusion comes from inflationary theory. Baryon asymmetry was generated in the course of the cosmological evolution due to processes that violates baryon number conservation. Today there is no unique answer to the question of the origin of this mechanism. We note only that baryon asymmetry was generated most probably at very high temperatures, at least 100 GeV and maybe much higher, although its generation at lower temperatures is not completely excluded.

Electroweak phase transition: At a thermal energy of about 100 GeV and below, the electromagnetic and weak forces start to behave distinctly. This happens because the vector bosons W^\pm and Z gain their masses, of roughly 80 and 90 GeV respectively, through the Higgs mechanism. In other words, at temperatures above 100 GeV (energy scale of electroweak interactions), the Higgs condensate is absent, and W^\pm and Z bosons have zero masses. The present phase with broken electroweak symmetry, Higgs condensate and massive W^\pm and Z bosons is the result of the electroweak transition that occurred at temperature of order 100 GeV.

QCD phase transition: Above energy scale of strong interactions which is about 200 MeV, quarks and gluons behave as individual particles (rather strongly interacting towards the transition epoch), while at lower temperatures they are confined in colorless bound states, hadrons. At the same time (or almost the same time) there was the transition associated with chiral symmetry breaking.

Neutrino decoupling: Neutrinos maintain thermal equilibrium with the primordial plasma through weak interactions down to a thermal energy of 1 MeV. Below this energy neutrino interactions with cosmic plasma terminates, and they decouple and freely propagate through the Universe. They are of the same order of magnitude as the temperature and number density of photons.

Big Bang Nucleosynthesis (BBN): At high temperatures protons and neutrons were free in thermal bath, but as the temperature of the Universe cooled down to the scale of binding energies in nuclei, i.e., 1 – 10 MeV due to expansion, neutrons have been captured into nuclei to form the light elements. Besides hydrogen, there are other light nuclei in primordial plasma: mostly helium-4 (the most tightly bound light nucleus) and also small amount of deuterium, helium-3 and lithium-7; heavier elements were not synthesized in the early Universe. This epoch of early Universe is the earliest epoch studied directly so far and good agreement between BBN theory and observations is one of the foundations of the theory of the early Universe. BBN epoch lasted from about 1 to 300 seconds after the Big Bang, corresponds to the temperatures range from 1 MeV to 50 keV [20].

Recombination and photon decoupling: At low temperatures the visible matter in the Universe was mainly in the state of neutral gas (hydrogen). At higher temperatures, the binding energy was not large enough to keep electrons in atoms, and the matter was in the state of baryon-electron-photon plasma. The temperature of the transition from plasma to neutral gas (recombination) is determined by the binding energy in hydrogen atom, 13.6 eV. Actually, due to the large photon-to-baryon ratio, recombination occurred at some lower temperature, $T \sim 0.3$ eV. This is a very special epoch in Universe history: before recombination photons actively scattered off electrons and were trapped in the plasma, while after it the neutral gas was transparent to photons and they could move freely in the Universe. These leftover photons form the cosmic microwave background radiation (CMB) that we see today. Therefore, it carries information about the properties of the Universe at the epoch when its temperature was about 0.26 eV or equivalently 3000 K and an age of about 370 thousand years.

2.2 EVIDENCE FOR DARK MATTER

In this section we discuss various evidences and observations that confirm the existence of a dark matter component in our Universe based on modern measurements and theoretical developments.

Rotation curves: Under the assumption of circular motion, the dependence of velocity of stars $v(r)$ on distance r from galactic center follows from Newton's law, $\sqrt{\frac{G_N M}{r}}$ where M is the enclosed mass, and G_N is the gravitational constant. For distances that extend beyond the Galactic disk, M should remain constant assuming all the mass is concentrated in the disk, and therefore $v(r) \propto r^{-1/2}$. Instead, observations find that the circular velocity curve flattens out at these distances, implying that $M(r) \propto r$ [21, 22]. Therefore one of the strongest pieces of evidence for dark matter comes from rotation curves of galaxies.

Gravitational lensing and the Bullet cluster: One of the predictions of General Relativity is that light can be bent by a gravitational potential and therefore does not propagate in a straight line around a massive object. This is called gravitational lensing. Another form of evidence for dark matter comes from utilizing gravitational lensing. If we look at a galaxy or galaxy cluster and the light coming from distant galaxies, we can see that the light is distorted or bent. This gives rise to multiple, distorted images of the distant galaxies. By measuring the masses of distant objects and comparing this to estimates of the amount of visible mass inferred from the luminosity of the object, it is possible to conclude that there is missing mass or not. Mergers of galaxy clusters provide an excellent opportunity to utilize this technique. In the famous case of the Bullet Cluster merger, 1E0657-558 [23, 24], weak gravitational lensing allows us to see a vivid separation between visible matter and dark matter. During the collision, individual galaxies within the clusters as well as dark matter behave as collisionless objects, streaming through the collision. But most of the ordinary matter in the clusters is in the form of hot gas within and between the galaxies, and the two merging gas clouds can also be seen from their X-ray emission to be interacting within the collision region. Gravitational lensing shows that most of the mass of the clusters passed through the collision region smoothly, an expected signature of dark matter.

Cosmic Microwave Background (CMB): As we explained in section. 2.1.2, the cos-

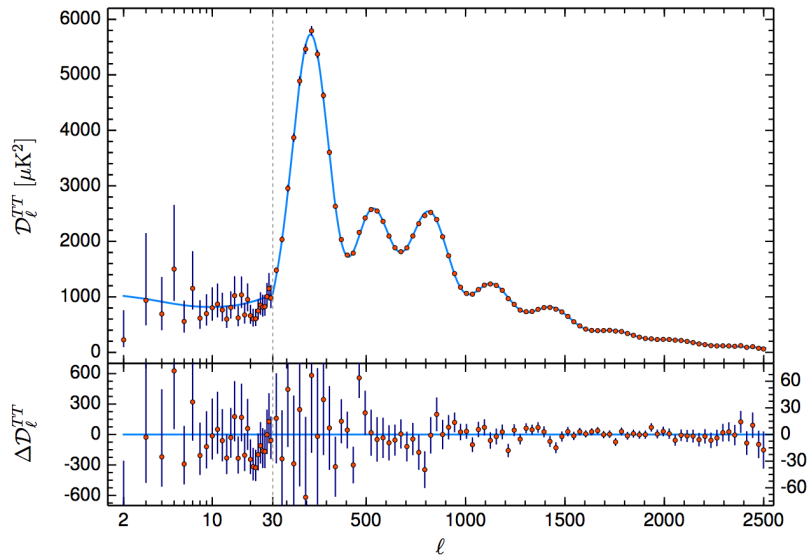


Figure 4: Planck 2018 temperature power spectrum, taken from Ref. [25]

mic microwave background is a relic radiation emitted around 300.000 years after the Big Bang, after recombination epoch. Photons emitted at this time could freely stream in the universe. The power spectrum of the CMB temperature anisotropy, the amount of fluctuation in the CMB temperature spectrum at different angular scales on the sky, reveals precise values for a host of cosmological parameters. Accurate measurements of this spectrum indicate the presence of a non-negligible Dark Matter component in the matter energy budget of the universe of the order of 85% and around 23% of its total energy density [25].

Structure Formation: To get structures like galaxies in a homogeneous and isotropic universe, we need to introduce some small nonuniformities in the matter distribution in the early universe. These perturbations will grow gradually in the expanding universe and eventually become galaxies. It can be shown that in a radiation-dominated universe, density perturbations in matter grow logarithmically with the expansion of the universe while they become larger linearly in a matter-dominated universe. So structures really form after the universe becomes matter-dominated. This leads to an argument for the existence of dark matter. If perturbations in matter began growing only after recombination, at redshift

$z \approx 1100$, and perturbations grow linearly in a matter-dominated universe, then we would not have nonlinear structure now unless we had begun with density perturbations $\delta\rho/\rho \sim 10^{-3}$. The CMB anisotropies, on the other hand, show us that the initial density perturbations were $\delta\rho/\rho \sim 10^{-5}$. Therefore the epoch of galaxy formation would occur substantially later in the universe than is observed. Dark matter resolves this problem: it provides a form of matter that was not coupled to the photon plasma. This allowed the Jeans instability to begin acting on dark matter well before redshift $z \approx 1100$.

2.3 PARTICLE DARK MATTER CANDIDATES

All the observational evidence of the existence of the dark matter that originate from its gravitational interaction, can lead us to a list of properties of a proper dark matter candidate. Indeed there is a plethora of dark matter candidates that can meet these properties. Dark matter (or at least a part of it) can be made of baryonic matter such as Massive Compact Halo Objects (MACHOs) in the form of primordial black holes, faint stars or stellar remnants. Since ordinary matter is made out of particles, therefore it is natural to make the hypothesis that non-baryonic dark matter is also made out of elementary particles. In that case these particles must be:

Cold or Warm, but not hot: At the time of decoupling from the thermal bath, dark matter should be non-relativistic (cold) or it is non-relativistic by radiation-matter equality epoch ($T \sim 1$ eV) (warm).

Dark (Dissipationless): no electromagnetic charge or color, at most weakly interacting with the bath.

Stable: Stable or long-lived such that they did not decay until today. In fact the lifetime should typically be much longer than the age of the universe.

Here we discuss briefly some of the non-baryonic dark matter particle candidates:

Neutrino: In the Standard Model, the only particles that can be considered as a viable Dark Matter candidate are neutrinos as they are stable, neutral and massive. But neutrino cannot be the only dark particle, since at the time of decoupling, it is still relativistic,

it would be a hot dark matter [26]. The other constrain on neutrino comes from phase space argument: it is a fermion and the occupancy number cannot be arbitrarily large, the so-called Tremaine-Gunn bound [27]. Assuming the existence of sterile neutrino, this new particle can play the role of the dark matter providing that its lifetime is larger than the age of the universe. Sterile neutrinos by masses of the order of the keV scale and a mixing angle of order of 10^{-9} can evade bounds from a plethora of constraints and be viable dark matter candidates [28].

WIMP: We can assume that dark matter is a weakly interacting massive particle (WIMP) that followed a thermal history similar to the Standard Model particles. In other words dark matter was initially in thermal equilibrium with the Standard Model bath, and it decoupled at some early stage of the universe. This idea that emerged in the 1980's is still one of the most popular dark matter candidates.

Since dark matter is stable, only annihilation and inverse annihilation processes

$$\chi\bar{\chi} \leftrightarrow \psi\bar{\psi} \quad (2.8)$$

can change the number of dark matter in a comoving volume, where χ the dark matter candidate and ψ is a Standard Model field which has a thermal distribution with zero chemical potential. Then dark matter number density is given by Boltzmann's equation:

$$\frac{dn_\chi}{dt} + 3Hn_\chi = -\langle\sigma v\rangle(n_\chi^2 - n_{\chi,\text{eq}}^2) \quad (2.9)$$

where $\langle\sigma v\rangle$ is the velocity averaged annihilation cross section of the process $\chi\bar{\chi} \rightarrow \psi\bar{\psi}$ and $n_{\chi,\text{eq}}$ is the expected DM density in case of thermal equilibrium with the Standard Model bath. The left-hand side of this equation represents the evolution of dark matter number density in the case where interaction processes are negligible, i.e. a dilution because of expansion. The right-hand side tends to ensure thermal equilibrium between dark matter and the bath, and lead the dark matter number density to evolve according to its thermal distribution. However, in the non-relativistic regime, $T \sim m_\chi$, the number density becomes suppressed, and the Hubble expansion rate wins. The result is the freeze-out of the dark

matter to its final abundance as illustrated in Fig.5. It can be shown that the fraction of the critical density, ρ_c , contributed by the WIMP dark matter of mass m_χ today is

$$\Omega_\chi h^2 \simeq 0.1 \left(\frac{m_\chi}{100 \text{ GeV}} \right) \left(\frac{10^{-26} \text{ cm}^3 \text{ s}^{-1}}{\langle \sigma v \rangle} \right) \quad (2.10)$$

The fact that a dark matter mass of the order of the electroweak scale $m_\chi \sim 100 \text{ GeV}$ and a typical electroweak cross section $\sigma \sim g^4 m_\chi^2 / m_Z^4 \sim 10^{-9} \text{ GeV}^{-2} \simeq 10^{-26} \text{ cm}^3 \text{ s}^{-1}$ lead to the observed dark matter relic density is known as the WIMP miracle and has become the dominant paradigm since many well-motivated models, such as supersymmetry, provide such candidates. Indeed the best WIMP candidate is motivated by Supersymmetry, the lightest neutralino in the Minimal Supersymmetric Standard Model. Another type of WIMP exists in models of universal extra dimensions [29]. In these models flat, compactified extra spatial dimensions with an extension of order of TeV^{-1} are introduced and all the Standard Model fields are allowed to propagate in the higher dimensional bulk. Higher dimensional momentum conservation in the bulk translates in four dimensions to Kaluza-Klein (KK) number (with boundary conditions to KK parity). The lightest KK particle, known as the LKP, does not decay and is a WIMP candidate [30].

It is worth mentioning that one important feature of the freeze-out mechanism is that it does not rely on any specific assumption regarding the prior dark matter history before thermalization with the Standard Model bath. As long as the thermalization condition is satisfied at some stage in the radiation domination era, this mechanism can be applied independently of the post-inflation history of the universe.

Axion: The QCD axion was first introduced by Peccei and Quinn in 1977 [31] as a solution to the strong CP problem (see section.1.1.2). Peccei and Quinn considered a global $U(1)_{\text{PQ}}$ symmetry that the spontaneous breaking of it, along with explicit breaking associated with the anomaly and instanton effects, leads to a very light pseudo-Goldstone boson known as an axion [32, 33]. The phenomenology of the axions is determined by the scale of the Peccei - Quinn symmetry breaking, denoted as f_a . It was initially assumed that the scale f_a would be comparable to the electroweak scale, but this was excluded experimentally. A still viable theory is the invisible axion, involving a very large f_a much larger than the weak

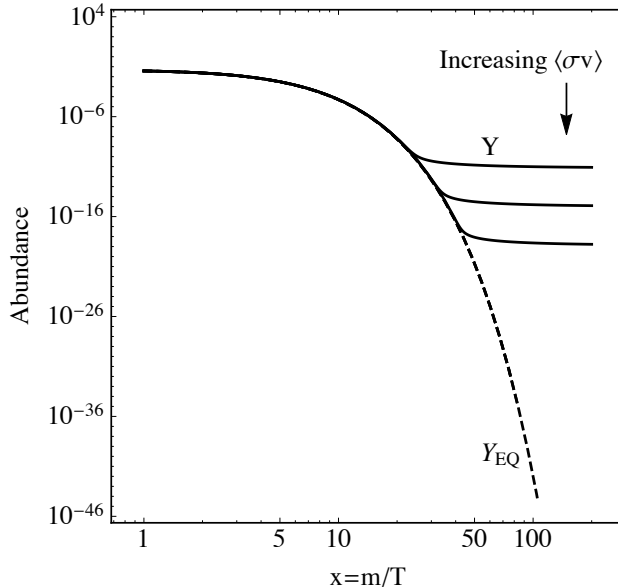


Figure 5: WIMP freeze-out to its final abundance

scale, and a very light axion, with a mass

$$m_a \sim \frac{\sqrt{m_u/m_d} f_\pi m_\pi}{1 + m_u/m_d \sqrt{2} f_a} \sim 0.6 \left(\frac{10^7 \text{ GeV}}{f_a} \right) \text{ eV} \quad (2.11)$$

where m_u , m_d , m_π and f_π are up quark mass, down quark mass, pion mass, and pion decay constant respectively. Axion couplings also scale as f_a^{-1} . Different experimental, astrophysical, and cosmological constraints suggest that f_a is in the range $10^9 - 10^{12}$ GeV, corresponding to $m_a \sim (10^{-5} - 10^{-2})$ eV [34]. Because of its negligible interaction strength, axion is a cold dark matter.

Axions and axion-like particles (ALPs), which are not necessarily associated with the strong CP problem and their masses do not follow Eq. 2.11 often occur in superstring theories [35].

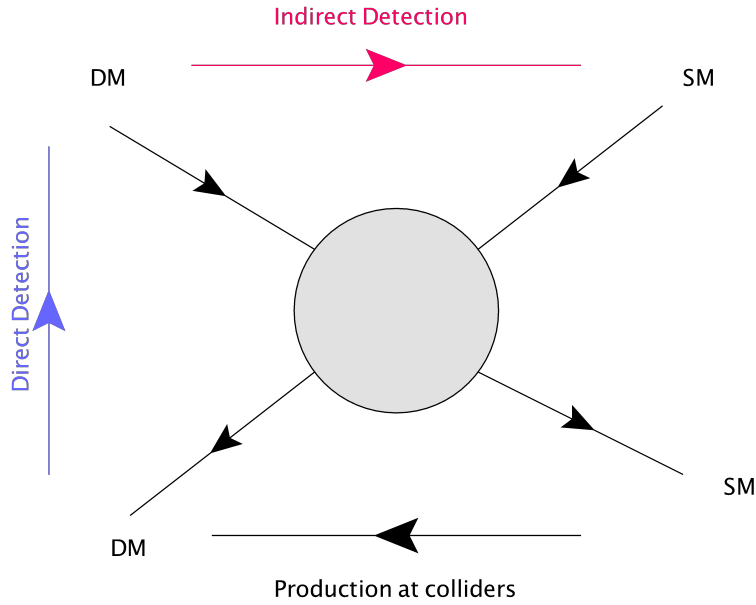


Figure 6: Dark matter search strategies

2.4 DARK MATTER DETECTION

If dark matter has non-gravitational interactions with the Standard Model particle content, then it is possible, as illustrated in Figure.6 to look for dark matter in three different directions:

Direct detection: dark matter scatters off the Standard Model particles elastically.

Indirect detection: dark matter annihilates into the Standard Model particles.

Collider searches: dark matter produces from the Standard Model particles.

In this section we review these dark matter searches briefly.

2.4.1 Direct Detection

The possibility of the dark matter interaction with ordinary matter such as nucleons is a reasonable assumption if we assume that dark matter particles were thermally produced in the early universe. Then dark matter particles that are flying around Earth can collide a

particle in a ground-based detector occasionally and scattering off with some recoil energy E_R . A large enough recoil energy can be used to detect scattered particle and infer the properties of the dark matter kinematically. This is called the direct detection of the dark matter which was first proposed in mid-1980s [36]. In the event of dark matter scatters off a nucleus with mass m_N , the nuclear recoil energy is

$$E_R = \frac{q^2}{2m_N} \simeq 50\text{keV} \left(\frac{m_\chi}{100 \text{ GeV}} \right)^2 \left(\frac{100 \text{ GeV}}{m_N} \right) \quad (2.12)$$

where $q \sim m_\chi v$ is the momentum transfer in the collision.

The basic quantity of interest is the scattering rate of the dark matter particle with mass m_χ off the nuclear target. The differential rate per unit detector mass is

$$\frac{dR}{dE_R} = \frac{\rho_\chi}{m_\chi m_N} \int_{v_{\min}}^{v_{\max}} d^3v v f(\mathbf{v}, t) \frac{d\sigma}{dE_R} \quad (2.13)$$

where ρ_χ is the density of dark matter in solar system, ($\sim 0.3 \text{ GeV}/c^2/\text{cm}^3$), $f(\mathbf{v}, t)$ is the dark matter velocity distribution in the lab frame, v_{\max} is the escape velocity of the Milky Way ($\sim 544 \text{ km/s}$), v_{\min} is the minimum velocity needed to cause a nucleus to scatter with energy E_R , and $d\sigma/dE_R$ is the differential dark matter-nucleus scattering cross section. The minimal velocity required for a WIMP to induce a nuclear recoil of energy E_R is

$$v_{\min} = \sqrt{\frac{E_R m_N (m_N + m_\chi)^2}{2 (m_N m_\chi)^2}} = \sqrt{\frac{E_R m_N}{2} \frac{1}{\mu^2}} \quad (2.14)$$

where μ denotes the reduced mass of the nucleon-WIMP system.

2.4.1.1 Spin-Independent and Spin-Dependent Interactions Because of its large de Broglie wavelength, the WIMP interacts coherently with all nucleons in the target nucleus. The WIMP-nucleus scattering cross section in Eq.2.13 is velocity and recoil-energy dependent and given by

$$\frac{d\sigma}{dE_R} = \frac{m_N}{2v^2\mu^2} [\sigma_{SI}F_{SI}^2(E_R) + \sigma_{SD}F_{SD}^2(E_R)] \quad (2.15)$$

Since the possible interaction of WIMPs with baryonic matter is still unknown, the cross section consists of two terms for spin-independent (SI, which can be described by a scalar $\mathcal{L}_S \sim \bar{\chi}\chi\bar{q}q$ or vector $\mathcal{L}_V \sim \bar{\chi}\gamma^\mu\chi\bar{q}\gamma^\mu q$ effective 4-fermion Lagrangian) and spin-dependent (SD, axial-vector $\mathcal{L}_A \sim \bar{\chi}\gamma^\mu\gamma_5\chi\bar{q}\gamma^\mu\gamma_5 q$) couplings. At small momentum transfers, q , all partial waves of the nucleons contribute and the WIMP scatters off the entire nucleus coherently. For higher q the WIMP's de Broglie wavelength is reduced and only part of the nucleus interacts. This loss of coherence is encapsulated in the finite form factors F_{SI} and F_{SD} .

The spin-independent (SI) cross section is given by

$$\sigma_{SI} = \sigma_n \frac{\mu^2}{\mu_n^2} \frac{[f_p Z + f_n(A - Z)]^2}{f_n^2} = \sigma_n \frac{\mu^2}{\mu_n^2} A^2 \quad (2.16)$$

where μ is the WIMP-nucleus reduced mass, and μ_n is the reduced mass of the WIMP-nucleon system. A is the nucleus mass number and Z its atomic number. To be able to compare different target nuclei utilized in different experiments, the WIMP-nucleus cross section, σ , is usually converted to a WIMP-nucleon cross section, σ_n . f_p and f_n are the WIMP coupling strength to protons and neutrons, respectively. The cross section reduces to the second expression provided $f_p = f_n$ which results in the A^2 dependence of the cross section: This implies that heavier targets observe higher event rates, however, at the same time the expected recoil energy, E_R is smaller that causes challenges on the detector's thresholds.

The current status of the search for spin-independent WIMP-nucleon scattering is shown in Figure.7.

The differential cross section for spin-dependent (SD) interactions, where the WIMP is assumed to be a (Dirac or Majorana) fermion coupling to nucleus of spin J is [38]

$$\frac{d\sigma_{SD}}{d|\vec{q}|^2} = \frac{8G_F^2}{\pi v^2} [a_p \langle S_p \rangle + a_n \langle S_n \rangle]^2 \frac{J+1}{J} \frac{S(|\vec{q}|)}{S(0)} \quad (2.17)$$

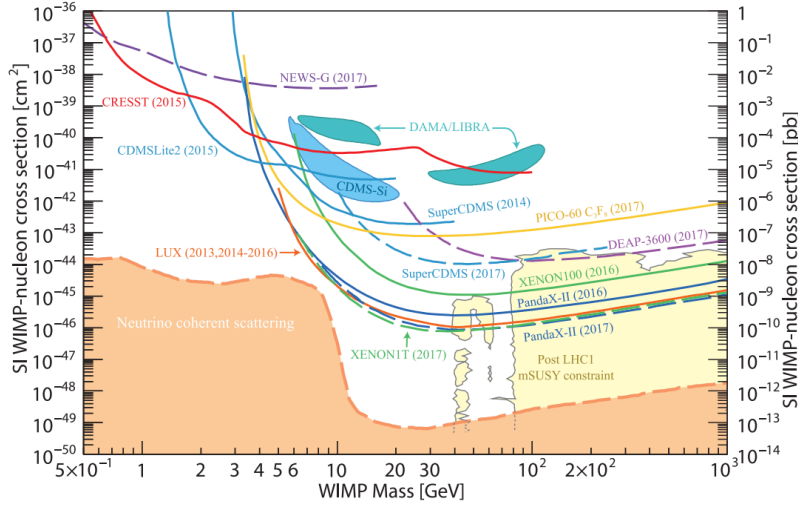


Figure 7: WIMP cross sections (normalized to a single nucleon) for spin-independent coupling versus mass, plot taken from Ref. [37]

where G_F is the Fermi constant and \vec{q} is the transferred momentum. $\langle S_p \rangle$ and $\langle S_n \rangle$ are the expectation values of the total spin operators for protons and neutrons in the target nucleus which are model dependent. It is clear that there is no A^2 -scaling from coherence effects as in the spin-independent case, Eq. 2.16, instead the cross section depends on the total nuclear spin J of the target nucleus and its spin-structure function, $S(|\vec{q}|)$.

2.4.2 Indirect Detection

In indirect searches for dark matter, the goal is to detect the products of dark matter annihilation or decay at objects with large dark matter density, in our galaxy or beyond. While WIMP dark matter annihilation is strongly suppressed after thermal freeze-out, it can still occur today and one can maximize the chance of discovery by searching in regions of very high dark matter density. If the dark matter particle is unstable (gravitino, sterile neutrino, ...), one can expect seeing some of them decaying today around us. Looking for the products of dark matter annihilations or decays are not limited to WIMPs and extend

to any framework where dark matter interactions with the SM particle content.

Dark Matter annihilations or decays into Standard Model particles could eventually produce quarks (q), leptons (ℓ), gauge bosons (W^\pm, Z, γ) or Higgs bosons (h) which will eventually decay to electrons (e^-), protons (p), nuclei (N), gamma-rays or neutrinos (ν). In order to claim the observation of some dark matter annihilation/decay event, an excess of these final stable particles has to be detected over the astrophysical background which is not well understood because of large uncertainties regarding the nature of the sources and propagation models.

In the following we discuss the most common signatures and associated detection strategies for indirect detection of dark matter.

2.4.2.1 Gamma Rays To quantify the amount of gamma rays produced from annihilation of dark matter content of some close region, e.g. Galactic Center, we introduce the flux

$$\frac{d\Phi}{dE_\gamma} = \frac{1}{4\pi} \sum_f B_f \frac{\langle \sigma_f v \rangle}{2m_\chi^2} \frac{dN_f}{dE_\gamma} \times \int_V \rho_\chi^2(\vec{x}) dV \quad (2.18)$$

where the summation is over all possible annihilation channels; B_f , is the branching fraction of final state f , $\langle \sigma_f v \rangle$, is the averaged annihilation cross section times relative velocity, dN_f/dE_γ , is the photon spectrum from annihilation or decay to the final state f , m_χ is the mass of the dark matter particle, and ρ_χ is the dark matter density. Eq.2.18 must be multiplied by an additional factor of 1/2 if the dark matter is not its own antiparticle.

All the astrophysical uncertainties in the determination of the flux are absorbed by the J -factor,

$$J \equiv \int_V \rho_\chi^2(\vec{x}) dV = \int_{\Delta\Omega} d\Omega' \int_{l.o.s} \rho_\chi^2 dl \quad (2.19)$$

while the particle physics input to the flux is absorbed by the factor of $\frac{\langle \sigma_f v \rangle}{m_\chi^2} dN_f/dE_\gamma$.

The larger the J -factor, the more promising the astrophysical target is for dark matter annihilation. But the size of the J -factor is not the only relevant factor, it together with the potential backgrounds help us to determine the ideal target. For example, dwarf galaxies are

dark matter-dominated and since they contain very few stars and little gas, therefore they are some of the cleanest systems to search for dark matter. On the other hand, while a signal from the center of the Galaxy enjoys enhancement due to the dark matter density and closeness, it has to cope with large systematic uncertainties on the astrophysical backgrounds.

2.4.2.2 Antiproton Cosmic rays are composed primarily of high-energy protons mainly originating outside the Solar System. For two reasons antiproton content of the astrophysical background is rare: first, the production of antiproton in the Galaxy happens through inelastic process of a proton hitting another proton, $p + p \rightarrow p + p + p + \bar{p}$, which costs us a lot of energy (threshold ~ 7 GeV). Second reason is that the energy flux of cosmic rays is falling steeply with energy ($\sim E^{-2.7}$), so compared to the maximal flux of cosmic-ray protons, observed at $E \sim 0.1$ GeV, antiprotons will be under abundant, at 0.1 GeV, by about a factor of

$$\frac{\Phi_{\bar{p}}(E)}{\Phi_p(E)} \Big|_{0.1\text{GeV}} \sim \left(\frac{0.1}{7.5}\right)^{2.7} \sim 10^{-5} \quad (2.20)$$

Dark matter particles could serve as a new primary component for cosmic rays. Proton is the common product of all dark matter models; annihilation or decay into quarks, gauge bosons, and even leptons due to ElectroWeak corrections, following by hadronization process generates proton abundantly. These processes will produce as much antiproton as proton. Antiprotons, as electrically charged particles, are deflected by the Galactic magnetic field and their propagation must be accounted for as a diffusion process. Any excess of antiprotons over the astrophysical background can be a hint of dark matter.

2.4.2.3 Neutrino Elusive weakly interacting neutrinos can travel over large distances without being affected, therefore they carry the spectral information of the source all along. They are detected by Cerenkov light produced by some detector material as neutrinos pass through it. One interesting scenario is capturing and accumulating dark matter inside the sun [39, 40], in the case where the DM-baryon scattering cross section is large enough. Then the only way to detect annihilations of these trapped dark matter particles would be via the

neutrino channel as only neutrinos can escape efficiently from the gravitational potential of the Sun.

2.4.3 Collider Searches

Another possibility to attempt at observing Dark Matter is to produce it at high energy colliders such as the Large Hadron Collider (LHC). LHC proton-proton collisions might result in the production of WIMPs in association with one or more QCD jets, photons as well as other detectable Standard Model debris. Since WIMPs are electrically neutral and cosmologically stable massive particles, they manifest at colliders as missing transverse energy. For this reason searches for dark matter are based on the observation of the visible counterpart as trigger of the event such as charged leptons, jets or a photon, generally referred to as mono-X searches. By selecting events with large missing energy one can reduce the Standard Model background and potentially disentangle a dark matter signal. However, colliders can allow to identify only missing energy, and therefore they cannot uniquely ascertain the presence of dark matter in a signal event. They can simply confirm the presence of a neutral and stable particle, that might have even decayed outside the detector. Anyhow, colliders offer an exciting and complementary search strategy to identify WIMPs. Indeed, assuming that the production of WIMPs at colliders is uniquely connected to WIMP-nucleon scatterings at underground laboratories, one can use the non-observation signals with large missing transverse momentum to derive limits on the WIMP-nucleon scattering cross-section.

3.0 INDIRECT DETECTION OF NEUTRINO PORTAL DARK MATTER

This chapter is devoted to the study of the feasibility of the indirect detection of dark matter in a simple model using the neutrino portal. The model is very economical, with right-handed neutrinos generating neutrino masses through the Type-I seesaw mechanism and simultaneously mediating interactions with dark matter. Given the small neutrino Yukawa couplings expected in a Type-I seesaw, direct detection and accelerator probes of dark matter in this scenario are challenging. However, dark matter can efficiently annihilate to right-handed neutrinos, which then decay via active-sterile mixing through the weak interactions, leading to a variety of indirect astronomical signatures. It is based on our work in Ref. [41].

3.1 INTRODUCTION

A wide array of gravitational phenomena over a range of cosmological scales strongly supports the hypothesis of dark matter (DM) [42, 43, 44]. There is, however, no firm evidence that DM couples to ordinary matter other than through gravity, and the search for such non-gravitational DM interactions has become one of the main drivers in particle physics today. Neutrinos (ν) in the Standard Model (SM) may be identified as a component of DM, since they are color-singlet, electrically neutral cosmic relics. However, the smallness of the lightest neutrino mass makes them relativistic at freeze-out in the early universe, and thus incompatible with current observations to account for the majority of the cold DM. One therefore must seek a solution beyond the SM. Since we do not know how DM couples (if at all) to the SM, it is important to explore a variety of models to understand in a comprehensive manner how non-gravitational DM interactions may manifest [45].

Since DM is presumably electrically neutral, it may be either the neutral component of an electroweak multiplet, as in the well motivated weakly interacting massive particle (WIMP) paradigm, or alternatively it may be a Standard Model (SM) gauge singlet state. In the latter case of gauge singlet DM, an economical and predictive mechanism for mediating DM interactions to the SM is provided by the so-called “portals” – renormalizable interactions of DM through gauge singlet SM operators. There are only three such portals in the SM—the Higgs portal [46, 47], the vector portal [48, 49], and the neutrino portal [8]. As applied to DM, the Higgs portal [46, 50, 51, 52], and the vector portal [53, 54, 55] have been extensively investigated, while the neutrino portal option has received comparatively little attention, despite the strong motivation due to its connection to neutrino masses. In this chapter we will examine a minimal model of neutrino portal DM in the simplest setup of a Type-I seesaw scenario [8].

The neutrino portal to DM relies on DM interactions being mediated by the right-handed neutrinos (RHNs). Since the RHNs are responsible for generating neutrino masses, one may typically expect the DM interaction strength with the SM to be very small since it is governed by the neutrino Yukawa coupling. In this case it is challenging to probe neutrino portal DM in accelerator experiments or in direct detection experiments. On the other hand, the DM coupling to the RHN can be sizable, thereby facilitating the efficient annihilation of DM to pairs of RHNs. This allows DM to be produced thermally in the early universe with the observed relic abundance and furthermore presents an opportunity to test the scenario through a variety of indirect detection channels. In this work we investigate the indirect detection signatures of neutrino portal DM. The scenario investigated here was first proposed in Ref. [53] and falls into the class of “secluded” DM scenarios. Some aspects of the thermal cosmology were investigated in Ref. [56]. In regards to indirect detection signatures, Ref. [57] explored a possible interpretation of the *Fermi* Galactic Center gamma ray excess [58, 59, 60, 61, 62] in terms of the DM annihilation to RHNs. Recently, Ref. [63] investigated the limits from gamma ray observations on DM annihilation to RHNs, although did not explore the implications for specific particle physics models. Extensions of the simplest scenario, which include additional states and/or interactions have also been discussed in Refs. [64, 65, 66, 67, 68, 69, 70, 71, 72, 73, 74]. Our work provides a comprehensive

and updated analysis of the indirect detection phenomenology of neutrino portal DM. In particular, we present constraints from *Planck* cosmic microwave background (CMB) measurements, *Fermi* dwarf spheroidal galaxies (dSphs) and Galactic Center gamma-rays studies, and AMS-02 antiproton observations, and also describe the future prospects for *Fermi* and the Cherenkov Telescope Array. Thermal relic annihilation rates are already constrained for DM masses below about 50 GeV. This scenario can also provide a DM interpretation of the *Fermi* Galactic Center gamma ray excess, although we demonstrate that such an interpretation faces some tension from dSphs and antiproton constraints. We also describe extensions of this scenario beyond the minimal model, including scenarios with large Yukawa and Higgs portal couplings, and highlight the potentially rich physics implications in cosmology, direct detection, and collider experiments. Besides these probes, there is also the interesting possibility of a hard gamma-ray spectral feature that arises from the radiative decays of N , which could place complementary constraints in the region $m_\chi \sim m_N$, $m_N \lesssim 50$ GeV. We will comment on this possibility below, and we refer the reader to Ref. [74] for a detailed study.

The outline of the chapter is as follows. In Section 4.2.1 we describe a minimal neutrino portal DM model, outline the expected range of couplings and masses, and discuss the cosmology. The primary analysis and results concerning the indirect detection limits and prospects are discussed in Section 3.3. In Section 3.5 we describe several features and phenomenological opportunities present in non-minimal neutrino portal DM scenarios. Our conclusions are presented in Section 4.5.

3.2 NEUTRINO PORTAL DARK MATTER

The simplest construction beyond the Standard Model to account for the neutrino masses is the introduction of right-handed neutrinos (RHN). Beside the normal Dirac mass terms with the Yukawa interactions, the RHN can also have a Majorana mass term since it is a SM gauge singlet. This is the traditional Type-I seesaw mechanism [8]. For the same reason of its singlet nature, N can serve as a mediator to the dark sector via the neutrino portal. A

simple model of neutrino portal DM based on the Type-I seesaw contains three new fields, N, χ, ϕ , where N and χ are two component Weyl fermions and ϕ is a real scalar field. They are charge-neutral with respect to the SM gauge interactions. The fermion N is identified as a RHN. We will assume that χ is lighter than ϕ , and they are charged under a Z_2 symmetry, which renders χ stable and a potential DM candidate.

The Lagrangian has the following new mass terms and Yukawa interactions

$$\mathcal{L} \supset -\frac{1}{2}m_\phi^2\phi^2 - \left[\frac{1}{2}m_N NN + \frac{1}{2}m_\chi\chi\chi + yLHN + \lambda N\phi\chi + \text{h.c.} \right], \quad (3.1)$$

where L and H are the SM $SU(2)_L$ lepton and Higgs doublets, respectively. There are two central features of this model. First, the RHN field N serves as a mediator between the dark sector fields χ, ϕ and the SM fields, due to the couplings λ and y . This mediation allows for non-gravitational signatures of the DM and a thermal DM cosmology. Second, after the Higgs obtains a vacuum expectation value, $\langle H \rangle = v/\sqrt{2}$ with $v = 246$ GeV, a small mass for the light SM-like neutrinos is generated via the seesaw mechanism:

$$m_\nu \sim \frac{y^2 v^2}{2m_N}. \quad (3.2)$$

Given the observed neutrino masses¹, the Yukawa coupling y depends on the RHN mass, m_N . For instance, fixing $m_\nu \sim \sqrt{(\Delta m_\nu)^{\text{atm}}} \sim 0.05$ eV suggests a small neutrino Yukawa coupling of order

$$y \simeq 10^{-6} (m_N/v)^{1/2}. \quad (3.3)$$

As we will discuss in more detail shortly, the requirement of thermal freeze-out of the DM puts an upper bound on the DM and RHN mass less than 20 TeV. Therefore, the Yukawa couplings that we will be interested in will generally be quite small. It will thus be extremely difficult to produce the DM at accelerators, or directly detect it through its scattering with SM particles. However, there is an opportunity to probe this type of DM via indirect detection, and this will be the primary focus of this chapter.

As alluded to already we will be interested in DM that is thermally produced in the early universe. The RHN mediator allows for the dark sector to couple to the SM thermal

¹In principle, we would need at least two right-handed states to generate the observed neutrino mass pattern. For our current interest, we will only focus on the lower-lying one N .

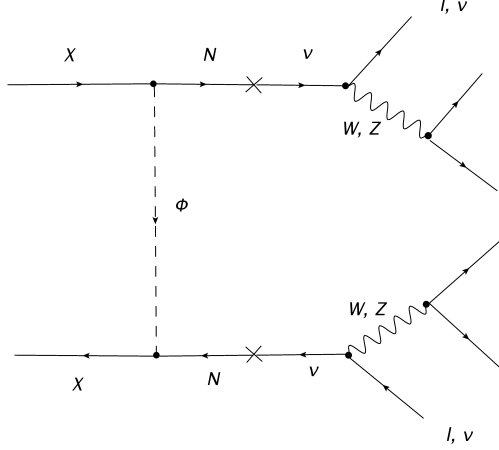


Figure 8: The Feynman diagrams for the DM particle annihilation to RHN pair and the decay of N to SM particles

bath in the early universe. Then, provided that $m_\chi > m_N$ and that all of the particles are sufficiently light, say below $\mathcal{O}(10 \text{ TeV})$, the DM can efficiently annihilate to RHNs, Fig. 8,

$$\chi\chi \rightarrow NN, \quad (3.4)$$

and achieve the correct relic abundance. The process Eq. (3.4) is governed by the coupling λ , which is a priori a free parameter. The thermally averaged annihilation cross section is

$$\langle\sigma v\rangle = \frac{[\text{Re}(\lambda)^2(m_\chi + m_N) + \text{Im}(\lambda)^2(m_\chi - m_N)]^2}{16\pi[m_\phi^2 + m_\chi^2 - m_N^2]^2} \left(1 - \frac{m_N^2}{m_\chi^2}\right)^{1/2}. \quad (3.5)$$

We observe that the annihilation cross section Eq. (3.5) depends on the coupling λ and the masses m_χ , m_N , m_ϕ . However, the indirect detection signatures that we will investigate will depend in a detailed way only on the size of the annihilation cross section $\langle\sigma v\rangle$, which determines the rate, as well as the masses m_χ and m_N , which will affect the energy spectrum of the SM annihilation products. Thus, it will be more convenient to simply work with the three parameters $\{\langle\sigma v\rangle, m_\chi, m_N\}$. Note that for a given set of masses, one can always

obtain the desired cross section by an appropriate choice of the coupling λ through Eq. (3.5), provided the coupling remains perturbative. We will discuss this point in detail shortly.

We can restrict the parameter space further if we demand that the DM saturates the observed relic density. For Majorana fermion DM the observed relic abundance is obtained for [75]

$$\langle\sigma v\rangle_{\text{thermal}} = 2.2 \times 10^{-26} \text{ cm}^3 \text{ s}^{-1}. \quad (3.6)$$

Once we fix the annihilation cross section to saturate the observed relic abundance, then all of the physics can be characterized in terms of the two masses m_χ and m_N . Parameter choices that predict cross sections smaller than (3.6) overproduce the DM.

We now discuss the expected range of masses and couplings of the new states in the model. A first constraint comes from demanding that the coupling λ be perturbative and thus the theory be predictive. Assuming $m_N \ll m_\chi$, the partial-wave perturbative unitarity bound for the DM annihilation amplitude requires that $\lambda < \sqrt{4\pi}$. The over-closure and perturbative unitarity constraints lead to the bound

$$m_\chi \lesssim \sqrt{\frac{\pi}{4\langle\sigma v\rangle_{\text{thermal}}}} \approx 20 \text{ TeV}, \quad (3.7)$$

which is in broad agreement with the general analysis of Ref. [76]. Furthermore, there are a variety of limits on the right-handed neutrinos N , which depend on its mass and mixing angle with active neutrinos. In particular, for seesaw motivated mixing angles, the lifetime of N is typically longer than $\mathcal{O}(1\text{ s})$ for $m_N \lesssim 1 \text{ GeV}$, and is thus constrained by Big Bang Nucleosynthesis [77, 78]. Then, considering $m_\chi > m_N$ in order to obtain an efficient DM annihilation cross section we will consider in this chapter masses in the range

$$1 \text{ GeV} < m_N < m_\chi \lesssim 20 \text{ TeV}. \quad (3.8)$$

The discussion above assumes a standard thermal history for the DM particle χ , which relies on χ being in equilibrium with the plasma. Since the dark sector particles χ and ϕ have no direct couplings to the SM, it is the RHN that is ultimately responsible for keeping χ and ϕ in equilibrium. It is therefore important that N remain in equilibrium with the SM during the freezeout process. The relevant processes to consider are the decay and

inverse decays of N to the SM. This question has been investigated recently in Ref. [57]². For Yukawa couplings dictated by the naive seesaw relation, these processes are very efficient when $m_N \gtrsim m_W$, since N decays through a two-body process. However, if N is light, $m_N \lesssim m_W$, the three-body decays of N become inefficient and N can fall out of equilibrium. As a consequence, this fact requires an annihilation cross section that is larger than the canonical thermal relic value by some order one factor in the early universe to efficiently deplete the χ abundance, as explored in detail in Ref. [57]. A detailed investigation of the cosmology is beyond the scope of this work, but we will take the standard thermal value for the annihilation cross section as a motivated benchmark.

Besides the terms in Eq. (3.1), an additional Higgs portal coupling, $\phi^2|H|^2$ is allowed in the model. This interaction provides an alternative means to keep ϕ , χ , and N in thermal equilibrium with the SM. We will assume for now that this coupling is small so that the phenomenology is dictated by the minimal neutrino portal interaction. However, a large Higgs portal coupling can lead to a variety of interesting effects, and we will discuss this topic in Section 3.5.

3.3 INDIRECT DETECTION CONSTRAINTS AND PROSPECTS

We now come to the main subject of this work: the constraints and prospects for indirect detection of neutrino portal DM. We will investigate several indirect signatures of DM annihilation in this scenario, including observations of the CMB, gamma rays, and antiprotons. For each of these indirect probes the relevant underlying reaction is DM annihilation to RHNs as in Eq. (3.4), followed by the weak decays of the RHNs to SM particles due to mixing. We will therefore require the energy spectrum dN/dE per DM annihilation in the photon, electron and antiproton channels as an input to our further analysis below. To compute these spectra we first simulate the decay of RHNs to SM particles in the N -rest frame using `MadGraph5_aMC@NLO` [225] in conjunction with the `SM_HeavyN_NLO` model files [81, 82]. These partonic events are then passed to `Pythia 8` [83] for showering and hadronization,

²See Ref. [79] for a similar discussion in the context of right-handed sneutrino DM.

thereby yielding the prediction for the resulting photon, electron, and antiproton spectrum coming from the N decay, dN'_i/dE' for $i = \gamma, e^-, \bar{p}$. These events are then boosted to the DM rest frame according to the formula (see, *e.g.*, Refs. [84, 85, 86, 87] for the case of massless particles):

$$\frac{dN_i}{dE} = \int_{\gamma(E-\beta\sqrt{E^2-m^2})}^{\gamma(E+\beta\sqrt{E^2-m^2})} \frac{dE'}{2\beta\gamma\sqrt{E'^2-m^2}} \frac{dN'_i}{dE'}, \quad \gamma = (1-\beta^2)^{-1/2} = m_\chi/m_N, \quad (3.9)$$

where m is the mass of the boosted particle, *i.e.*, photons, or electrons, antiprotons; see Appendices A and B for a derivation of Eq. (3.9). This gives the prediction for the required spectrum in each channel. We note that spin correlations are not accounted for in our simulation, but these are expected to have only a modest effect on the broad continuum spectra of interest to us (see Ref. [86] for an explicit example where this expectation is borne out).

We display in Figure 9 examples of the predicted continuum γ -ray, electron, and antiproton spectra for $(E_i^2 dN_i/dE_i$ versus E_i for $i = \gamma, e^-, \bar{p}$), where we have fixed the DM mass to be $m_\chi = 200$ GeV and chosen three values for the RHN masses $m_N = 20$ GeV (solid), 50 GeV (dashed), 100 GeV (dotted). Here we have assumed that N couples solely to the first generation (electron-type) lepton doublet. In the case of the γ -ray and antiproton spectrum, one observes a broad spectrum that peaks in the $\mathcal{O}(10$ GeV) range. The location of the peak is largely dictated by the DM mass, which controls the total injected energy. There is a mild sensitivity to the RHN mass, with harder spectra resulting from a larger mass gap between the DM and RHN. For the electron case, in addition to the continuum component, there is a hard component resulting from the primary $N \rightarrow We$ decay, which is clearly seen in Figure 9.

In this work we will restrict to the case in which N couples to the electron-type lepton doublet, but it is worth commenting on the cases of couplings to muon and/or tau flavor. In these cases, we have checked that the continuum spectra is very similar to the electron-flavor case, as is expected since these particles dominantly originate from decay of the electroweak bosons. The primary difference for muon or tau-flavor couplings will be the absence of the hard electron component from the primary N decay. The electron spectrum will be used

below as an input to the CMB bounds, so one may expect a mild difference in the resulting limits in the case of muon or tau flavor couplings.

We now present in turn the constraints on neutrino portal DM from the *Planck* cosmic microwave background measurements, *Fermi* observations of gamma rays from the Galactic Center and from dwarf spheroidal galaxies, and AMS-02 observations of antiprotons. A summary of these constraints, as well as a discussion of other indirect searches not considered here, and an analysis of the future prospects, is presented below in Section 3.3.5.

3.3.1 Cosmic Microwave Background

The Cosmic Microwave Background (CMB) provides a sensitive probe of DM annihilation around the epoch of recombination. In particular, if the annihilation products include energetic electrons and photons, the photon-baryon plasma can undergo significant heating and ionization as these particles are injected into the bath, modifying the ionization history and altering the temperature and polarization anisotropies. Using precise measurements of the CMB by a number of experiments, including WMAP [88], SPT [89, 90], ACT [91], and *Planck* [92], robust, model-independent constraints on DM annihilation have been derived by several groups [93, 94, 95, 96, 97, 98, 99, 100, 101, 102, 103, 104, 105, 106, 107].

The relevant quantity of interest for DM annihilation during recombination is the energy absorbed by the plasma per unit volume per unit time at redshift z ,

$$\frac{dE}{dV dt} = \rho_c^2 \Omega_\chi^2 (1+z)^6 \left[f(z) \frac{\langle \sigma v \rangle}{m_\chi} \right], \quad (3.10)$$

where ρ_c is the critical density of the Universe today and Ω_χ is the DM density parameter today. Production of neutrinos as daughter particles and free-streaming of electrons and photons after creation until their energy is completely deposited into the intergalactic medium (IGM) (via photoionization, Coulomb scattering, Compton processes, bremsstrahlung and recombination) affect the the efficiency of energy deposition. This is accounted for in Eq. (3.10) by the efficiency factor, $f(z)$, which gives the fraction of the injected energy that is deposited into the IGM at redshift z and depends on the spectrum of photons and electrons arising from DM annihilations. Furthermore, since the CMB data are sensitive to energy injection

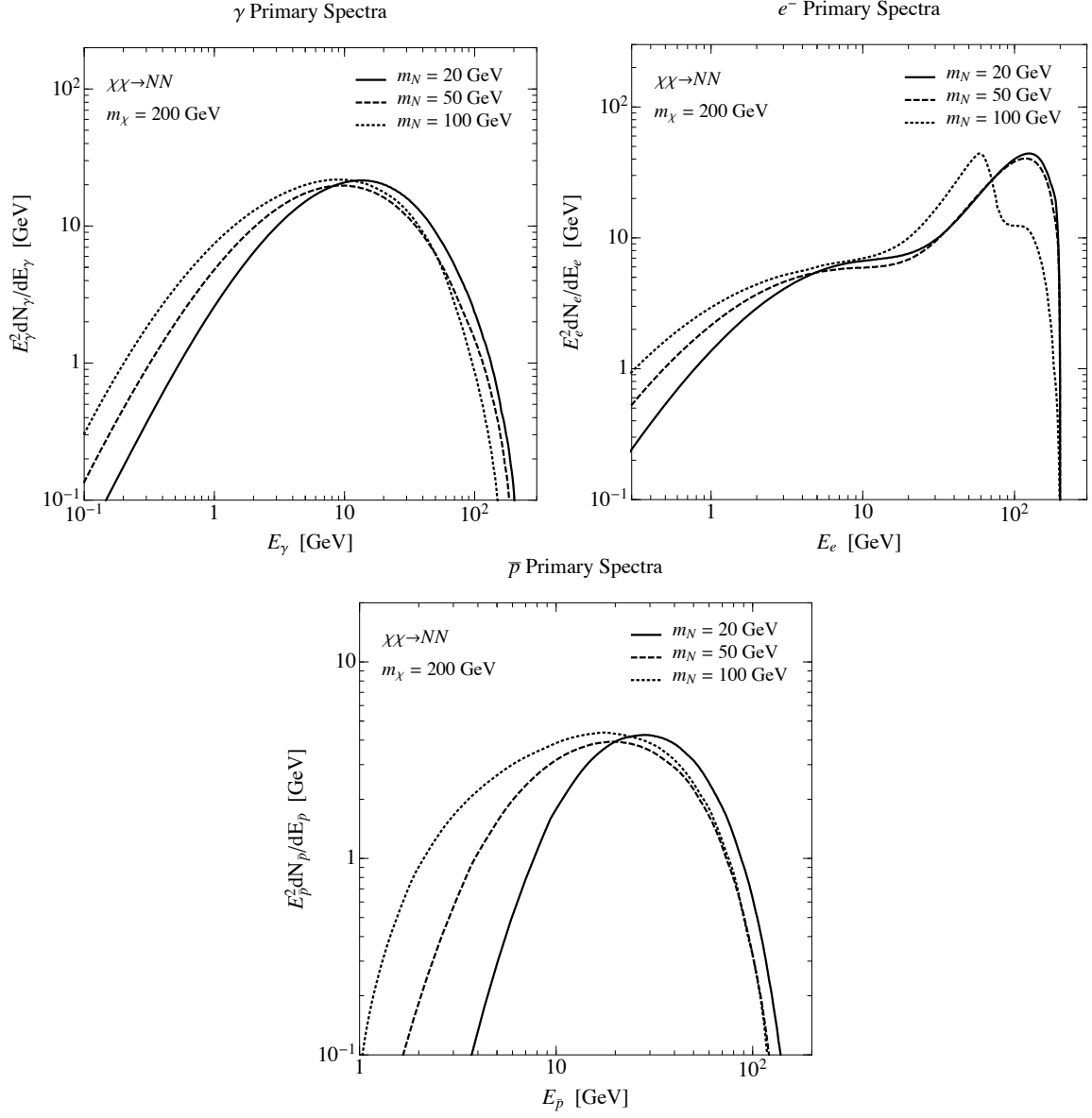


Figure 9: Continuum γ -ray, electron, and antiproton spectra $E_i^2 dN_i/dE_i$ versus E_i ($i = \gamma, e^-, \bar{p}$) for DM mass $m_\chi = 200$ GeV and RHN masses $m_N = 20$ GeV (solid), 50 GeV (dashed), 100 GeV (dotted). The RHN is assumed to couple to the electron-type lepton doublet.

over a narrow range of redshift, *i.e.*, 1000–600, $f(z)$ can be well-approximated by a constant parameter f_{eff} .

The additional energy injection from DM annihilation in Eq. (3.10) alters the free electron fraction (the abundance ratio of free electrons to hydrogen), which in turn affects the ionization history. These effects are quantitatively accounted for with new terms in the Boltzmann equation describing the evolution of the free electron fraction. The additional terms are added to the baseline Λ CDM code and used to derive limits on the energy release from DM annihilation. *Planck* sets a limit on the particle physics factors in Eq. (3.10)

$$f_{\text{eff}}(m_\chi) \frac{\langle \sigma v \rangle}{m_\chi} < 4.1 \times 10^{-28} \text{ cm}^3 \text{ s}^{-1} \text{ GeV}^{-1}, \quad (3.11)$$

which is obtained from temperature and polarization data (TT,TE,EE+lowP) [92].

To apply the *Planck* constraints of Eq. (3.11) to the neutrino portal DM model, it remains to compute the efficiency factor $f_{\text{eff}}(m_\chi)$ in our model. We use the results of Ref. [106], which provides $f_{\text{eff}}^{\gamma(e^-)}(E)$ curves for photons and electrons to compute a weighted average with the photon/electron spectrum $(dN/dE)_{\gamma,e^-}$ predicted in our model according to

$$f_{\text{eff}}(m_\chi) = \frac{1}{2m_\chi} \int_0^{m_\chi} dE E \left[2f_{\text{eff}}^{e^-}(E) \left(\frac{dN}{dE} \right)_{e^-} + f_{\text{eff}}^\gamma(E) \left(\frac{dN}{dE} \right)_\gamma \right]. \quad (3.12)$$

The photon and electron spectra for each DM and RHN mass point are computed with Monte Carlo simulation described at the beginning of this section and are displayed for a few benchmarks in Figure 9. Using these spectra and Eqs. (3.11) and (3.12), we obtain a limit on the annihilation cross section from the CMB as a function of m_χ and m_N . These limits are displayed in Figure 10 as contours of the 95% C.L. upper limit on $\log_{10} [\langle \sigma v \rangle / (\text{cm}^3 \text{ s}^{-1})]$ (black curves) from the CMB from *Planck* [92] in the $m_\chi - m_N$ plane. The thick (red) line indicates the region where the cross section limit is equal to the thermal relic value of Eq. (3.6). The constraints on the annihilation cross section are translated to limits on the minimum value of the coupling constant λ (which occurs for $m_\phi = m_\chi$) as shown by the vertical (blue) lines. The shaded (blue) region indicates where the perturbative unitarity bound is violated, $\lambda > \sqrt{4\pi}$. Since the efficiency factor f_{eff} is essentially constant over a broad range of m_χ , Eq. (3.11) implies that the limit on $\langle \sigma v \rangle$ scales with m_χ irrespective of

the value of m_N , and this feature is clearly present in Figure 10. We observe that *Planck* is able to constrain the thermal relic value based on Eq. (3.6) for DM masses below about 20 GeV. A small feature in the limit contour is apparent in the region near $m_W \lesssim m_N \lesssim m_Z$. This is a consequence of the dominance of the two body decay to $N \rightarrow W\ell$ in this small mass window.

3.3.2 Gamma rays from the galactic center

One of the primary signatures of DM annihilation are high-energy gamma rays. In comparison to other cosmic ray signatures involving electrically charged particles, gamma rays are essentially unperturbed by magnetic fields and the astrophysical environment as they travel to us from their source, yielding information about both the energy and location of the underlying DM reaction. One can search for both gamma ray line signatures as well as a continuum signal. While a line signature is unfortunately not present in the neutrino portal DM model, there can be a distinct continuum gamma ray signal, and this will be the subject of investigation here. Significant advances in our study of the gamma-ray sky have been achieved over the past several years by the *Fermi* Gamma Ray Space Telescope, and data from the *Fermi* collaboration can be used to probe DM annihilation over a wide range of models and DM masses. In this section we will consider gamma ray signatures from the center of the Milky Way. The Galactic Center has long been recognized as the brightest source of DM induced gamma rays, a consequence of its proximity and the rising DM density in this region. At the same time extracting a signal from this region is challenging due to significant and not well-understood astrophysical backgrounds. Below we will also investigate gamma ray signals from dwarf spheroidal galaxies, which provide a cleaner, albeit dimmer, source of gamma rays.

The quantity of interest for gamma ray signals of DM annihilation is the gamma ray flux per unit energy per unit solid angle in a given direction, $\Phi_\gamma(E, \hat{n})$, where E is the energy and \hat{n} is a unit vector along the path of the line of sight. The gamma ray flux can be written as

$$\Phi_\gamma(E, \hat{n}) = \frac{1}{4\pi} \left[\frac{\langle \sigma v \rangle}{2m_\chi^2} \frac{dN_\gamma}{dE} \right] J(\hat{n}). \quad (3.13)$$

Planck CMB 95% C.L. Limit

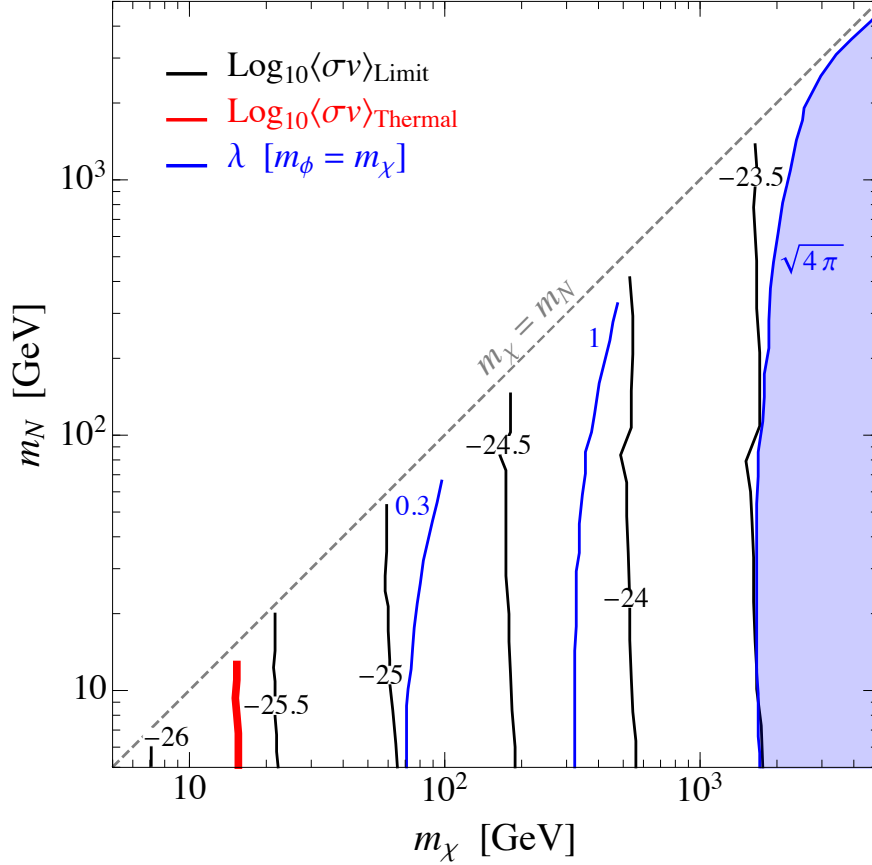


Figure 10: Contours of the 95% C.L. upper limit on $\log_{10} [\langle\sigma v\rangle/(\text{cm}^3 \text{s}^{-1})]$ in the $m_\chi - m_N$ plane (black curves) from *Planck* [92]. The thick (red) line indicates the region where the cross section limit is equal to the thermal relic value of Eq. (3.6). The vertical (blue) lines show the limits on the minimum value of the coupling constant λ . The shaded (blue) region indicates the perturbative unitarity bound.

The term in square brackets in Eq. (3.13) above depends only on the underlying particle physics properties of the DM model, including m_χ , $\langle\sigma v\rangle$, and the spectrum of photons emitted per DM annihilation dN_γ/dE . This spectrum is shown in Figure 9 for the channel $\chi\chi \rightarrow NN$ for several choices of χ and N masses.

The quantity $J(\hat{n})$ in Eq. (3.13), also called the J -factor, depends only on astrophysics and involves an integral over the DM density profile $\rho_\chi(\mathbf{r})$ that runs along the path of the line of sight defined by \hat{n} :

$$J(\hat{n}) = \int_{\text{l.o.s.}} \rho_\chi^2(\mathbf{r}) dl. \quad (3.14)$$

In practice, the J -factor is averaged over a particular region of interest relevant for the analysis. The J -factor depends sensitively on the DM distribution and can vary by several orders of magnitude depending on this assumption, which translates into a substantial uncertainty in the derived annihilation cross section limit. At present, there is no consensus on the expected DM halo profile. Cuspy profiles such as NFW [108, 109] or Einasto [110] find support from N -body simulations [111, 112]. These simulations only involve DM, and the inclusion of baryonic processes may significantly impact the shape of the profile, especially towards the inner region of the Milky Way. However, even the qualitative nature of the resulting DM distribution is a matter of debate, and it is possible that the resulting profile is either steepened [113, 114, 115, 116] or flattened [117] due to baryonic effects. Besides the assumption of the DM distribution, a separate, smaller $\mathcal{O}(1)$ uncertainty arises from the overall normalization of the profile, which is fixed to match the local DM density ρ_0 [118].

The current situation regarding the observed gamma ray flux from the Galactic Center is somewhat murky. A number of analyses, starting from the works of Goodenough and Hooper [59, 60] and culminating most recently in the *Fermi* analysis [58], have found a broad excess of gamma rays from the Galactic Center, which peaks in the 1 – 3 GeV range. All analyses conclude that there is a highly statistically significant excess above the currently accepted diffuse background models (see for example Refs. [61, 62]). However, the origin of these gamma rays is still not clear. While there has been a significant effort devoted to possible DM interpretations, recently it has been argued that the excess is more likely to be a new population of unresolved point sources, which would disfavor the simplest DM

interpretations [119, 120, 121, 122] (see however [123]). It is certainly interesting to speculate on a possible DM origin, and we will carry out this exercise below in Section 3.4. Here we will instead take a conservative approach and use the *Fermi* data to place limits on DM annihilation.

To obtain limits on the neutrino portal DM scenario, we use the model independent results of Ref. [124]. In that work, four years of data from the *Fermi* Large Area Telescope was used to construct maps of the gamma ray flux in the region around the Galactic Center in four energy bins in the range from 300 MeV–100 GeV. Backgrounds templates from known point sources and emission from the Galactic Disk are then subtracted to yield the residual flux. Assuming that DM annihilation accounts for the remaining emission, the authors then place limits on DM annihilation for several choices of halo profiles. This procedure yields conservative limits since it is expected that additional background sources, such as the central supermassive black hole, unresolved point sources, and cosmic ray interactions with the gas, also contribute significantly to the residual emission. Limits on the the particle physics factor that governs the gamma ray flux, $(\langle\sigma v\rangle/m_\chi^2) \int dE dN_\gamma/dE$, are provided in Ref. [124].

For the neutrino portal DM model, we can use these results to derive a limit on the annihilation cross section for the process $\chi\chi \rightarrow NN$ as a function of the DM and RHN mass. In Figure 11 we show contours of the 95% C.L. upper limit on the annihilation cross section in the $m_\chi - m_N$ plane labelled by the black curves. These limits are derived under the assumption of an NFW profile and local DM density $\rho_0 = 0.3 \text{ GeV cm}^{-3}$. We see that under these assumptions, the *Fermi* data probes the thermal relic cross sections of Eq. (3.6) for $m_\chi \lesssim 10 \text{ GeV}$ (thick red contour). The constraints on the annihilation cross section are again translated to limits on the minimum value of the coupling constant λ as shown by the vertical (blue) lines. The shaded (blue) region indicates the perturbative unitarity bound. However, we again emphasize that there are significant uncertainties associated with halo profile, and the limits will become stronger (weaker) by a factor of a few to 10 (depending of course on the detailed shape) if one assumes a contracted (cored) DM distribution [124]. We observe a small feature near $m_W \lesssim m_N \lesssim m_Z$ where the two body decay $N \rightarrow W\ell$ dominates.

Fermi GC 95% C.L. Limit

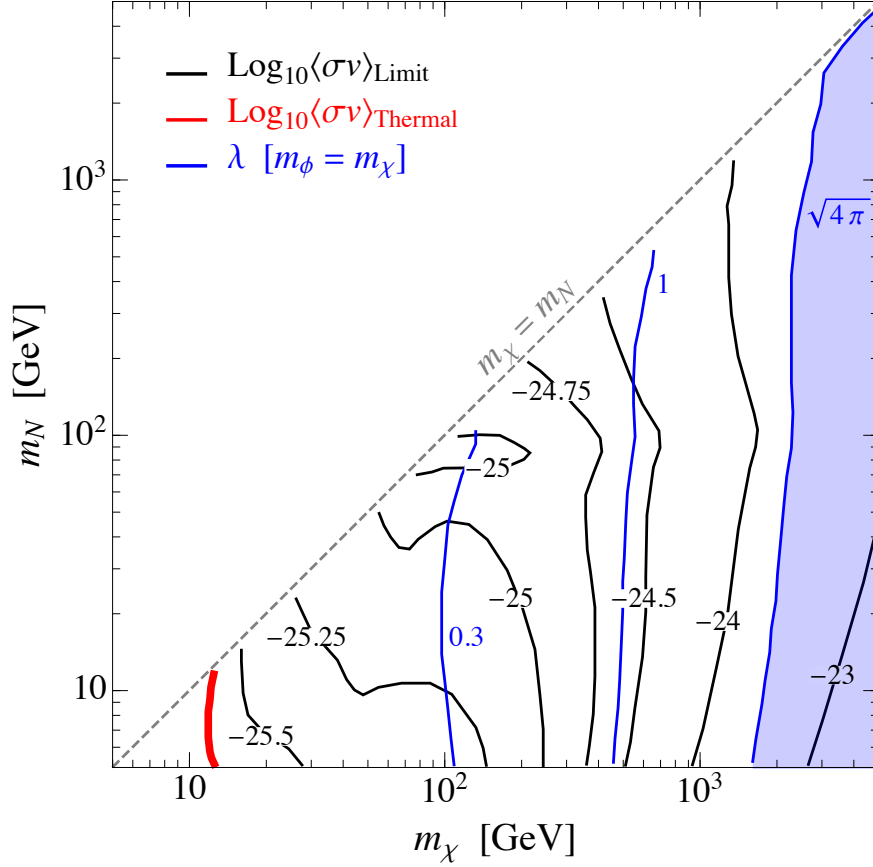


Figure 11: Contours of the 95% C.L. upper limit on $\log_{10} [\langle\sigma v\rangle/(\text{cm}^3 \text{s}^{-1})]$ in the $m_\chi - m_N$ plane (black curves) from *Fermi* observations of gamma-rays from the Galactic Center, using the model independent results of Ref. [124]. The thick (red) line indicates the region where the cross section limit is equal to the thermal relic value of Eq. (3.6). The vertical (blue) lines show the limits on the minimum value of the coupling constant λ . The shaded (blue) region indicates the perturbative unitarity bound.

3.3.3 Gamma rays from dwarf spheroidal galaxies

Gamma ray observations of dwarf spheroidal satellite galaxies (dSphs) of the Milky Way offer a promising and complementary indirect probe of DM annihilation. There are several reasons to consider dSphs. They are DM-dominated, having mass to light ratios in the 10-2000 range. Being satellites of the Milky Way, the dSphs are nearby. There are many of them, $\mathcal{O}(40)$, allowing for a joint analysis to increase statistics. And, crucially, while the Galactic Center provides a significantly brighter source of DM, the dSphs are known to have substantially smaller astrophysical gamma-ray backgrounds in comparison to the Galactic Center, making them very clean sources for indirect searches. The *Fermi*-LAT collaboration has analyzed 6 years of gamma ray data from Milky Way dSphs, finding no significant excess above the astrophysical backgrounds [125]. Here we will discuss the implications of these null results for the neutrino portal DM scenario.

The *Fermi* analysis [125] is based on a joint maximum likelihood analysis of 15 dSphs for gamma ray energies in the 500 MeV - 500 GeV range. The quantity of interest in the likelihood analysis is the energy flux,

$$\varphi_{k,j} = \int_{E_{j,\min}}^{E_{j,\max}} E \Phi_{\gamma,k}(E) dE, \quad (3.15)$$

for k th dwarf and j th energy bin. For each dwarf and energy bin, *Fermi* provides the likelihood, $\mathcal{L}_{k,j}$ as a function of $\varphi_{k,j}$. The likelihood function accounts for instrument performance, the observed counts, exposure, and background fluxes. For a given DM annihilation channel, the energy flux depends on m_χ , $\langle\sigma v\rangle$, and J_k (the J -factor of the dSph – see Eq. (3.14)) according to Eqs. (3.13,3.14,3.15), *i.e.*, $\varphi_{k,j} = \varphi_{k,j}(m_\chi, \langle\sigma v\rangle, J_k)$. The likelihood for a given dwarf, \mathcal{L}_k , is

$$\mathcal{L}_k(m_\chi, \langle\sigma v\rangle, J_k) = \mathcal{LN}(J_k|\bar{J}_k, \sigma_k) \prod_j \mathcal{L}_{k,j}(\varphi_{k,j}(m_\chi, \langle\sigma v\rangle, J_k)), \quad (3.16)$$

where \mathcal{LN} accounts for statistical uncertainty in the J -factor determination (from the stellar kinematics in the dSphs), incorporated as a nuisance parameter in the likelihood. The *Fermi*-LAT collaboration employs a log-normal distribution parameterized by \bar{J}_k, σ_k :

$$\mathcal{LN}(J_k|\bar{J}_k, \sigma_k) = \frac{1}{\ln(10)J_k\sqrt{2\pi}\sigma_k} e^{-(\log_{10}(J_k)-\log_{10}(\bar{J}_k))^2/2\sigma_k^2}, \quad (3.17)$$

where J_k is the true value of the J -factor and \bar{J}_k is the measured J -factor with error σ_k on the quantity $\log_{10} \bar{J}_k$. The combined likelihood for all the dwarfs is then

$$\mathcal{L}(m_\chi, \langle\sigma v\rangle, \{J_i\}) = \prod_k \mathcal{L}_k(m_\chi, \langle\sigma v\rangle, J_k), \quad (3.18)$$

where $\{J_i\}$ is the set of J -factors.

Given that no significant excess is observed, a delta-log-likelihood method is used to set limits on DM model parameters, treating the J -factors as nuisance parameters. The delta-log-likelihood $\Delta \ln \mathcal{L}$ is given by

$$\Delta \ln \mathcal{L}(m_\chi, \langle\sigma v\rangle) = \ln \mathcal{L}(m_\chi, \langle\sigma v\rangle, \{\tilde{J}_i\}) - \ln \mathcal{L}(m_\chi, \widehat{\langle\sigma v\rangle}, \{\hat{J}_i\}) \quad (3.19)$$

where $\widehat{\langle\sigma v\rangle}$ and $\{\hat{J}_i\}$ are the values of $\langle\sigma v\rangle$ and $\{J_i\}$ that jointly maximize the likelihood at the given m_χ , and $\{\tilde{J}_i\} = \{\tilde{J}_i(m_\chi, \langle\sigma v\rangle)\}$ are the values of the J -factors that maximize the likelihood for a given m_χ and $\langle\sigma v\rangle$. A 95% C.L. upper limit is then defined by demanding $-\Delta \ln \mathcal{L}(m_\chi, \langle\sigma v\rangle) \leq 2.71/2$.

We follow a similar approach to the *Fermi* prescription defined above, with one minor modification to speed up the numerical optimization. Rather than optimize over each of the 15 nuisance J -factors for each dSph, we introduce a single parameter, δ , which represents the deviation of the J -factor of the dwarfs from their central values according to $\log_{10}(J_k) = \log_{10}(\bar{J}_k) + \delta \sigma_k$. Since no gamma-ray excess is observed in any individual dSph, it is reasonable to expect that the fit tends to move all J -factors up or down simultaneously depending on the assumed values of m_χ and $\langle\sigma v\rangle$, and this effect that is captured well by our δ prescription. As a validation, we have checked that our prescription reproduces the *Fermi* limits on DM annihilation in the $b\bar{b}$ channel [125] at the 10-20% level throughout the entire mass range.

Using the gamma ray spectra produced with the Monte-Carlo simulation described at the beginning of this section (examples are shown in Figure 9), we derive limits on the neutrino portal DM model for the channel $\chi\chi \rightarrow NN$. In Figure 12 we show contours of the 95% C.L. upper limit on the annihilation cross section in the $m_\chi - m_N$ plane. The *Fermi* data from the Milky Way dSphs are able to probe thermal relic cross sections (3.6) for $m_\chi \sim 40 - 80$ GeV

Fermi dSphs 95% C.L. Limit

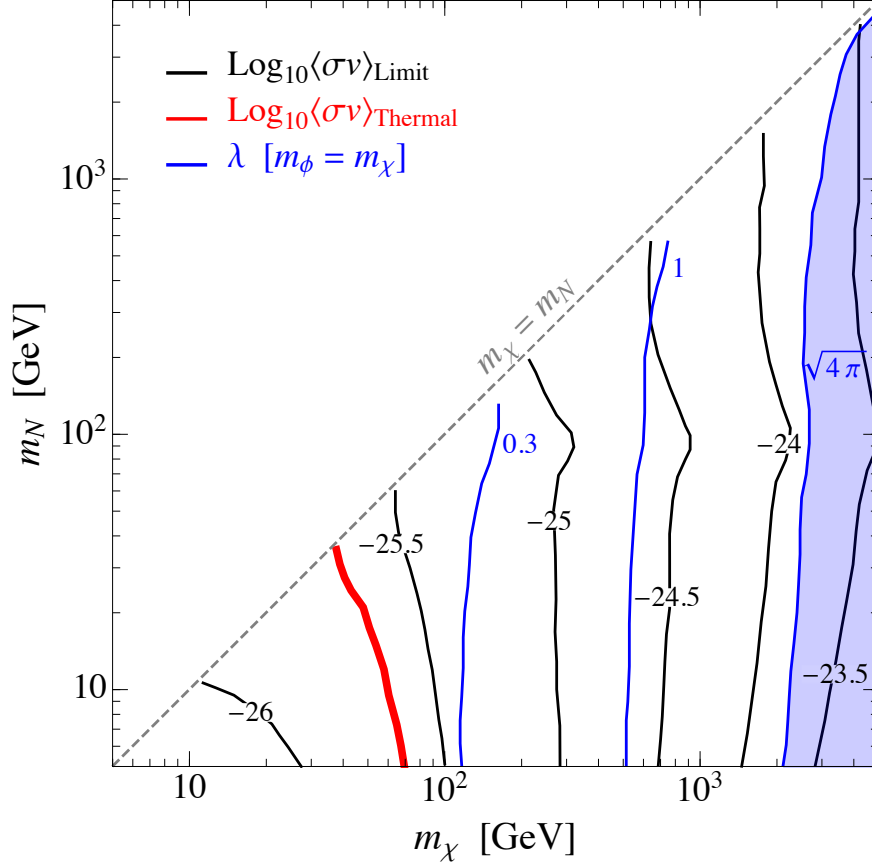


Figure 12: Contours of the 95% C.L. upper limit on $\log_{10} [\langle\sigma v\rangle/(\text{cm}^3 \text{s}^{-1})]$ in the $m_\chi - m_N$ plane (black curves) from *Fermi* observations of gamma-rays from the Milky Way dSphs. The thick (red) line indicates the region where the cross section limit is equal to the thermal relic value of Eq. (3.6). The vertical (blue) lines show the limits on the minimum value of the coupling constant λ . The shaded (blue) region indicates the perturbative unitarity bound.

as shown by the thick (red) line, depending on the mass of the RHN ³. The vertical (blue) lines and the associated numbers show the limits on the minimum value of the coupling constant λ . The shaded (blue) region indicates the perturbative unitarity bound. In the region $m_W \lesssim m_N \lesssim m_Z$ the two body decay $N \rightarrow W\ell$ opens up and saturates the branching ratio, which is clearly seen in Figure 12.

3.3.4 Antiprotons

Antiprotons (\bar{p}) have long been recognized as a promising indirect signature of DM. While DM annihilation typically produces equal numbers of protons and antiprotons, the astrophysical background flux of antiprotons is very small in comparison to that of protons. On the other hand, describing the production and propagation of these charged hadrons is a challenging task, and any statement regarding DM annihilation rests on our ability to understand the associated astrophysical uncertainties. The Alpha Magnetic Spectrometer (AMS-02) experiment has provided the most precise measurements of the cosmic ray proton and antiproton flux to date [126], and here we will explore the implications of this data on our neutrino portal DM scenario. Since DM annihilates to RHNs, which subsequently decay via W , Z , and Higgs bosons, the resulting cascade decay, showering and hadronization produce a variety of hadronic final states including antiprotons. AMS-02 will therefore provide an important probe of the model.

The propagation of antiprotons through the galaxy to earth is described by a diffusion equation for the distribution of antiprotons in energy and space (see, *e.g.*, Ref. [127] and references therein). The transport is modeled in a diffusive region taken to be a cylindrical disk around the galactic plane and is affected by several physical processes. These include diffusion of the antiprotons through the turbulent magnetic fields, convective winds that impel antiprotons outward, energy loss processes, solar modulation, and a source term describing the production and loss of antiprotons. The source term accounts for astrophysical sources such as secondary and tertiary antiprotons, and antiproton annihilation with the interstellar

³Our annihilation cross section limits are weaker than those derived in Ref. [63] by roughly a factor of two. We have not been able to find the source of the discrepancy, although it is perhaps possible to attribute the difference to the uncertainties in the dSph J -factors. We are grateful to Farinaldo Queiroz for correspondence on this issue.

gas, as well as primary antiprotons produced through DM annihilation. The propagation depends on a number of input parameters, and a set of canonical models, called MIN, MED, MAX are often employed [128]. The diffusion equation is solved assuming the steady state condition to find the flux of antiprotons from DM annihilation at earth,

$$\Phi_{\bar{p},\chi}(K) = \frac{v_{\bar{p}}}{4\pi} \left(\frac{\rho_0}{m_\chi} \right)^2 R(K) \frac{1}{2} \langle \sigma v \rangle \frac{dN_{\bar{p}}}{dK}, \quad (3.20)$$

where $dN_{\bar{p}}/dK$ is the kinetic energy (K) spectrum of antiprotons per DM annihilation, $v_{\bar{p}}$ is the antiproton velocity, and ρ_0 is the local DM density. The propagation function $R(K)$ accounts for the astrophysics of production and propagation, and we use the parameterization provided in Ref. [129].

AMS-02 has provided precise measurements of the proton flux, $\Phi_p(K)$ [130], and the antiproton-to-proton flux ratio, $r(K)$ [126], which can be used to place constraints on DM annihilation. To proceed, we require an estimate of the secondary background antiproton flux originating from astrophysical sources. For this purpose we use the best-fit secondary flux, $\Phi_{\bar{p},\text{bkg}}(K)$, from [131], which provides an acceptable fit to the AMS-02 data. With the total antiproton flux, $\Phi_{\bar{p},\text{tot}}(K, m_\chi, \langle \sigma v \rangle) = \Phi_{\bar{p},\text{bkg}}(K) + \Phi_{\bar{p},\chi}(K, m_\chi, \langle \sigma v \rangle)$, and the measured proton flux from AMS-02, $\Phi_p(K)$, in hand, we form the ratio of these two fluxes and fit it to the observed ratio. The test statistic is

$$\chi^2(m_\chi, \langle \sigma v \rangle) = \sum_i \frac{[r(K_i) - (\Phi_{\bar{p},\text{tot}}(K_i, m_\chi, \langle \sigma v \rangle) / \Phi_p(K_i))]^2}{\sigma_i^2}, \quad (3.21)$$

where i runs over energy bins, and σ_i is the reported uncertainty of the flux ratio [126]. Following Ref. [131], we define a limit on $\langle \sigma v \rangle$ as a function of m_χ , m_N according to the condition

$$\chi^2(m_\chi, \langle \sigma v \rangle) - \chi_0^2 \leq 4. \quad (3.22)$$

where χ_0^2 is the best fit chi-squared statistic assuming no primary DM antiproton source from Ref. [131]. The limit is derived under the assumption of a Einasto profile and using the MED propagation scheme. Contours of the limit on the annihilation cross section in the $m_\chi - m_N$ plane are displayed in Figure 13. For DM masses in the range of 20 - 80 GeV, AMS-02 is able to probe the thermal cross section Eq. (3.6), as indicated by the thick (red)

AMS-02 Antiproton 95% C.L. Limit

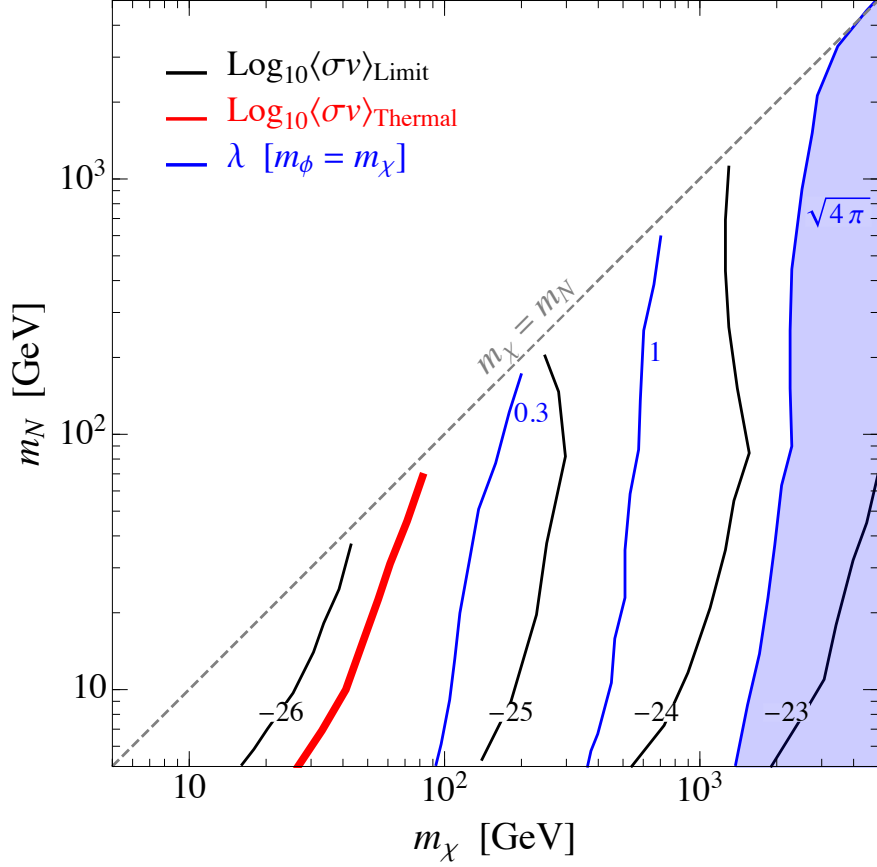


Figure 13: Contours of the upper limit on $\log_{10}[\langle\sigma v\rangle/(\text{cm}^3 \text{s}^{-1})]$ in the $m_\chi - m_N$ plane (black curves) from the AMS-02 measurement of the antiproton-to-proton flux ratio [126]. The thick (red) line indicates the region where the cross section limit is equal to the thermal relic value of Eq. (3.6). The vertical (blue) lines show the limits on the minimum value of the coupling constant λ . The shaded (blue) region indicates the perturbative unitarity bound.

line. The vertical (blue) lines show the limits on the minimum value of the coupling constant λ . The shaded (blue) region indicates the perturbative unitarity bound. It is important to note again that there are significant uncertainties associated with the DM halo profile and the propagation scheme, which can lead to a variation in the cross section limits by one order of magnitude or more [131]. Note that for a fixed m_χ , the limits in Figure 13 become stronger as m_N is increased. This is because for fixed m_χ , heavier RHNs tend to produce more low energy antiprotons (see Figure 9). However, the ratio $r(K)$ shows good agreement with the astrophysical background model at low value of kinetic energy K and a slight excess at larger values of K , explaining the behavior seen in Figure 13.

3.3.5 Summary of limits and future prospects

In Figure 14 we show the combined limits on the neutrino portal DM model for the case in which the annihilation cross section is fixed to the thermal value, $\langle\sigma v\rangle = 2.2 \times 10^{-26} \text{ cm}^3 \text{ s}^{-1}$. Constraints from *Planck* CMB measurements, *Fermi* observations of gamma-rays from the Galactic Center and dSphs, and AMS-02 antiproton measurements are shown. We remind the reader that the *Fermi* Galactic Center limits are derived for the choice of an NFW halo profile, while the AMS-02 antiproton limits are based on an Einasto profile and MED propagation scheme. Under the stated assumptions, we conclude that thermal annihilation is constrained for DM masses up to 50 – 70 GeV depending on RHN mass. AMS-02 provides the best probe in the case $m_N \lesssim m_\chi$, while *Fermi* dSphs provides the superior constraint for $m_N \ll m_\chi$. We have also illustrated the impact of astrophysical uncertainties on the antiproton and dSphs limits in Figure 14. For antiproton constraints, we show Burkert profile and MED propagation (green dotted line) and Einasto profile and MAX propagation (green dashed line). For dSphs, we show $\log_{10}(J_k) = \log_{10}(\bar{J}_k) - 2\sigma_k$ (blue dotted line) and $\log_{10}(J_k) = \log_{10}(\bar{J}_k) + 2\sigma_k$ (blue dashed line).

There are several other notable indirect DM searches that we wish to comment on here. AMS-02 has provided detailed measurements of the cosmic ray positron spectrum [132]. Much attention has been paid to these results (and those of its forerunner PAMELA [133]) due to the observation of a striking rise in the fractional positron flux, which potentially

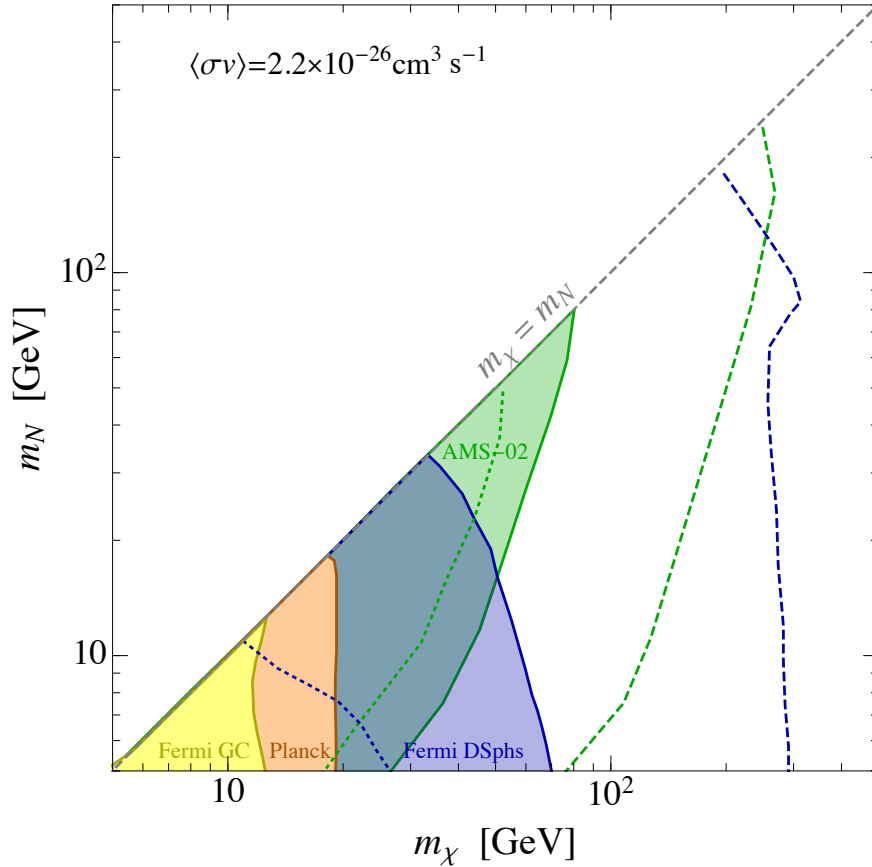


Figure 14: Constraints on the neutrino portal DM model in the $m_\chi - m_N$ plane from the CMB (*Planck*), Galactic Center gamma rays (*Fermi*), dSphs gamma rays (*Fermi*), and antiprotons (AMS-02). A thermal annihilation cross section $\langle\sigma v\rangle = 2.2 \times 10^{-26} \text{ cm}^3 \text{ s}^{-1}$ is assumed throughout. See the text and Figures 10,11,12,13 for further details. Dotted and dashed lines illustrate the impact of DM-related astrophysical uncertainties.

points to a new primary source of positrons. While it is true that DM annihilation in our scenario produces a significant positron flux, the cross section limits from *Fermi* dSphs gamma rays and AMS-02 antiproton observations are expected to be stronger than those from AMS-02 positron measurements by an order of magnitude or more, and thus we have chosen to focus on these stronger tests.

Another well-known indirect DM probe is high energy neutrinos from DM annihilation in the sun, which can be probed with the IceCube experiment [134]. But under the minimal assumption of typical seesaw values for the neutrino Yukawa coupling (see Eq. (3.3)) the DM-nucleon scattering rate will be too small to allow for the efficient capture of DM in the sun, so we do not consider this possibility further.

Along with the continuum gamma-ray signatures studied here, there is also the possibility of a harder gamma-ray spectral feature that arises from the radiative decay $N \rightarrow \gamma\nu$ [74]. This signature will be relevant in the region $m_\chi \sim m_N$, $m_N \lesssim 50$ GeV. For the benchmark thermal relic cross section, there are already relevant limits in this region from AMS-02 (see Figure 14), which however are subject to sizable astrophysical uncertainties. In that regard, the spectral “triangle” feature would provide a complementary probe. On the one hand, the hard spectral feature has the advantage of being more easily discernible over the power law background, while at the same time it is expected that the overall rate will be significantly less than the gamma-ray continuum signal due to its radiative origin. A full quantitative study of this signature goes beyond our scope here and we refer the reader to Ref. [74] for further details.

As we have demonstrated, the data collected so far by *Fermi*-LAT already leads to stringent limits on DM parameter space, and the sensitivity will improve significantly in the coming years. The projected sensitivities for 10 and 15 years of data taking has been studied in detail by the collaboration in Ref. [135]. The fast discovery of new dSphs is the primary upcoming change in dSph targeted DM searches. The identification of new dSph candidates by the Dark Energy Survey (DES) [136] over the past two years, if confirmed, will double the number of known dSphs. Following on important discoveries of the Sloan Digital Sky Survey (SDSS) [137], which covered 1/3 of the sky and discovered 15 ultra-faint dSphs, surveys like DES and especially the Large Synoptic Survey Telescope (LSST) [138] will cover

complementary regions of the sky which are expected to discover potentially $\mathcal{O}(100)$ dSphs. Ref. [135] takes 60 total dSphs as an estimate of the number of dSphs that can be used for LAT searches. They find that the sensitivity of searches targeting dwarf galaxies will improve faster than the square root of observing time. Following Ref. [135] we expect an improvement on the cross section limit from *Fermi*-LAT 15 years dSph observations by a factor of a few, which will probe thermal relic DM with masses $m_\chi \gtrsim 100$ GeV in the neutrino portal DM scenario. Due to their large effective areas, ground-based imaging air Cherenkov telescopes (IACTs), such as H.E.S.S. [139], VERITAS [140], and MAGIC [141], and in the future CTA [142] and HAWC [143], are well suited to search for higher energy gamma rays originating from heavy DM annihilation. In particular, H.E.S.S. has presented a search for DM annihilation towards the Galactic Center using 10 years of data [139]. Assuming a cuspy NFW or Einasto profile the search sets the strongest limits on TeV mass DM that annihilates to WW or quarks, and almost reach thermal annihilation rates. Taken at face value, the H.E.S.S. limits are indeed stronger than the *Fermi* dSphs limits for DM masses above a few hundred GeV, but are however less robust due to the inherent astrophysical uncertainties associated with the central region of the Milky way, both in terms of conventional gamma-ray sources and the DM distribution. The H.E.S.S data is not publicly available, so unfortunately we are not able to properly recast their limit. However, for a fixed DM mass, the continuum photon spectrum produced in our model from $\chi\chi \rightarrow NN$ is qualitatively similar to the spectrum produced by $\chi\chi \rightarrow WW$. We can therefore obtain a rough estimate of the H.E.S.S. sensitivity by translating their limits in the WW channel to our parameter space. The H.E.S.S. limits are approaching the canonical thermal relic annihilation rate for DM masses around 1 TeV.

In the future, the Cherenkov Telescope Array (CTA) will be able to further probe heavy TeV-scale DM annihilation, with the potential to improve by roughly an order of magnitude in cross section sensitivity over current instruments depending on the annihilation mode and DM mass. Here we estimate the sensitivity of future CTA gamma-ray observations of the Galactic Center using a “Ring” method technique [144]. Our projections are based on a simplified version of the analysis carried out in Ref. [145] that we now briefly describe. The analysis begins with the definition of signal (referred to as “ON”) and background (“OFF”)

regions. A binned Poisson likelihood function is constructed in order to compare the DM model $\boldsymbol{\mu}$ to a (mock) data set \boldsymbol{n} :

$$\mathcal{L}(\boldsymbol{\mu}|\boldsymbol{n}) = \prod_{i,j} \frac{\mu_{ij}^{n_{ij}}}{n_{ij}!} e^{-\mu_{ij}}. \quad (3.23)$$

where μ_{ij} is the predicted number of events for a given model $\boldsymbol{\mu}$ in the i th energy bin and the j th region of interest, corresponding to ON ($j = 1$) and OFF ($j = 2$) regions. These model predictions are compared to the corresponding observed counts n_{ij} . We use 15 logarithmically-spaced energy bins, extending from 25 GeV to 10 TeV. The number of gamma-ray events predicted by each model consists of three components: a DM annihilation signal, an isotropic cosmic-ray (CR) background, and the Galactic diffuse emission (GDE) background:

$$\mu_{ij} = \mu_{ij}^{\text{DM}} + \mu_{ij}^{\text{CR}} + \mu_{ij}^{\text{GDE}}. \quad (3.24)$$

The details for the regions of interest that have been used in our analysis, including the corresponding solid angles and J -factors, can be found in Ref. [142]. Furthermore, we have used the effective area produced by MPIK group [146] and fixed the time of observation to be 100 hours.

We account for differential acceptance uncertainties (i.e. acceptance variations across different energy bins and regions-of-interest) by rescaling the predicted signals μ_{ij} by parameters α_{ij} and profiling the likelihood over their values. Following Ref. [145] we assume Gaussian nuisance likelihoods for all α with respective variance σ_α^2 independent of i and j . Our limits correspond to differential acceptance uncertainties of 1%. The mock data \boldsymbol{n} we employ includes a fixed isotropic cosmic-ray background component in all bins, and no signal from DM annihilation. We derive 95% CL upper limits (sensitivity) on the annihilation cross-section $\langle\sigma v\rangle$ in the usual way by requiring $-\Delta \ln \mathcal{L} \leq 2.71/2$. Our projections are shown in Figure 15. We have not included systematic uncertainties for the background components, which can be as large as order one and thus significantly degrade the CTA sensitivity. However, this can be partially overcome through a more sophisticated morphological analysis, which leverages the shape differences between the galactic diffuse emission and DM signal [145]. In the end, we expect that Figure 15 provides a reasonable ballpark

estimate of the CTA sensitivity, which can improve over H.E.S.S. by a factor of a few to ten in the 100 GeV - TeV DM mass range. We expect *Fermi* dSphs observations to provide superior limits for lower mass DM, $m_\chi \lesssim 100$ GeV.

3.4 GALACTIC CENTER GAMMA RAY EXCESS INTERPRETATION

As mentioned in Section 3.3.2, various analyses of *Fermi*-LAT data show a spherically symmetric excess of gamma rays coming from the central region of the Milky Way peaking in the 1-3 GeV energy range [59, 60, 61, 62, 58]. Since DM annihilation to RHNs abundantly produces gamma rays, it is interesting to explore a possible interpretation of this excess in the context of the neutrino portal DM model. In fact, this possibility was previously investigated in Ref. [57], which found that DM annihilation to RHNs could indeed provide a good fit to the Galactic Center excess. Here we will additionally confront this interpretation with existing constraints from other indirect probes, and notably *Fermi* gamma-ray observations from dSphs and AMS-02 antiproton observations.

We fit the neutrino portal DM model parameters to the Galactic Center excess spectrum given in Ref. [62]. We adopt Navarro-Frenk-White (NFW) profile with $\gamma = 1.2$. Following [62] we define the χ^2 as

$$\chi^2(\boldsymbol{\theta}) = \sum_{ij} [\Phi_i(\boldsymbol{\theta}) - (\Phi_i)_{\text{obs}}] \cdot \Sigma_{ij}^{-1} \cdot [\Phi_j(\boldsymbol{\theta}) - (\Phi_j)_{\text{obs}}], \quad (3.25)$$

where $\boldsymbol{\theta} = \{\langle\sigma v\rangle, m_\chi, m_N\}$, Φ_i ($(\Phi_i)_{\text{obs}}$) is the predicted (observed) γ -ray flux (see Eq. (3.13)) in the i^{th} energy bin, and Σ is the covariance matrix. We find that the best-fit point is $\{\langle\sigma v\rangle = 3.08 \times 10^{-26} \text{ cm}^3 \text{ s}^{-1}, m_\chi = 41.3 \text{ GeV}, m_N = 22.6 \text{ GeV}\}$ with $\chi^2 = 14.12$ for 23 degrees-of-freedom. Figure 16 depicts the best-fitted spectrum induced from the right-handed neutrinos. Figure 17 displays $1\sigma, 2\sigma$, and 3σ CL regions in the $m_N - m_\chi$ parameter space. We see that neutrino portal DM can provide an acceptable fit over a significant range of mass parameters.

Next, we would like to confront this interpretation with the other constraints derived in Section 3.3. To this end, we perform the Galactic Center excess while fit fixing the

Projected sensitivity of CTA at 95% C.L.

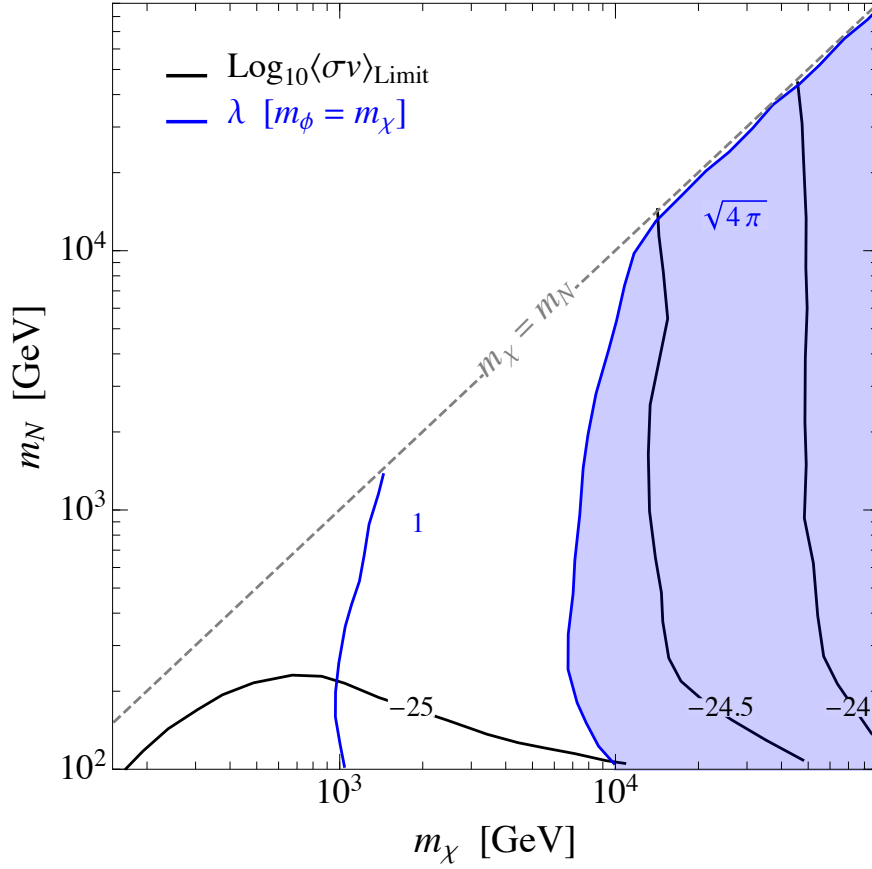


Figure 15: Contours of the 95% C.L. projected sensitivity on $\log_{10} [\langle\sigma v\rangle/(\text{cm}^3 \text{s}^{-1})]$ in the $m_\chi - m_N$ plane (black curves) from CTA γ -ray observations of the Galactic Center using Ring method, assuming 100hr of observation [145].

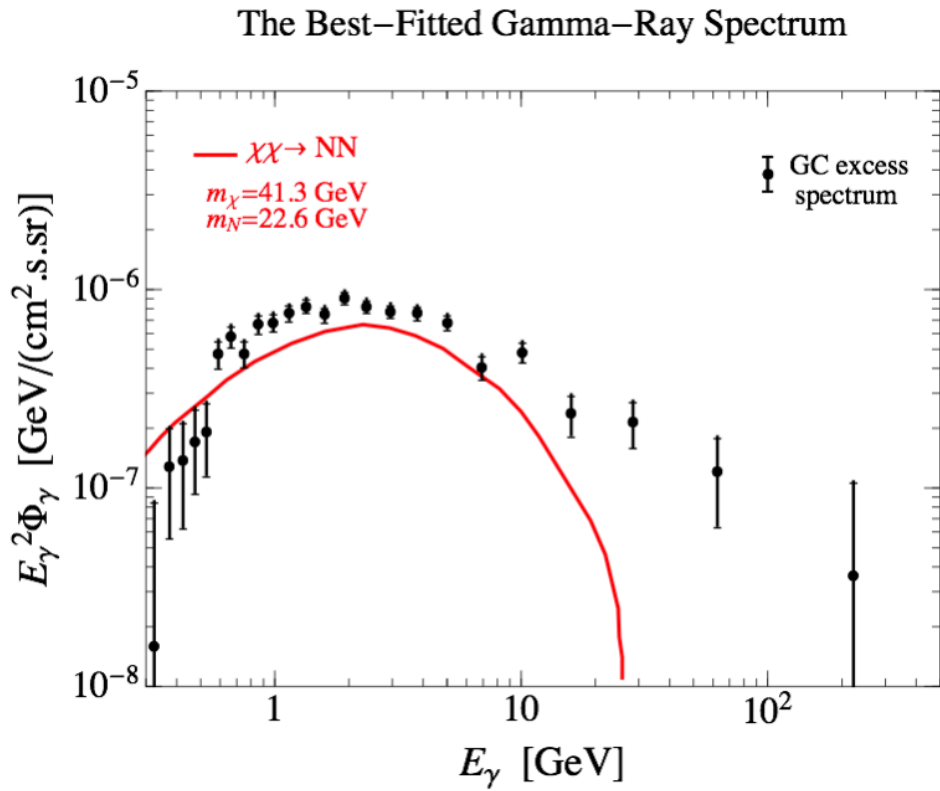


Figure 16: The best-fitted gamma-ray spectrum together with the observed central values and the error bars. The data and error bars are from Ref. [62].

annihilation cross section to its thermal value, and overlay the limits derived from *Planck* CMB, *Fermi* dSphs, and AMS-02 antiproton observations. The result is displayed in the right panel of Figure 17. We see that this interpretation faces some tension with limits from dSphs and antiprotons. However, it is too early to conclude from this analysis that the DM interpretation of the excess is not viable given the significant astrophysical uncertainties in the local DM density, dSphs DM densities, and the modeling of the antiproton propagation.

3.5 BEYOND THE MINIMAL SCENARIO

We have explored what is perhaps the simplest scenario of neutrino portal DM. The primary probe of this model comes from indirect detection, and we have presented a comprehensive picture of the current constraints. However, it is possible that the neutrino mass model is more complex than the simplest Type-I seesaw, or that there are additional interactions of the scalar mediator with the Higgs, in which case a much richer phenomenology is possible. In this section we will highlight some of these possibilities.

3.5.1 Large neutrino Yukawa coupling

Taking the naive seesaw relation in Eq. (3.2) as a guide, one generally expects very small active-sterile mixing angles, $\theta \sim \sqrt{m_\nu/m_N} \simeq 10^{-6} \times (m_N/100 \text{ GeV})^{-1/2}$, suggesting poor prospects for direct detection and accelerator experiments. However, the neutrino Yukawa coupling and active sterile-mixing angle can be much larger if one goes beyond the simplest Type-I seesaw. For example, in the inverse seesaw model [147], the RHNs are pseudo-Dirac fermions, with splitting governed given by a small Majorana mass. The SM neutrino masses are light due to the same small Majorana mass, while the Yukawa coupling can in principle be as large as $y \sim 0.1$, while being compatible with experimental constraints.

Such large Yukawa couplings not only offer increased chances to probe the RHNs directly (see, *e.g.*, Ref. [148, 149] for a review), but will also enhance the detection prospects of the DM sector. For instance, one can induce sizable DM couplings to the Z and Higgs boson at one

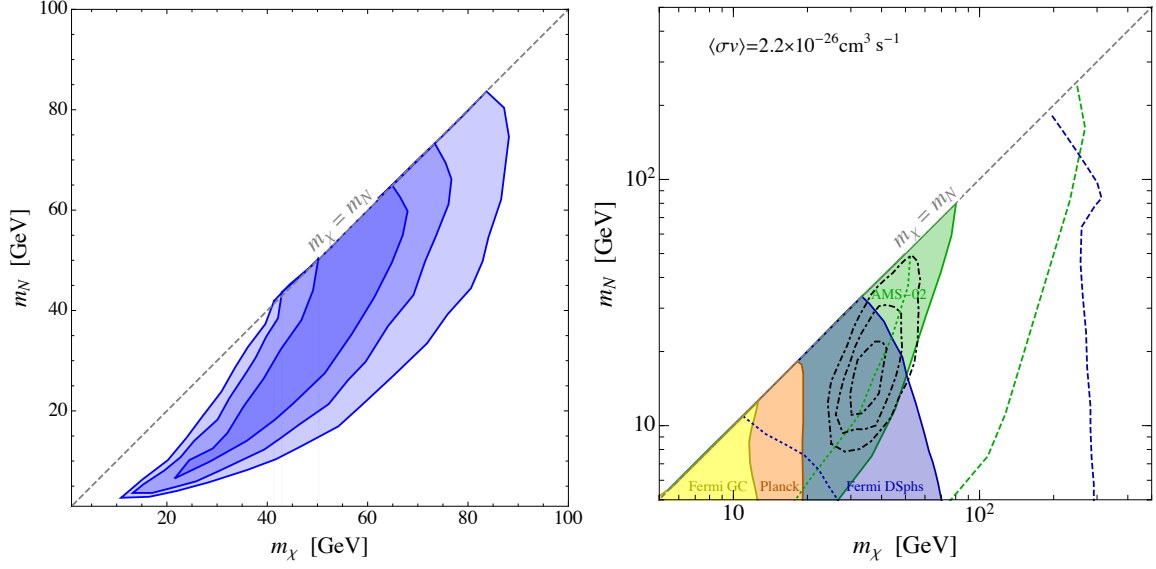


Figure 17: Interpretation of the Galactic Center gamma ray excess. The left panel displays the 1σ , 2σ , and 3σ preferred regions in the $m_\chi - m_N$ plane, with the best-fit point of $\{\langle\sigma v\rangle = 3.08 \times 10^{-26} \text{ cm}^3 \text{ s}^{-1}, m_\chi = 41.3 \text{ GeV}, m_N = 22.6 \text{ GeV}\}$ with $\chi^2 = 14.12$ for 23 degrees of freedom. The right panel shows the best-fit region for the case of a fixed thermal annihilation cross section, $\langle\sigma v\rangle = 2.2 \times 10^{-26} \text{ cm}^3 \text{ s}^{-1}$, as well as the existing limits from *Planck* CMB, *Fermi* dSphs, and AMS-02 antiproton observations.

loop that mediate large scattering rates with nuclei, which is relevant for direct detection experiments and capture of DM in the sun. One can also potentially produce the RHNs directly in accelerator experiments.

This also opens up the possibility for the RHN to be heavier than the dark sector particles, while still having a thermal cosmology. Due to the large mixing angle, it is possible for DM to annihilate efficiently into light active neutrinos, and furthermore the DM may annihilate to other SM particles through the loop-induced Z and h couplings. We refer the reader to Refs. [73, 68, 69] for recent investigations of these issues.

3.5.2 Higgs portal coupling

The scalar particle ϕ can couple to the Higgs portal at the renormalizable level

$$\mathcal{L} \supset \frac{\lambda_{\phi H}}{2} \phi^2 |H|^2. \quad (3.26)$$

We have so far assumed that this coupling is small. The reason we have made this assumption is primarily for simplicity, as then the phenomenology and cosmology is solely dictated by the neutrino portal link to the SM. However, this assumption can certainly be questioned.

Restricting to the fields and interactions of our scenario in Eq. (3.1), we observe that the Higgs portal coupling (3.26) will be induced at one loop with strength of order $\lambda_{\phi H} \sim \lambda^2 y^2 / 16\pi^2$, which is very small due to the small neutrino Yukawa coupling. Still, one may expect unknown UV physics to generically induce a larger coupling. This is because there is no enhanced symmetry in the limit $\lambda_{\phi H} \rightarrow 0$, and so even though the operator (3.26) is marginal, we cannot rely on technical naturalness ensure a small value without further information about the UV physics. That being said, one can certainly imagine completions in which the Higgs portal coupling is suppressed. For example if ϕ is a composite scalar state of some new strong dynamics, then the Higgs portal operator would fundamentally be a higher dimension operator and could be therefore be naturally suppressed.

Another good reason to consider the Higgs portal operator is that it provides additional opportunities to probe the dark sector in experiment. A one loop coupling of the DM to the Higgs will be induced and this can mediate scattering of DM with nuclei, or invisible decays of the Higgs to DM [68, 69, 70, 71].

An even more distinctive signature at colliders can arise if the Higgs could decay into a pair of light scalars, $h \rightarrow \phi\phi$. These scalars, once produced would then cascade decay via $\phi \rightarrow N\chi$. The resulting RHN N , being lighter than the W boson, will have a macroscopic decay length and could leave a striking displaced vertex signal (see, *e.g.*, [150]). The signature would thus be an exotic Higgs decay with two displaced vertices.

3.6 SUMMARY AND OUTLOOK

In this chapter we have investigated a simple model of neutrino portal DM, in which the RHNs simultaneously generate light neutrino masses via the Type-I seesaw mechanism and mediate interactions of DM with the SM. The model, presented in Section 4.2.1, is quite minimal and contains a dark sector composed of a fermion χ (the DM candidate) and scalar ϕ , along with the RHN N . Given the generic expectation of tiny neutrino Yukawa couplings, testing this model with direct detection or accelerator experiments is likely to be challenging. However, it is possible in this model that DM efficiently annihilates to RHNs, which allows for a number of indirect probes of this scenario.

We have carried out an extensive characterization of the indirect detection phenomenology of the neutrino portal DM scenario in Section 3.3. Restricting to an experimentally and theoretically viable mass range, $1 \text{ GeV} \lesssim m_N < m_\chi \lesssim 10 \text{ TeV}$, we have derived the constraints on the $\chi\chi \rightarrow NN$ annihilation cross section from *Planck* CMB measurements, *Fermi* gamma-ray observations from the Galactic Center and from dSphs, and AMS-02 antiproton observations. Currently, the dSphs and antiproton measurements constrain DM masses below 50 GeV for thermal annihilation rates. In the future, *Fermi* dSphs observations will be able to probe DM masses above the 100 GeV range for thermal cross sections, while CTA will be able to approach thermal cross section values for DM masses in the 100 GeV - 1TeV range.

This model can also provide a DM interpretation of the *Fermi* Galactic Center gamma ray excess as discussed in Section 3.4. We have verified that the predicted spectrum of gamma rays is compatible with the observed excess for RHN and DM masses in the 20–60 GeV range

and annihilation rates close to the thermal value. However, we have also shown that this interpretation faces some tension with the existing constraints from *Fermi* dSphs and AMS-02 antiprotons (subject of course to various astrophysical uncertainties). It will be interesting to see how this situation develops as *Fermi* and AMS-02 collect more data. However, at least in the simplest model explored here, it will be challenging to find complementary probes outside of indirect detection.

It is possible that the neutrino mass generation mechanism is more intricate than the simplest Type-I seesaw, as discussed in Section 3.5. If so, the implications for neutrino portal DM could be dramatic, particularly if the neutrino Yukawa coupling is large, as this could lead to direct detection prospects, accelerator probes, and new annihilation channels. Additionally, it is possible in this scenario for additional Higgs portal couplings to be active, which could yield further phenomenological handles.

Portals provide a simple and predictive theoretical framework to characterize the allowed renormalizable interactions between the SM and DM. Furthermore, the existence of neutrino masses already provides a strong hint that the neutrino portal itself operates in nature. These two observations provide a solid motivation for testing the neutrino portal DM scenario, both through the generic indirect detection signals investigated in this chapter, and also the additional signals present in more general models. It is worthwhile to broadly explore these scenarios and their associated phenomenology in detail, and we look forward to further progress in this direction in the future.

4.0 THERMAL DARK MATTER THROUGH THE DIRAC NEUTRINO PORTAL

This chapter is devoted to the study of a simple model of thermal dark matter annihilating to standard model neutrinos via the neutrino portal. A (pseudo-) Dirac sterile neutrino serves as a mediator between the visible and the dark sectors, while an approximate lepton number symmetry allows for a large neutrino Yukawa coupling and, in turn, efficient dark matter annihilation. The dark sector consists of two particles, a Dirac fermion and complex scalar, charged under a symmetry that ensures the stability of the dark matter. A generic prediction of the model is a sterile neutrino with a large active-sterile mixing angle that decays primarily invisibly. The existing constraints and future projections from direct detection experiments, colliders, rare meson and tau decays, electroweak precision tests, and small scale structure observations are derived. It is based on our work in Ref. [151].

4.1 INTRODUCTION

The search for non-gravitational dark matter (DM) interactions is one of the chief enterprises in modern experimental particle physics and observational astrophysics [42, 43, 44, 45]. While not required on general grounds, such interactions find strong motivation in the context of a cosmological origin of the dark matter abundance. Indeed, a compelling hypothesis is that DM is a thermal relic from the hot Big Bang, which requires non-gravitational couplings between DM and the Standard Model (SM) to ensure thermal contact and deplete the DM abundance. These couplings in turn predict a variety of novel phenomena associated with DM that can be sought through experiment and observation, offering the prospect of

testing the thermal relic hypothesis. The most popular possibility for the non-gravitational couplings is the ordinary electroweak gauge interactions. This scenario is theoretically attractive due to the coincidence of the predicted and observed DM abundance for a TeV-mass relic with electroweak interactions and its potential connection to the Higgs naturalness problem, and has inspired an expansive and diverse experimental search program that has probed a significant portion of the parameter space.

Nevertheless, thermal relic DM need not have SM gauge interactions. It is quite plausible that DM is instead a new electroweak gauge singlet particle, in which case an additional mediator particle is generally required to couple the dark and visible sectors [152, 153]. While there are in principle many ways that this mediation can occur, three renormalizable *portal* couplings stand out on account of their economy and uniqueness. These are the well-known vector portal [154, 48, 49], Higgs portal [46, 47], and neutrino portal [8]:

$$B_{\mu\nu} V^{\mu\nu}, \quad H^\dagger H S, \quad \bar{L} H N + \text{h.c.}, \quad (4.1)$$

where V_μ , S , and N are new vector, scalar, and fermionic mediators, respectively, which can be straightforwardly coupled to the singlet DM particle. It is possible to distinguish two cases according to the dominant DM annihilation channel [53]. The first case is *secluded annihilation*, in which dark matter annihilates directly to mediator particles. This occurs when DM is heavier than the mediator. The second, more predictive case, is *direct annihilation*, in which the dark matter annihilates through the mediator to SM particles. This occurs when DM is lighter than the mediator. In the secluded regime, the annihilation rate is set entirely by dark sector couplings. The mediator need only have a minuscule coupling to the SM to ensure kinetic equilibrium between the sectors, making it challenging to robustly test the scenario.¹ In contrast, efficient direct annihilation necessitates a substantial mediator-SM coupling to avoid DM overproduction, leading to a predictive and experimentally testable scenario. For the predictive case of thermal DM directly annihilating to SM particles, a broad experimental effort is developing that will decisively test vector portal mediation [55], while the case of Higgs portal mediation is already strongly constrained [156].

¹Departing from kinetic equilibrium can have change the standard relationship between DM annihilation and its relic abundance. For a detailed study of this, see Ref. [155].

Neutrino portal DM has been studied only a handful of times, despite sterile neutrinos N being arguably the best motivated mediator candidate due to their role in neutrino mass generation. One likely reason for this is a theoretical prejudice for tiny neutrino Yukawa couplings, which in the simplest Type I seesaw with Majorana sterile neutrinos are generally far too small to allow efficient direct DM annihilation to SM neutrinos. Most studies have therefore focused on the secluded regime, in which DM annihilates directly to the sterile neutrino mediators [53, 57, 56, 70, 71, 72, 63, 41]. In this case the most robust signatures are indirect, and include cosmic gamma-rays antiprotons, and imprints of DM annihilation on the cosmic microwave background (see e.g., the recent study of Ref. [41]).

However, the case of direct annihilation to SM neutrinos can also be viable if the Yukawa couplings are large. Small neutrino masses are easily compatible with large neutrino Yukawa couplings provided sterile neutrinos are pseudo-Dirac states and an approximate $U(1)_L$ global lepton number symmetry is present. A model incorporating these basic ingredients was first studied in Ref. [73], where the implications of a large neutrino-DM interaction for small scale structure were investigated. A similar model was analyzed in Ref. [68, 69], where the focus was on heavy DM phenomenology. It is also worth mentioning that direct annihilation to light neutrinos allows for thermal relic DM lighter than ~ 10 GeV that does not disturb cosmic microwave background (CMB) observations without resorting to velocity suppression, as opposed to annihilation into electromagnetically interacting final states [106]. For other dark matter studies utilizing the neutrino portal, see Ref. [64, 66, 67].

Our aim in this work is to provide a systematic analysis of thermal neutrino portal DM in the direct annihilation regime, over the entire cosmologically viable DM mass range from 1 MeV–1 TeV. The basic model consists of a dark sector containing a Dirac fermion DM χ and a complex scalar ϕ , along with a Dirac sterile neutrino mediator N , and is essentially the one constructed in Ref. [73]. Beyond the particular motivation of Ref. [73], this model is of interest more generally as a scenario in which dark sector interactions with light neutrinos lead to thermalization and annihilation. We derive the existing constraints and future sensitivity projections from direct detection experiments, colliders, rare meson and tau decays, electroweak precision tests, cosmology. We also indicate the parameter regions that are favored by perturbativity and technical naturalness. In analogy with predictive vector and

Higgs portal models, we also present a transparent strategy to compare these constraints and projections with the thermal relic target, under minimal and conservative assumptions on model parameters. We identify new probes of this model that can be undertaken with existing or near future experiments, including 3-body decays of stopped kaons and transverse momentum distributions of charged leptons in W boson production at colliders. Furthermore, we emphasize the impact that a high statistics $\tau^+\tau^-$ sample at a future B -factory could have on testing this scenario.

The rest of this chapter is organized as follows. In Sec. 4.2, we outline the basic ingredients of the model, discuss its simple cosmology, and the decay modes of the new states. Section 4.3 describes constraints and probes of the heavy, mostly sterile neutrino in this scenario. The phenomenology of the DM in this model and ways to test it are in Sec. 4.4. In Sec. 4.5 we conclude and discuss future prospects.

4.2 FRAMEWORK

In this section we begin by defining a simple model in which DM couples to SM neutrinos through mixing generated with a neutrino portal coupling. We then discuss the cosmology and define the thermal relic target. We also discuss some basic features of the model that will be needed to understand the phenomenology, including the decays of the new heavy states, and the radiative couplings. We conclude this section with a brief discussion of technical naturalness in this scenario.

4.2.1 Model

As discussed in the introduction, the basic scenario we have in mind is thermal DM annihilating directly to SM neutrinos through the neutrino portal.² To allow for a large neutrino Yukawa coupling, and in turn an efficient annihilation rate, we take our mediator N to be a Dirac particle. The dark sector is very minimal, and consists of a Dirac fermion

²More precisely, the dark matter annihilates into very light, mostly SM flavor neutrinos which we refer to here as “SM neutrinos” for simplicity.

DM candidate χ and a complex scalar ϕ . Along with the kinetic terms, the Lagrangian is given by [73]

$$\begin{aligned}
-\mathcal{L} \supset & m_\phi^2 |\phi|^2 + m_\chi \bar{\chi}\chi + m_N \bar{N}N \\
& + \left[\lambda_\ell \bar{L}_\ell \hat{H} N_R + \phi \bar{\chi} (y_L N_L + y_R N_R) + \text{h.c.} \right],
\end{aligned} \tag{4.2}$$

where H ($\hat{H} = i\tau_2 H^*$) is the Higgs doublet, $L_\ell = (\nu_{\ell L}, \ell_L)^T$ are SM lepton doublets with $\ell = e, \mu, \tau$ labeling the charged lepton mass eigenstates, λ_ℓ are the neutrino Yukawa couplings, and $y_{L,R}$ are couplings of the sterile neutrino mediator to the dark sector fields. The Lagrangian of Eq. (4.2) respects a global $U(1)_L$ lepton number symmetry, under which L_ℓ , N and ϕ^* have equal charges, as well as a \mathbb{Z}_2^D dark matter parity under which χ and ϕ are odd while all other fields are even. This \mathbb{Z}_2^D could be the remnant of a gauge symmetry broken at a high scale [157]. At the level of Eq. (4.2), the lepton number symmetry forbids light SM neutrino masses, allowing us to take λ_ℓ as free parameters and in particular much larger than the usual naive Type I seesaw expectation.

We will assume $m_\chi < m_\phi$, such that the \mathbb{Z}_2^D symmetry ensures the stability of χ . If, instead, $m_\chi > m_\phi$ then the \mathbb{Z}_2^D symmetry would render ϕ stable and it would be a good DM candidate. The phenomenology in this case would be essentially the same. The main difference is that the DM annihilation cross section is velocity-suppressed (in the limit that either y_L or y_R dominates), requiring larger couplings to provide efficient annihilation. Since the fermionic DM scenario can tolerate smaller couplings, it is more conservative. For this reason, we specify that $m_\chi < m_\phi$ and the fermion is the DM for definiteness in our detailed study.

In the electroweak vacuum, $\langle H \rangle = v = 174$ GeV, the SM neutrinos ν_i mix with N . Diagonalizing the Lagrangian, we find a heavy sterile Dirac neutrino state, which we label ν_4 . The physical mass of this state is $m_4 = \sqrt{m_N^2 + \sum_\ell \lambda_\ell^2 v^2}$, and its left chiral component is a combination of sterile and active flavors,

$$\nu_4 = \begin{pmatrix} U_{N4}^* N_L + \sum_\ell U_{\ell 4}^* \nu_{\ell L} \\ N_R \end{pmatrix}, \tag{4.3}$$

where the mixing angles are given by

$$U_{\ell 4} = \frac{\lambda_\ell v}{m_4}, \quad |U_{N4}| = \frac{m_N}{m_4} = \sqrt{1 - \sum_\ell |U_{\ell 4}|^2}. \quad (4.4)$$

This is the crucial feature of the model: the mixing angles are not proportional to the light neutrino masses (in this limit, zero) and can be viewed as more or less free parameters.

The linear combinations of N_L and $\nu_{\ell L}$ that are orthogonal to ν_{4L} are the light neutrinos, ν_{iL} with $i = 1, 2, 3$, which remain massless at this level. N_L contains an admixture of light neutrinos, and so the light neutrinos interact with the DM via Eq. (4.2):

$$\begin{aligned} & y_L \phi \bar{\chi}_R N_L + \text{h.c.} \\ & \rightarrow y_L |U_{N4}| \phi \bar{\chi}_R \nu_{4L} - y_L \sqrt{1 - |U_{N4}|^2} \phi \bar{\chi}_R \nu_{iL} + \text{h.c.} \end{aligned} \quad (4.5)$$

where ν_i is an admixture of light neutrinos $\nu_{1,2,3}$ with unit norm. The active neutrinos get an orthogonal admixture of heavy and light neutrinos,

$$\nu_{\ell L} = \sum_{i=1,2,3} U_{\ell i} \nu_{iL} + U_{\ell 4} \nu_{4L} \quad (4.6)$$

for $\ell = e, \mu, \tau$.

The 4×4 matrix U describes the relationship between gauge and mass eigenstates. Since the light neutrinos are all degenerate (i.e. massless) at the level we are dealing with them now, we can ignore mixing amongst the active neutrinos. Thus, the upper-left 3×3 block of this matrix, corresponding to the usual Pontecorvo-Maki-Nakagawa-Sakata matrix [158] and which governs ordinary neutrino oscillations, is unimportant for our purposes and the phenomenology is determined by the active-sterile mixing angles $U_{\ell 4}$.³

There are a few simple ways to extend the model to incorporate light neutrino masses. The most interesting possibility is to endow N with couplings that violate lepton number. For example, one can add the Majorana mass term, $\mu \bar{N}_R^c N_L + \text{h.c.}$ as in the ‘‘inverse seesaw’’ scenario [147, 159], or the Yukawa couplings, $\lambda'_\ell \bar{L}_\ell \hat{H} N_R^c + \text{h.c.}$ as done in [160]. This will lead to small neutrino masses, of order $\lambda'_\ell v^2 \mu / m_N^2$ or $\lambda'_\ell \lambda_\ell v^2 / m_N$ respectively, governed by $U(1)_L$ breaking interactions, while the $\Delta L = 0$ neutrino Yukawa coupling, λ_ℓ , in Eq. (4.2)

³See Sec. 4.3.4, however, for a discussion of atmospheric neutrino oscillations in the context of a large τ -sterile mixing.

may still be large. These possibilities give N the dual responsibility of generating neutrino masses and mediating DM interactions. In fact, only one Dirac sterile neutrino (made up of two Weyl fermions) is required to produce phenomenologically viable neutrino masses and mixings. Another possibility is that there are additional states N' that participate in the mass generation, in either lepton-number-preserving or -violating ways with some other UV dynamics. In any event, generating realistic neutrino masses while keeping the Yukawa couplings λ_ℓ large requires that N is a Dirac or pseudo-Dirac state; in the latter case, the small mass splitting between the mass eigenstates will, however, have no significant phenomenological consequences for the parameter choices of interest to us.

Note that we have not written the renormalizable operator $\lambda_{\phi H}|\phi|^2|H|^2$ which is allowed by the symmetries in Eq. (4.2) and is generated radiatively. After electroweak symmetry breaking, this operator contributes to the ϕ mass and to decays of the Higgs boson to $\phi\phi^*$ (which as we show in Sec. 4.2.3 are invisible at colliders). In a natural theory, we would expect the coefficient of this operator to be at least as large as the radiative contributions $\lambda_{\phi H} \gtrsim \delta\lambda_{\phi H} \sim (y_L^2 \lambda_\ell^2 / 16\pi^2) \log(\Lambda_{\text{UV}}^2 / m_4^2)$ where Λ_{UV} is a cutoff of the theory. The current limit on the invisible Higgs width translates to the upper bound $\lambda_{\phi H} \lesssim 0.01$. We describe the implications from potential fine-tuning of m_ϕ and the limit on the invisible Higgs width further in Secs. 4.2.2 and 4.3.5, respectively. We find that the effects of a value of $\lambda_{\phi H}$ near the radiative estimate (in fact, up to factor $\sim 1/|U_{\ell 4}|^2$ larger) are always subdominant to other contributions.

4.2.2 Cosmology

As is well-known, the relic density obtained through thermal freezeout is determined by the thermally averaged DM annihilation cross section $\langle\sigma v\rangle$. The relevant process in this case is annihilation into light neutrinos, $\chi\bar{\chi} \rightarrow \nu\bar{\nu}$, and the cross section can be computed from

the interaction Lagrangian, Eq. (4.5):

$$\begin{aligned} \langle\sigma v\rangle &= \frac{y_L^4}{32\pi} \left(\sum_{\ell} |U_{\ell 4}|^2 \right)^2 \frac{m_{\chi}^2}{m_{\phi}^4} \left(1 + \frac{m_{\chi}^2}{m_{\phi}^2} \right)^{-2} \\ &\simeq 1 \text{ pb} \left(\frac{y_L \sqrt{\sum_{\ell} |U_{\ell 4}|^2}}{0.2} \right)^4 \left(\frac{10 \text{ GeV}}{m_{\chi}} \right)^2 \left(\frac{3}{m_{\phi}/m_{\chi}} \right)^4, \end{aligned} \quad (4.7)$$

where in the second step we have normalized the cross section to the canonical value $\langle\sigma v\rangle = 3 \times 10^{-26} \text{ cm}^3/\text{s} \simeq 1 \text{ pb}$, which yields a DM abundance that is in close agreement with the measured value.

In analogy with simple vector portal DM scenarios [55, 161], it is useful to define a dimensionless parameter Y that governs the annihilation rate,

$$Y \equiv y_L^4 \left(\sum_i |U_{i4}|^2 \right)^2 \frac{m_{\chi}^4}{m_{\phi}^4}. \quad (4.8)$$

In terms of this parameter Eq. (4.8), $\langle\sigma v\rangle \approx Y/(32\pi m_{\chi}^2)$ and constraints on the model can be conveniently compared to the thermal relic target in the $m_{\chi} - Y$ plane. In Fig. 18 we show in this parameter space where the cross section Eq. (4.7) is $3 \times 10^{-26} \text{ cm}^3/\text{s} = 1 \text{ pb}$ as a function of DM mass m_{χ} with solid, dark gray diagonal lines. Along this line, the DM thermal relic density is close to the observed value. Above this line, the relic density is smaller than the measured density if DM is symmetric (equal populations of particles, χ , and antiparticles, $\bar{\chi}$), but it is easy to imagine obtaining the correct abundance in this region through an initial asymmetry (i.e., exactly what happens in the baryon abundance case). Below this line, if the DM is in thermal equilibrium then it naively overcloses the Universe, and obtaining the correct DM density here requires a more complicated nonthermal cosmology. From this point of view, parameter space above the $\langle\sigma v\rangle = 1 \text{ pb}$ line is a well motivated target. Accordingly, we shade the region where $\langle\sigma v\rangle < 1 \text{ pb}$ to indicate that it is disfavored in a simple thermal cosmology. Our goal in this work is to place conservative bounds and projections on the cosmologically motivated region of parameter space, which suggests a particular set of benchmark model parameter choices.

We also display a variety of experimental constraints in Fig. 18, which will be surveyed in detail below. The first class of constraints, including direct detection experiments and

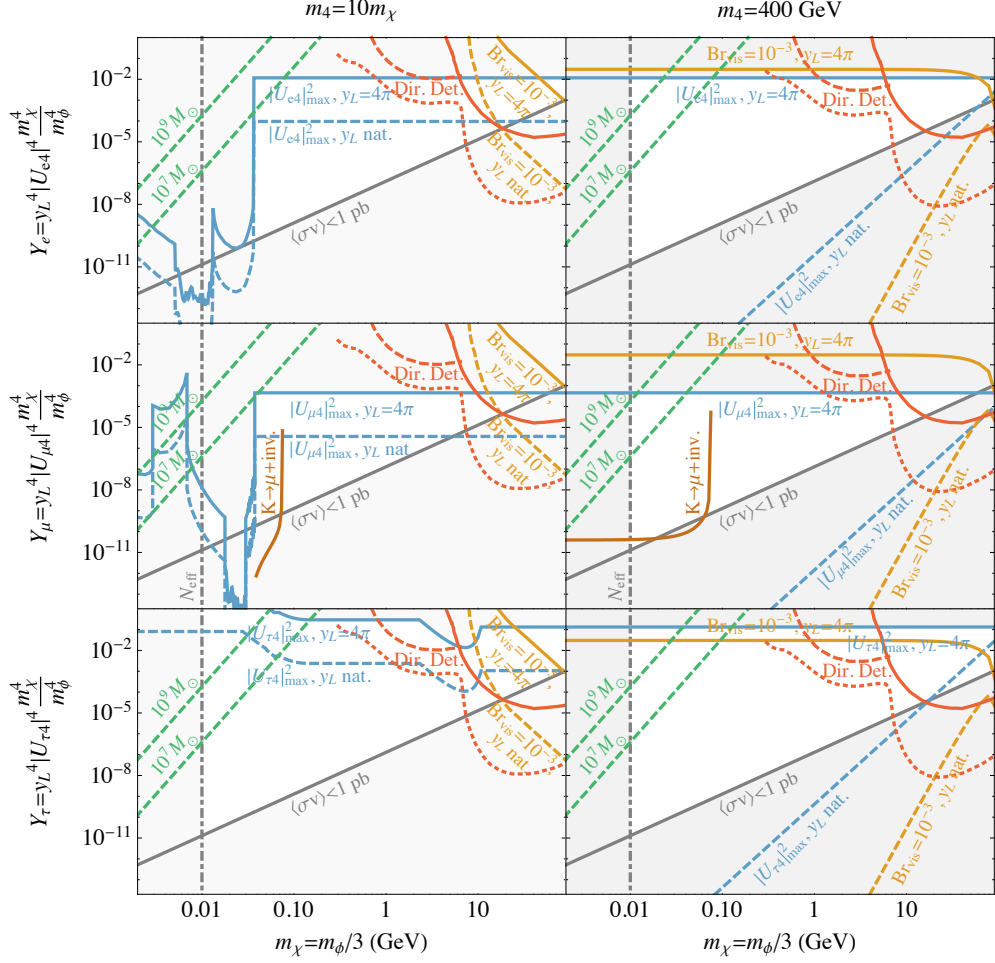


Figure 18: Limits and constraints on the parameter $Y = y_L^4 (\sum_i |U_{i4}|^2)^2 (m_\chi/m_\phi)^4$ as a function of the DM mass m_χ , assuming mixing dominantly with the e , μ , τ flavors from top to bottom. We have fixed the mediator mass to be $m_\phi = 3m_\chi$. On the left we take the heavy neutrino's mass to be $m_4 = 10m_\chi$ and on the right we fix it to $m_4 = 400$ GeV. The solid gray line shows where the annihilation cross section is 1 pb, roughly the value required for a thermal relic. We also show direct detection limits through the effective DM coupling to the Z (red, solid), as well as the direct detection cross sections corresponding to the “ ν floor” (red, dotted).

the small scale structure of dark matter, scale in approximately the same way on Y , m_χ as the annihilation cross section and can be compared to the thermal target without further assumption on the model parameters. However, there are a number of other constraints on sterile neutrinos which limit the mixing angle as a function of the heavy neutrino mass and thus require further assumptions about the model parameters to obtain a constraint on Y . Noting Eq. (4.8), we see that for this class of constraints, the weakest (and thus most conservative) constraint on Y as a function of m_χ is obtained by 1) saturating the experimental bound on the mixing angle, 2) taking y_L close to nonperturbative values, and 3) maximizing the ratio of masses m_χ/m_ϕ while keeping $m_\chi < m_\phi$. For these limits, we therefore fix a set of conservative benchmark values of $y_L = 4\pi$ and $m_\chi/m_\phi = 1/3$.

Note that to represent the constraints on the invisible heavy neutrino in the $m_\chi - Y$ plane, we further require an assumption about the heavy neutrino mass. There are two important comments in this regard, First, these constraints become stronger in the low m_4 regime. Thus to place conservative bounds we should take m_4 to be heavy. Second the dark scalar ϕ suffers from the usual naturalness problem associated with light scalar particles. The scalar receives a quadratically divergent correction to its mass coming from the same Yukawa coupling that enters into the DM annihilation cross section, $\delta m_\phi^2 \sim y_L^2 \Lambda_{UV}^2 / 16\pi^2$. To conservatively implement a naturalness “bound,” we choose to cut this off at the scale $\Lambda_{UV} = m_4$ (typically the heaviest particle in the low energy theory). Further UV contributions could be screened in a low scale UV completion which stabilizes the ϕ mass, e.g. supersymmetry or compositeness. The operator $\lambda_{\phi H} |\phi|^2 |H|^2$ gives a contribution $\lambda_{\phi H} v^2$ to m_ϕ^2 . Given the radiative estimate of $\lambda_{\phi H}$ above, this contribution is suppressed by the relative factor $(|U_{e4}|^2 m_4^2 / \Lambda_{UV}^2) \log(\Lambda_{UV}^2 / m_4^2)$ so we do not include it in our “bound.”

The naturalness “constraint” becomes weaker as m_4 is lowered. It is clear that the naturalness consideration is complementary to the invisible neutrino experimental constraints, since the latter prefer large m_4 while the former prefer small m_4 . We thus show two sets of plots in Fig. 18 with the following assumptions: 1) light ν_4 , fixing $m_\chi : m_\phi : m_4 = 1 : 3 : 10$, in the left column and 2) heavy ν_4 , fixing $m_4 = 400$ GeV, in the right column.

We also derive limits under the assumption that one of the mixing angles $|U_{e4}|$, $|U_{\mu 4}|$, $|U_{\tau 4}|$ dominates, while the others are negligible. This assumption is not necessarily conservative

in terms of constraining the thermal target, since some of the limits may be weakened by $\mathcal{O}(1)$ factors while still obtaining a viable DM cosmology if two or more sizable mixing angles are present. This concern is relatively minor in our view, and is outweighed by the transparency of this assumption, which allows us to clearly display the flavor dependence inherent in certain limits. In this case we specify the flavor content of the coupling relevant for DM annihilation in Eq. (4.8) via $Y_\ell \equiv y_L^4 |U_{\ell 4}|^4 m_\chi^4 / m_\phi^4$ for $\ell = e, \mu, \tau$.

Only the coupling y_L enters the annihilation cross section Eq. (4.7). The coupling y_R does not lead to a tree-level DM-SM interaction, and for most DM masses plays no role in the cosmology. For simplicity, we therefore will assume in this work that y_R is small and can be neglected. However, we note that for $m_\chi \sim m_Z/2$ or $m_\chi \sim m_h/2$, DM can annihilate at one loop through an s -channel Z or Higgs to the SM, which can potentially compete with the tree level process due to the resonant enhancement. It is easy to see that the radiative coupling of DM to the Higgs, $h\bar{\chi}\chi$, vanishes in the limit $y_R \rightarrow 0$. As discussed further below, a radiative $Z\bar{\chi}\chi$ coupling, proportional to y_L^2 , is still generated in this limit. For the benchmark choices described above, we have checked that annihilation through the Z on resonance is subdominant to the tree level annihilation process Eq. (4.7). It would be worthwhile to explore in more detail these resonance regions under different parameter assumptions, as this may allow certain constraints to be relaxed. However, these are fairly special regions of parameter space and their detailed exploration goes beyond our scope here. See Ref. [68, 69] for work in this direction.

Light DM that is in thermal equilibrium with neutrinos can affect the number of relativistic degrees of freedom, N_{eff} , as inferred by measurements of the CMB [162] and primordial light element abundances. The agreement of these with standard CMB and big bang nucleosynthesis (BBN) expectations can be used to set a lower limit on the DM mass of around 10 MeV [163, 164] which we show in Fig. 18 with vertical dot-dashed lines.

4.2.3 Decays of new states

From the interactions in Eq. (4.5) we can obtain the partial decay widths of the new unstable particles. The dark scalar ϕ decays to χ and a light anti-neutrino with a rate

$$\Gamma_{\phi \rightarrow \chi \bar{\nu}_l} = \frac{y_L^2}{16\pi} \sum_i |U_{i4}|^2 m_\phi \left(1 - \frac{m_\chi^2}{m_\phi^2}\right)^2. \quad (4.9)$$

The heavy neutrino ν_4 decays (invisibly) to χ and ϕ through either y_L or y_R . Assuming that y_R is negligible, the rate for this is

$$\begin{aligned} \Gamma_{\nu_4 \rightarrow \chi \phi^*} &= \frac{y_L^2}{32\pi} |U_{N4}|^2 m_4 \left(1 - \frac{m_\phi^2}{m_4^2} + \frac{m_\chi^2}{m_4^2}\right) \\ &\times \lambda^{1/2} \left(1, \frac{m_\phi^2}{m_4^2}, \frac{m_\chi^2}{m_4^2}\right), \end{aligned} \quad (4.10)$$

where $\lambda(a, b, c) \equiv a^2 + b^2 + c^2 - 2ab - 2ac - 2bc$. This rate should be compared with the usual weak decay rate that occurs due to active-sterile mixing. The weak decay rate is negligible for $m_4 \ll m_W$, as it must proceed via off-shell weak bosons. For $m_4 > m_W$, two body weak decays are kinematically allowed, and the rate for $\nu_4 \rightarrow \ell^- W^+$ is

$$\begin{aligned} \Gamma_{\nu_4 \rightarrow \ell^- W^+} &= \frac{G_F m_4^3}{8\pi\sqrt{2}} |U_{\ell 4}|^2 \left(1 - \frac{m_W^2}{m_4^2}\right)^2 \left(1 + \frac{2m_W^2}{m_4^2}\right) \\ &\simeq \frac{\lambda_\ell^2 m_4}{32\pi}, \end{aligned} \quad (4.11)$$

where in the second step we have assumed $m_W \ll m_4$ and used the mixing angle relation Eq. (4.4). Comparing Eqs. (4.10) and (4.11), we see that weak decays can be competitive if λ_ℓ is as large as y_L . However, given the mixing angle relation in Eq. (4.4), this only occurs in practice when m_4 is very large, of order 1 TeV or more. Therefore, weak decays of ν_4 are subdominant over the entire parameter space consistent with thermal dark matter. To illustrate this, in Fig. 18 we show contours where the weak branching fraction of the heavy neutrino is 10^{-3} , fixing y_L to either its perturbative maximum, $y_L = 4\pi$ (orange, solid curves), or to its ‘‘bound’’ from naturalness, $y_L = 4\pi m_\phi/m_4$ (orange, dashed curves). Below these lines, values of the weak branching fraction can be chosen to be less than 10^{-3} , which is sufficient to reduce the limits derived from visible decays of the heavy neutrino (see, e.g. [148, 149, 165]) to be subdominant. In this setup, where N is Dirac or pseudo-Dirac,

$\Delta L = 2$ decays of the heavy neutrino are either absent or highly suppressed. In the two specific possibilities mentioned in Sec. 4.2.1 where the light neutrino masses are due to either a lepton-number-violating Majorana mass μ or Yukawa coupling λ'_ℓ , the $\Delta L = 2$ decay rate is suppressed relative to the $\Delta L = 0$ rate by the factor $(\mu/m_N)^2$ or $(\lambda'_\ell v/m_N)^2$, respectively.

4.3 STERILE NEUTRINO CONSTRAINTS

As discussed in the previous section, the sterile neutrino mediator ν_4 decays invisibly into the dark sector in our scenario. In Ref. [73], the limits on the mixing angle for invisibly decaying heavy neutrinos were presented (see also Ref. [166]). These limits impact the cosmologically motivated DM parameter space since the annihilation cross section Eq. (4.7) (or equivalently the Y parameter in Eq. (4.8)) depends on this mixing angle. In this section we briefly review the existing limits and take note of a few updates due to recent searches. The limits are summarized in the $m_4 - |U_{i4}|^2$ plane in Fig. 19.

4.3.1 μ, τ decays

A massive neutrino with non-vanishing $|U_{e4}|$ and/or $|U_{\mu 4}|$ leads to a modified value of the Fermi constant extracted from the muon lifetime. Because the Fermi constant governs a host of precision electroweak and high-energy observables, the general agreement of this data [167, 168] with the SM predictions constrains these mixing angles (labelled τ_μ/EWPT in Fig. 19). Similarly, the Fermi constant enters into the semi-leptonic weak decays used to measure the CKM elements, V_{ud} and V_{us} , and CKM unitarity can therefore be used to derive limits on $|U_{\mu 4}|$ [73, 168]. Furthermore, the lack of distortions in the e^+ energy spectrum in μ^+ decays measured by the TWIST collaboration [169] can be used to constrain $|U_{e4}|$ and $|U_{\mu 4}|$ for masses $m_4 < m_\mu - m_e$ [73, 166, 170].

The constraints on mixing in the τ sector are generally much weaker than in the e and μ sector. Relevant limits on $|U_{\tau 4}|$ can be derived from τ decays, including the leptonic decays $\tau \rightarrow e\bar{\nu}\nu$, $\tau \rightarrow \mu\bar{\nu}\nu$ [168, 171, 172], as well as certain hadronic modes like $\tau \rightarrow \nu 3\pi$ [73, 173].

4.3.2 Rare meson decays

Rare meson decays, $M^+ \rightarrow \ell^+ \nu_4$, provide some of the best probes of an invisible heavy neutrino. One striking signature is a peak in the energy spectrum of the outgoing lepton in the meson rest frame due to the two-body kinematics. Strong limits on $|U_{e4}|$ arise from peak searches in $\pi \rightarrow e\nu$ [174], $K \rightarrow e\nu$ [175], and $B \rightarrow e\nu$ [176] decays, while similar searches in the decays $\pi \rightarrow \mu\nu$ [177], $K \rightarrow \mu\nu$ [178], and $B \rightarrow \mu\nu$ [176] decays constrain $|U_{\mu 4}|$. Furthermore, a comparison of the experimental value of the ratio $\Gamma_{\pi \rightarrow e\nu}/\Gamma_{\pi \rightarrow \mu\nu}$ to its SM prediction can be used to set constraints on $|U_{e4}|$ and $|U_{\mu 4}|$ [179].

4.3.3 Three body decays

One of the most sensitive probes of sterile neutrinos comes from decays of a charged meson, M^+ , to a charged lepton, ℓ^+ , and heavy, mostly sterile neutrino, as discussed in Sec. 4.3. If the mass of the heavy neutrino, m_4 , is larger than $m_M - m_\ell$, this two-body decay is kinematically forbidden from happening. However, in this model, if $m_\chi + m_\phi < m_M - m_\ell$, then three-body decays $M^+ \rightarrow \ell^+ \chi \phi$ can proceed through off-shell (heavy and light) neutrinos. In the limit that $m_4 \gg m_M$, the rate for this decay is

$$\begin{aligned} \frac{1}{\Gamma_{M^+ \rightarrow \ell^+ \nu_\ell}} \frac{d\Gamma_{M^+ \rightarrow \ell^+ \phi \chi}}{dx} &= \frac{y_L^2 |U_{\ell 4}|^2}{32\pi^2} (1 - |U_{\ell 4}|^2) \\ &\frac{\sqrt{x^2 - 4x_\ell}}{x_\ell (1 - x_\ell)^2} \frac{(1 - x)x + 2x_\ell}{(1 + x_\ell - x)^3} (1 + x_\ell - x - x_\phi + x_\chi) \\ &\times \lambda^{1/2}(1 + x_\ell - x, x_\phi, x_\chi), \end{aligned} \quad (4.12)$$

where $x = 2E_\ell/m_M$ is the energy fraction carried by the charged lepton in the meson rest frame and $x_{\chi, \phi, \ell} = m_{\chi, \phi, \ell}^2/m_M^2$.

The signature of this decay is a charged lepton recoiling against something unobserved (χ and ϕ are both invisible) with a momentum different from the value expected for the standard decay into a charged lepton and massless neutrino, just as in the two-body case (where the decay products of the heavy neutrino are unobserved). The ℓ^+ momentum is distributed over a range of values in the three-body case instead of being monochromatic as in the two-body case.

Armed with the expression in Eq. (4.12) (including terms that survive with finite m_4) for the decay rate, we can use the search for heavy neutrinos in $K^+ \rightarrow \mu^+ + \text{inv.}$ by the E949 experiment [180] to set an upper limit on $y_L^2 |U_{\mu 4}|^2$ or, equivalently, $Y_{\nu\mu}$. To perform this estimate we assume that the μ^+ momentum distribution in the K^+ rest frame measured by E949 is well described by a power law background (dominantly from the radiative decay $K^+ \rightarrow \mu^+ \nu \gamma$) and ask what level of signal, $K^+ \rightarrow \mu^+ \chi \phi$, is allowed. We show the resulting 90% CL upper limits on $Y_{\nu\mu}$ as a function of m_χ (assuming $m_\phi = 3m_\chi$) for both the light m_4 and large m_4 cases in Fig. 18. In both cases, E949 data appear to be sensitive to an interesting region of parameter space close to thermal relic annihilation cross sections. The NA62 experiment plans to collect about 10^{13} kaon decays [181, 182] and could, assuming systematic errors can be kept under control, probe values of $Y_{\nu\mu}$ about an order of magnitude smaller than E949.

4.3.4 Neutrino oscillations

Given the rather weak direct constraints on mixing in the τ sector, it is interesting to consider the consequences of mixing on neutrino oscillations. Notably, atmospheric neutrino oscillations are affected by $\nu_\tau - \nu_4$ mixing due to a suppression of the matter potential by the factor $(1 - |U_{\tau 4}|^2)$ (see [73] for a detailed discussion). An analysis by Super-Kamiokande using the atmospheric muon neutrino zenith angle distribution leads to constraints on $|U_{\tau 4}|$ [183].

If the heavy neutrino is light, it can affect the number of relativistic species present during BBN. This sets a lower bound of $m_4 \gtrsim 10$ MeV [164] which we show in Fig. 19, labelled “ N_{eff} ”.

4.3.5 Invisible Higgs and Z decays

In addition to the flavor-specific constraints discussed above, invisible Higgs and Z boson decays can be used to constrain the mixing angles. These are most relevant for larger values of m_4 where they become competitive with other constraints. We show the limit on the mixing angles from the constraint that the invisible branching of the Higgs is less than 0.24 at 95% C. L. [184] as solid blue lines in Fig. 19. We also show the reach that a future limit

of 5% [185] on this branching could achieve as dotted blue lines. In setting these limits, we only consider decays of the Higgs to neutrinos through the Yukawa coupling with a rate proportional to λ_ℓ^2 . Since ϕ decays invisibly, $h \rightarrow \phi\phi^*$ decays generated by the operator $\lambda_{\phi H}|\phi|^2|H|^2$ also contribute to the invisible Higgs width. However, this mode is suppressed relative to the neutrino mode by at least a further factor of λ_ℓ^2 given the radiative estimate of the coefficient $\lambda_{\phi H}$ and we therefore ignore it.

The effect on the invisible branching of the Z due to heavy sterile neutrinos that mix with the active neutrinos is well-known. The 90% C. L. limits on the mixing angles that comes from the measurement of the invisible Z width of 499.0 ± 1.5 MeV [168] are shown in Fig. 19 as solid, orange lines.

4.3.6 LHC searches

Furthermore, a heavy neutrino with a relatively large admixture of active flavors can be produced in large numbers in leptonic W^\pm decays. Since, in the case we consider here, the heavy neutrino decays invisibly into the dark sector the only effect is a distortion of the kinematics of this decay. In particular, at a hadron collider, the W transverse mass (M_T^W) endpoint or the transverse momentum (p_T) spectra of electrons and muons measured in Drell-Yan production of W^\pm would be affected. For heavy neutrinos light enough to be produced on-shell in $W^\pm \rightarrow \ell^\pm$ decays, this would appear as a kink in the lepton p_T at p_T^{peak} with the M_T^W endpoint, M_T^{peak} , shifted as

$$M_T^{\text{peak}} = M_W \left(1 - \frac{m_4^2}{M_W^2} \right), \quad p_T^{\text{peak}} = \frac{1}{2} M_T^{\text{peak}}. \quad (4.13)$$

The relative size of the kink in this spectrum is at the level $\sim |U_{\ell 4}|^2$ for neutrinos kinematically allowed in W decay. Neutrinos that are heavier than the W simply dilute the rate by the factor $1 - |U_{\ell 4}|^2$. Lepton p_T spectra in W^\pm production and decay at a hadron collider are very well studied because accurate measurements of these spectra, in particular their endpoints, are crucial in determining the W^\pm mass. Since the recent ATLAS measurement of the W^\pm mass [186] has e^\pm and μ^\pm p_T spectra that agree with theoretical expectations at the subpercent level, we can reasonably expect a sensitivity to mixing angles of $\mathcal{O}(10^{-2})$

or smaller. This would be comparable to the limit from electroweak precision tests and therefore very interesting.

To estimate the sensitivity of the measurement of lepton p_T spectra at the LHC to $|U_{e4}|$ and $|U_{\mu4}|$, we generated samples of $pp \rightarrow W^+ \rightarrow e^+, \mu^+ + \text{inv.}$ including massless and massive neutrinos [81, 82] corresponding to 4.1 fb^{-1} of 7 TeV pp collisions using MadGraph5 [225], interfaced with Delphes [187] to model the detector response. We examine the resulting e^\pm and μ^\pm p_T distributions between 30 GeV and 50 GeV with bins of 0.5 GeV. Assuming that the standard model expectation describes these data and that statistical errors dominate (which are $\mathcal{O}(\text{few} \times 0.1\%)$ as in Ref. [186]) aside from the overall normalization, we perform a fit to the underlying theory expectation (a function of $|U_{e4}|$ and $|U_{\mu4}|$) at each value of m_4 . We allow the overall measured cross section to vary by 2% from the theoretical prediction to take the systematic error on the overall normalization, which comes mainly from the measurement of the total luminosity, into account.

In Fig. 19 we show the resulting regions of parameter space ruled out at 90% C.L. with dashed brown lines labeled “ $W \rightarrow e$ ” and “ $W \rightarrow \mu$ ”. As anticipated, the limit on the mixing angle for heavy neutrinos that can be produced on-shell is at the level of the statistical errors which dominate the shape of the p_T spectra while for $m_4 > m_W$ the limit corresponds to the uncertainty on the overall cross section. For lighter neutrino masses the difference in the lepton p_T is difficult to distinguish from that for a massless neutrino so the limit is weakened.

4.4 DARK MATTER PHENOMENOLOGY

4.4.1 Direct Detection

At one loop χ picks up an effective coupling to the Z boson, which can be written after EWSB as

$$\mathcal{L} \supset a_Z \frac{g}{c_W} Z_\mu \bar{\chi} \gamma^\mu P_R \chi, \quad (4.14)$$

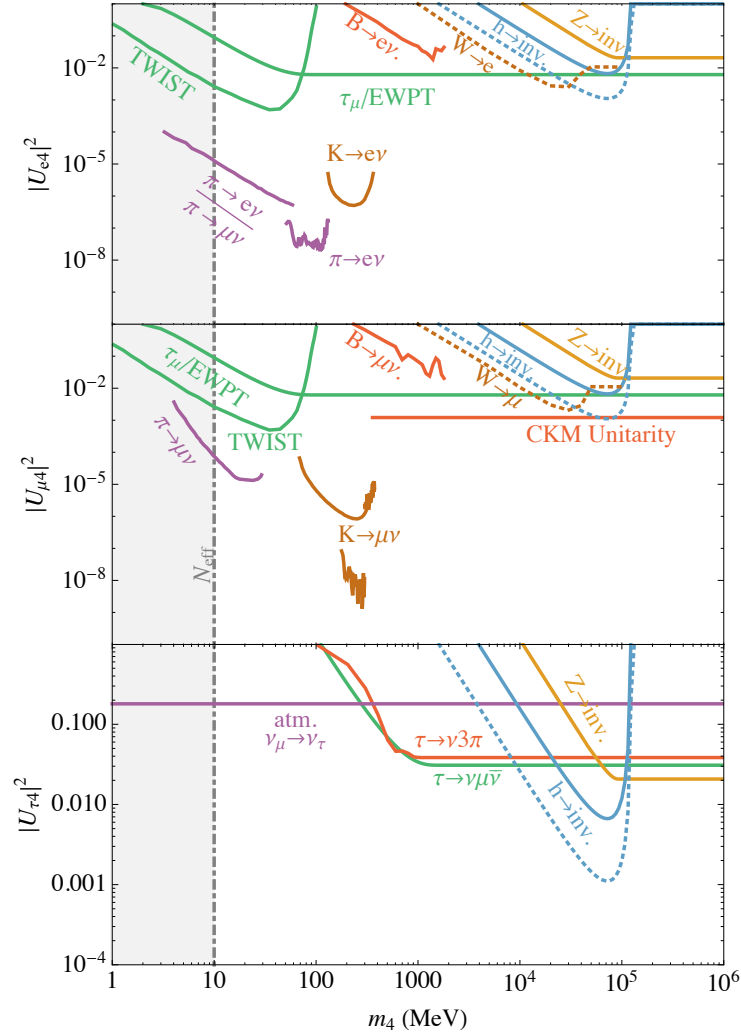


Figure 19: 90% C.L. upper limits on the mixing angles $|U_{\ell 4}|^2$ as functions of the heavy neutrino mass m_4 in the case that the heavy neutrino decays invisibly.

where the coupling a_Z is given by

$$a_Z = |U_{N4}|^2(1 - |U_{N4}|^2) \frac{y_L^2}{16\pi^2} G\left(\frac{m_\phi^2}{m_4^2}\right), \quad (4.15)$$

with $G(x) = (x - 1 - \log x)/(4(1 - x)^2)$. In Eqs. (4.14) and (4.15) we work in the limit $m_\chi \ll m_\phi, m_4$ and zero external momentum (we use the full loop integral for our numerical results). This coupling mediates spin-independent scattering of DM with nuclei via Z boson exchange, and therefore direct detection experiments provide an important probe of the model. The effective DM-nucleon spin-independent scattering cross section is given by

$$\sigma_n = \frac{\mu_n^2}{\pi} \frac{(Zf_p + (A - Z)f_n)^2}{A^2} \quad (4.16)$$

where $f_n = G_F a_Z / \sqrt{2}$, $f_p = -(1 - 4s_W^2)G_F a_Z / \sqrt{2}$.

The strongest constraints in the high DM mass region come from recent results of XENON1T [188] and PandaX-II [189] searching for spin-independent scattering of DM on nuclei, and are shown as a solid red curve in Fig. 18. These constraints rule out the thermal DM benchmark for DM masses heavier than about 15 GeV. We also show projections from SuperCDMS SNOLAB [190], which will cut further into $m_\chi \sim \text{GeV}$ mass region, as a dashed red curve. In addition, to get a sense of what region of parameter space can potentially be probed with direct detection, we show values of the coupling that correspond to a direct detection cross section at the “neutrino floor” [191] as a dotted red curve.

Clearly, direct detection experiments provide a powerful probe of the high DM mass region in this scenario, but it is important to note that these limits can be weakened or evaded altogether if the DM obtains a mass splitting. This can be implemented by adding a Majorana mass terms for the chiral components of χ . In this case upper limits on the DM mass are provided by constraints on the mixing angles for heavy, invisibly decaying neutrinos, notably electroweak precision tests as well as decays of electroweak bosons. Thus, these searches provide a complimentary probe of this scenario to direct detection.

There has been a significant effort devoted to exploring new methods of direct detection to probe low mass DM candidates [192], although in our scenario the scattering cross section with electrons is unfortunately too small to be detected.

4.4.2 DM structure

There has been growing evidence that observations of dark matter structure on sub-galactic scales differs from the expectation from N -body simulations that assume that dark matter only interacts gravitationally (which, with respect to structure formation, essentially corresponds to the expectation for standard cold DM candidates). One of the longstanding problems in this area is the so-called “missing satellites” [193] problem—the apparent observation of fewer satellite galaxies of the Milky Way than expected. While the gravitational feedback of normal matter at small scales, resulting from complicated astrophysics, could resolve this discrepancy, it is also possible to address these issues with nongravitational interactions of dark matter. One such possibility is if the dark matter is relatively strongly coupled to the light neutrinos as in this scenario [194].

A large coupling of dark matter to light (relativistic) neutrinos produces a pressure that resists the gravitational collapse of the dark matter. Because both the number density of light neutrinos and the interaction cross section are larger at high temperatures, this pressure is important at early times when the Universe is hotter and eventually becomes unimportant at some critical temperature determined by the strength of the dark matter-neutrino interaction. Structures in the Universe form hierarchically, with smaller structures forming before larger ones, since only density perturbations with wavelengths smaller than the (expanding) horizon size can grow. The structures formed gravitationally by dark matter before matter-radiation equality provide the seeds for the growth of objects containing normal matter that we later observe. At early times when the dark matter-neutrino interactions are important, the pressure felt by the dark matter means that structures do not efficiently grow due to gravity, while, after the dark matter-neutrino interactions become unimportant, structures can form [195].

In other words, dark matter-neutrino interactions can address the missing satellites problem by suppressing the growth of small scale structures. The scale below which structures do not efficiently form in this scenario can be characterized in terms of a cutoff mass, M_{cut} , which is the mass of dark matter inside the horizon at the critical temperature when DM-neutrino interactions become unimportant (for detailed discussion of these issues, see, e.g., [196]).

This mass is a useful heuristic expected to correspond roughly to the size of the smallest gravitationally bound objects at late times. In this model the cutoff mass is estimated to be [73]

$$M_{\text{cut}} \simeq 10^8 M_{\odot} \left(\frac{g_*}{3.36} \right)^{-7/8} \left(\frac{0.1 \text{ GeV}}{m_{\chi}} \right)^{-14/4} Y^{3/4}, \quad (4.17)$$

assuming $m_{\phi} \gg m_{\chi}$. In this expression, g_* refers to the effective number of relativistic degrees of freedom at the time of decoupling which we will always take to be 3.36 which is relevant for the phenomenologically interesting case where the decoupling happens when the Universe's temperature is around a keV.

We take values of the cutoff, M_{cut} , between about 10^7 and $10^9 M_{\odot}$ to roughly represent DM-neutrino interactions strong enough to explain the missing satellites problem. An upper bound on M_{cut} of around $10^9 M_{\odot}$ can be obtained analyzing Milky Way satellites [197], looking for small scale structures in the Lyman- α forest [198], or through gravitational lensing of small, distant objects [199].

4.5 SUMMARY AND OUTLOOK

We have presented a general analysis of thermal relic DM that annihilates directly to SM neutrinos through the neutrino portal. This possibility is very well motivated theoretically but has been relatively less well studied than other scenarios involving vector or scalar mediators. Indeed, directly annihilating to light neutrinos can allow for thermal relic dark matter below roughly 10 – 50 GeV without spoiling CMB measurements.

The model described in Sec. 4.2.1 is simple and economical, adding just three new states, fermions N and χ and a scalar ϕ , with masses from about 10 MeV to $\mathcal{O}(100 \text{ GeV})$. It allows for a very simple cosmological history, detailed in Sec. 4.2.2, with the DM number density being set either by annihilation to light neutrinos or by an initial asymmetry, with annihilation reducing the number density to the measured level. The relatively large dark matter-light neutrino coupling needed for annihilation requires that the sterile neutrino mediator N be (pseudo-)Dirac. We discussed the impact of radiative corrections to the scalar mass, identifying regions of parameter space that do not require fine-tuning.

In Sec. 4.2.3, we pointed out an interesting feature of this scenario: the fact that the heavy (mostly N) neutrino decays primarily invisibly into the dark sector, allowing for relatively larger active-sterile mixing angles. Sections 4.3 and 4.4 were devoted to fully exploring the model. We discussed and updated limits on the sterile neutrino in this scenario where it decays invisibly in Sec. 4.3. The direct detection signature of this model was examined in Sec. 4.4.1 and we find that it sets an upper limit on the DM mass of around 10 GeV in the simplest scenario. The impact on the small scale structure of DM, which could signal strong interactions between light neutrinos and DM, was also presented in Sec. 4.4.2. Addressing this would likely imply a large mixing with the τ neutrino.

We identified several new measurements or analyses that can be done to probe large regions of viable parameter space in this setup. First, we discussed the possibility that the heavy, invisibly decaying neutrino required for this scenario can affect the kinematics of charged leptons in Drell-Yan W^\pm production at the LHC. The sizable active-sterile mixing angle needed as well as the large number of W bosons produced at the LHC could allow for unconstrained regions of viable parameter space to be probed by such a measurement. In our simple mock analysis, we only considered e^+ and μ^+ transverse momenta above 30 GeV as in the ATLAS measurement of the W mass [186]. Including smaller p_T values in this analysis would extend sensitivity to smaller values of the heavy neutrino mass m_4 and we urge any experimental analysis to push the lepton p_T threshold as low as possible while still being able to deal with, e.g., issues from pile up.

Secondly, we discussed the sensitivity of three-body decays of kaons into the dark sector to this scenario. One virtue of this search is that it scales on the parameters of the model in the same way as the DM annihilation cross section and can therefore probe the parameter space without having to assume particular values of some parameters. We estimated the region of parameter space ruled out by the E949 experiment which collected around 10^{12} stopped kaon decays—this includes a large region of parameter space consistent with thermal relic DM that is unconstrained by other experiments. The NA62 experiment will collect around an order of magnitude more kaons and will therefore be able to probe even more of the viable thermal relic parameter space, providing an excellent test of this scenario.

Additionally, the active-sterile mixing angle is relatively less well constrained when it

involves the τ flavor, particularly for $m_4 \lesssim 300$ MeV, which can allow for DM-neutrino interactions to be strong enough to affect small scale structure. In this region, the dominant constraint comes from the impact of nonstandard matter effects on the oscillation of atmospheric neutrinos as measured by Super-Kamiokande [183]. It is important to note that this measurement is statistics limited and further data will probe a very interesting region, especially from the point of view of small scale structure effects. Models in which dark matter annihilates directly to light neutrinos are well-motivated, simple and far-reaching phenomenologically, in both particle physics and cosmology. New ideas to probe this class of models should be strongly encouraged. It could well herald a discovery that uncovers the particle nature of dark matter.

5.0 SUSY SIGNALS FROM QCD PRODUCTION AT THE UPGRADED LHC

This chapter is devoted to evaluating the sensitivities of the High Luminosity (HL) and High Energy (HE) upgrades of the LHC to gluinos and stops, decaying through the simplified topologies $\tilde{g} \rightarrow q\bar{q}\chi^0$, $\tilde{g} \rightarrow t\bar{t}\chi^0$ and $\tilde{t} \rightarrow t\tilde{\chi}^0$. It is based on our work in Ref. [200].

5.1 INTRODUCTION AND METHODOLOGY

As one of the leading resolutions of the hierarchy problem associated with the weak scale and the Planck scale, supersymmetry (SUSY) has attracted enormous attention as an experimental target for past, present, and future colliders. The lamppost of naturalness suggests that super-partners should appear near the electroweak scale [201]. Although experimental searches have not established any observable signal thus far, it is conceivable that the SUSY scale may still be just out of reach or that SUSY experimental signatures are unconventional in nature. With this in mind, it is essential to develop and quantify the impact of SUSY search strategies at the Large Hadron Collider (LHC) and its potential successors.

At the end of Run 2 of the LHC, preparations for the luminosity upgrade of the LHC are well underway [202]. In addition, there has been significant interest in the possibility of augmenting the LHC energy with new stronger magnets [203]. The energy upgrade of the LHC could take us to the next energy frontier. We thus find it timely to reexamine SUSY searches. In this chapter, we describe the ability of luminosity- and energy-upgraded versions of the LHC to probe supersymmetry.

Supersymmetric theories are broad in scope, and even if one is to focus solely on collider

searches, there is much model-dependence in signature space (see, *e.g.*, [204]). A variety of search strategies are necessary to cover the multitude of potential signatures of SUSY. In this work we consider two well-motivated and leading channels, namely, pair production of the gluinos and top-quark partners (stops). Once kinematically accessible, gluino pair production will be the leading channel because of its octet representation under QCD. On the other hand, owing to the large top-quark Yukawa coupling and the resulting stop soft-mass evolution over scales, it is motivated to consider the stops as the lightest quark partners and thus the most kinematically favored for production. Specifically, we evaluate the leading decay modes of hadronic jets plus large missing transverse energy (\cancel{E}_T), resulting from the missing neutral lightest SUSY partner (LSP), taken to be the neutralino (χ^0). We also include flavor tagging, requiring that some of the jets be b -tagged. Thus the standard decay chains of gluinos and stops under consideration are

$$\tilde{g} \rightarrow q\bar{q}\chi^0, \quad \tilde{g} \rightarrow t\bar{t}\chi^0, \quad \text{and} \quad \tilde{t} \rightarrow t\chi^0.$$

From a bottom-up perspective, the stop and gluino are important to search for because they affect the Higgs mass parameter at one and two loops respectively, and with their strong couplings are expected to be some of the most important super-particles with respect to tuning of the electroweak scale¹. Throughout, we consider simplified models [205, 206] wherein the new particle production is entirely due to gluinos and stops which decay through the above modes to a bino LSP [207, 208]. We note that while the analyses which we consider are some of the most common collider SUSY searches, their relevance depends on SUSY breaking scenarios and parameter assumptions, including the mass splitting between the colored super-partners and the LSP. Nevertheless, they give a representative starting point and a perspective for well-motivated channels.

We estimate the potential reach of these searches at both the High Luminosity LHC (HL-LHC), with 3 ab^{-1} of 14 TeV proton collisions, and the High Energy LHC (HE-LHC), with the energy and integrated luminosity increased to 27 TeV and 15 ab^{-1} , respectively. While over the past several years HL-LHC and 100 TeV analyses have sought to project

¹The Higgsino affects the Higgs mass at tree level, but is uncolored and thus more challenging to produce at a hadron collider. We note that while we consider models with bino LSPs, there is an implicit tuning at large LSP mass because the Higgsino must be even heavier than the LSP.

the potential of future colliders to search for the same superparticles as we consider (see, e.g., [209, 210, 211, 212] for reviews), HE-LHC studies are less common (though some 33 TeV studies exist [213]), and have considered different final states with varying motivations [214, 215]. This work is most closely related to the ATLAS HL-LHC studies [216, 217], which we have both improved upon with cut optimization and the inclusion of currently accepted detector projections, and extended to the HE-LHC. One of the gluino searches presented here has appeared in the report of the Beyond the Standard Model Physics Working Group [218] in the *Workshop on Physics at the HL-LHC, and perspectives on HE-LHC*, while the other extended results appear here for the first time.

The rest of this chapter is organized as follows. In Section 5.2, we project the HL-LHC and HE-LHC gluino reach in the 4 jets plus \cancel{E}_T final state, both in the cases where the gluino decays through light-flavor or heavy-flavor off-shell squarks. In Section 5.3, we estimate the reach of the luminosity- and energy-upgraded LHC for the stop in the b -jets plus jets plus \cancel{E}_T final state. Section 5.4 contains a discussion of our results and our conclusions.

5.2 GLUINOS

While the gluino only affects the Higgs mass at two loops, it nevertheless plays an important numerical role in contributing to Higgs mass corrections [219], and enjoys a relatively large production cross section as a fermionic color octet. The total production cross section including NLO and NLL QCD corrections [220] is, for gluinos of mass 2 TeV,

$$1.7 \text{ fb at } 14 \text{ TeV and } 68 \text{ fb at } 27 \text{ TeV.}$$

The latter figure is estimated using the K-factor from 33 TeV gluino production, and shows an increase of a factor of 40 by going to the HE-LHC. In our study, we evaluate the sensitivity of future proton colliders to gluino pair production with gluinos decaying to the LSP through off-shell squarks, using standard jets + \cancel{E}_T searches. Given the simplified model we are considering as signal with SUSY masses as free parameters, we elect to optimize search regions requiring four jets and missing energy.

Before moving to the details of our studies, we comment briefly on our choice of final state. First, if light flavor squarks are kinematically accessible, $\tilde{q}\tilde{q}^*$, $\tilde{q}\tilde{q}$, and $\tilde{q}\tilde{g}$ production would lead to events with only two or three hard jets. In addition, if a squark is present in the spectrum which weighs less than the gluino, the cascade decay $\tilde{g} \rightarrow q\tilde{q}, \tilde{q} \rightarrow q\tilde{\chi}^0$ can lead to somewhat different kinematics with a squark two-body decay, depending on the masses of the intermediate squark and the LSP. We have chosen the particular topology $\tilde{g} \rightarrow q\tilde{q}\tilde{\chi}^0$ for two main reasons. First, from a bottom-up perspective there is less reason to expect the light flavor squarks to be very closely related to the weak scale, and indeed in the limit of decoupled squarks final states with light-flavor quarks can be important. In addition, adding more particles such as intermediate squarks would increase the dimensionality of the parameter space to consider, and we prefer to avoid this complication here. Finally, in the compressed region where the gluino and LSP masses are similar, a search region with fewer jets is expected to be somewhat more effective [221]. We will nevertheless find that by loosening our cuts on \cancel{E}_T and related kinematic variables, we can achieve reasonable sensitivity in this scenario. Typically, the four jets plus missing energy final state is the most powerful in constraining this simplified model [222].

Similar considerations apply in the case of gluinos decaying through off-shell 3rd generation squarks. It is useful to separate this topology both because of the motivation from naturalness for the stop to be close in mass to the electroweak scale, and because the b -quarks from top and bottom decays can be tagged, yielding different experimental signatures than for gluinos decaying through off-shell light flavor squarks. We thus choose to also consider the decay topology $\tilde{g} \rightarrow t\bar{t}\tilde{\chi}^0$. Due to the different decay modes of the tops, multiple final states can occur, including same-sign dileptons plus missing energy [223, 224], but common to all of the possibilities are multiple b -jets. We will follow the authors of [215] and consider purely hadronic top decays, performing a search in a jets plus missing energy final state where leptons are vetoed and some of the jets are required to be tagged as originating from b quarks. In principle there can be up to 12 hard jets in the final state when gluino decays proceed through off-shell stops and the resulting tops decay hadronically, but we consider only the first four jets in our analysis. We expect that with this choice, gluino decays through off-shell sbottoms will enjoy a similar limit.

5.2.1 $\tilde{g} \rightarrow q\bar{q}\tilde{\chi}^0$

The main SM backgrounds in the $4j + \cancel{E}_T$ final state are $Z(\rightarrow \nu\nu) + \text{jets}$, $W(\rightarrow \ell\nu) + \text{jets}$, and $t\bar{t}$ production. There are additional small contributions to the background from single top and diboson production, which we ignore. We generate signal and background using MadGraph 5 [225] at parton level and Pythia 8 [226] to perform showering with MLM matching [227]. At parton level, the background is generated in bins of H_T , where H_T is the scalar sum of the p_T of all jets, to ensure sufficient statistics. We simulate the detector response using Delphes 3 [187], which employs FastJet [228] to cluster jets using the anti- k_T algorithm [229], with the commonly accepted HL-LHC card corresponding to the upgraded ATLAS and CMS detectors. For the signal, we normalize the cross sections to NLL+NLO calculations [220]. To encapsulate higher-order effects for background, we apply a universal K-factor of 1.25.

Following previous works [221, 216, 217], we apply a set of baseline cuts

$$p_T(j_1) > 160 \text{ GeV}, N_{\text{jets}}(p_T > 60 \text{ GeV}, |\eta| < 5.0) \geq 4, \cancel{E}_T > 160 \text{ GeV}. \quad (5.1)$$

We further require that signal events contain no isolated electrons (muons) with p_T above 10 (10) GeV and $|\eta|$ below 2.47 (2.4). We reject events with $\Delta\phi(j, \cancel{E}_T)_{\min} < 0.4$, where $\Delta\phi(j, \cancel{E}_T)_{\min}$ is the minimum transverse angle between \cancel{E}_T and the first three leading jets, to avoid contamination from QCD background with mismeasured jets. To further reduce the background, we demand $\cancel{E}_T/\sqrt{H_T} > 10 \text{ GeV}^{1/2}$ and $p_T(j_4)/H_T > 0.1$, and j_4 indicates the fourth leading jet. After this baseline selection, a two dimensional optimization over cuts on \cancel{E}_T and H_T is performed to obtain the maximum significance. The latter cuts are optimized at each signal point to maximize the significance defined as

$$\mathcal{S} = \frac{S}{\sqrt{B + \sigma_B^2 B^2 + \sigma_S^2 S^2}}, \quad (5.2)$$

where S and B are the number of signal and background events, respectively, and $\sigma_B = 20\%$ and $\sigma_S = 10\%$ are our assumed background and signal systematic uncertainties. To assure a reasonable description of the statistical significance, we require at least 8 background events throughout our studies. For the HL-LHC (HE-LHC), we vary \cancel{E}_T in steps of 0.5 (0.5) TeV

from 0.5 (0.5) up to 3.0 (7.0) TeV and H_T in steps of 0.5 (0.5) TeV from 0.5 (0.5) up to 5.0 (7.0) TeV. Because of our cut optimization, our search is predicted to enjoy better sensitivity than the existing ATLAS HL-LHC study [216].

To present the qualitative features of our analyses, we choose two gluino benchmark points

$$m(\tilde{g}, \tilde{\chi}^0) = (1020 \text{ GeV}, 1000 \text{ GeV}) \text{ and } (2000 \text{ GeV}, 300 \text{ GeV}). \quad (5.3)$$

The first benchmark represents the nearly-degenerate (compressed) mass spectrum – a challenging scenario for collider searches. The second set has a typical light LSP, implying large missing energy in the final state. In Table 3, we show the cut flow for two benchmark points, using our baseline selection cuts in addition to the optimal \cancel{E}_T and H_T cuts that we have found for each point. We also show sample kinematic distributions of H_T for both signal and background in Figure 20, after all cuts except for the last cut are applied. We see that the value of H_T is broadly peaked at $m_{\tilde{g}}$ as expected. The tail of the H_T distribution extends further for a lighter LSP due to larger \cancel{E}_T . With our preferred cuts, the significance is maximized.

We show exclusion and discovery contours in Figure 21 (left panel), indicating where the significance reaches 2σ (exclusion) and 5σ (discovery), respectively. We find that, for a massless LSP, a gluino of approximately 3.2 TeV can be probed by the HL-LHC with 3 ab^{-1} of integrated luminosity. At 27 TeV with 15 ab^{-1} of integrated luminosity, the exclusion (discovery) reach is roughly 5.7 (5.2) TeV. We see that for a nearly-degenerate gluino and LSP, the exclusion (discovery) reach of HL-LHC and HE-LHC approximate 1.5 (1) TeV and 2.2 (2) TeV respectively. For comparison, a 100 TeV collider with 3 ab^{-1} of data would be able to discover gluinos with the same decay topology up to 11 TeV, again assuming a massless LSP [221].

5.2.2 $\tilde{g} \rightarrow t\bar{t}\tilde{\chi}^0$

For the simplified model with heavy flavor quarks in the final state, we still require four jets plus missing energy, as explained above, but now impose the additional demand that two of the jets be b -tagged, reducing the backgrounds of the previous subsection considerably.

$m(\tilde{g}, \tilde{\chi}^0)$	(1020, 1000)	(2000, 300)	Background
Generator-level cuts	396	1.70	$3.43 \cdot 10^4$
Lepton veto	396	1.69	$1.93 \cdot 10^4$
Jet $p_T > (160, 60, 60, 60)$ GeV	30.8	1.64	$5.45 \cdot 10^3$
$\cancel{E}_T > 160$ GeV	27.8	1.59	$1.73 \cdot 10^3$
$\Delta\phi(j_{1,2,3}, \cancel{E}_T) > 0.4$	23.1	1.27	$1.10 \cdot 10^3$
$\cancel{E}_T/\sqrt{H_T} > 10$ GeV ^{1/2}	18.6	0.97	358
$p_T(j_4)/H_T > 0.1$	8.82	0.48	246
$\cancel{E}_T > 500$ GeV	2.82	–	17.6
$H_T > 1000$ GeV	1.65	–	5.21
$\cancel{E}_T > 500$ GeV	–	0.46	17.6
$H_T > 3500$ GeV	–	0.09	0.004

Table 3: Cut flow for the two gluino benchmark points in Eq. (5.3) at HL-LHC. At each step, the cross section remaining after the indicated cut is shown in fb. The baseline cuts are identical for both points as stated in the text.

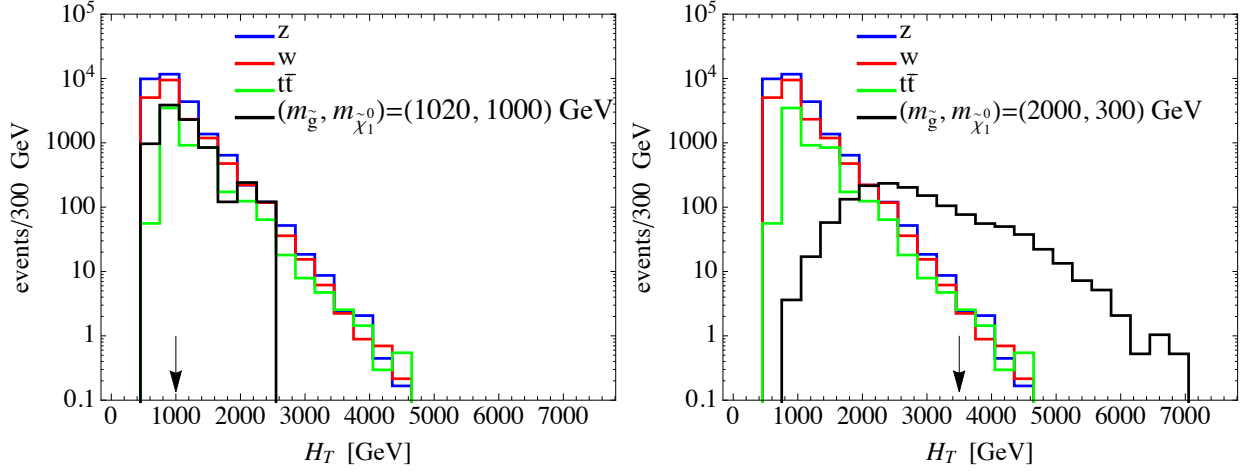


Figure 20: The H_T distribution after all cuts except for that on the H_T are applied, at HL-LHC. In the left/right panel, the signal corresponds to the benchmark points in Eq. (5.3). The arrows indicate the final cuts on H_T for the chosen signal regions.

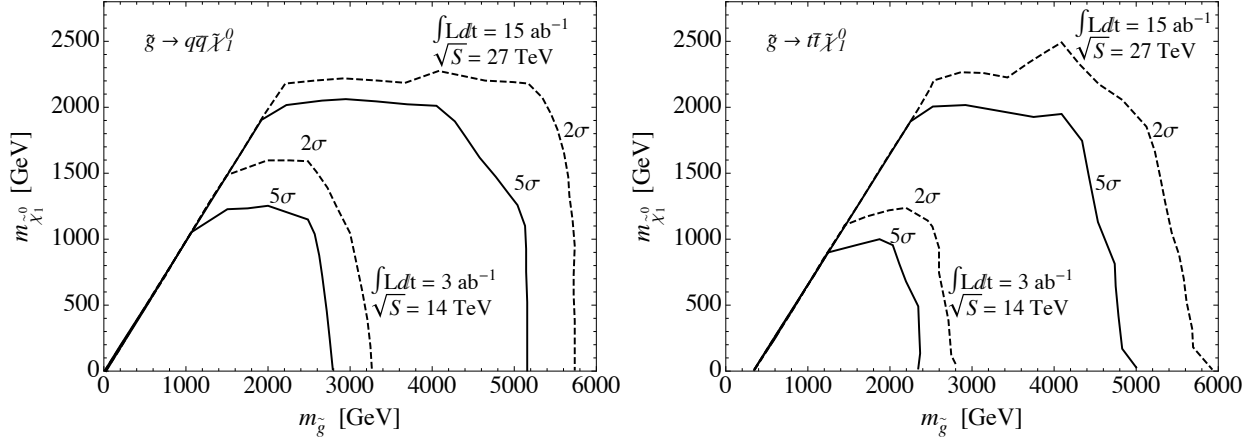


Figure 21: The expected reach of LHC upgrades in probing gluinos decaying through off-shell squarks $\tilde{g} \rightarrow q\bar{q}\tilde{\chi}_1^0$ (left panel) and $\tilde{g} \rightarrow t\bar{t}\tilde{\chi}_1^0$ (right panel), in the gluino-LSP mass plane. The plots show the gluino mass reach at the LHC for 14 (27) TeV with 3 ab^{-1} (15 ab^{-1}) of data.

Instead, the main sources of background events are $t\bar{t}$, $t\bar{t}Z$ and $b\bar{b}Z$ production. We use the same event generation pipeline as for the $\tilde{g} \rightarrow q\bar{q}\tilde{\chi}^0$ topology.

We initially veto on leptons with p_T above 10 GeV and $|\eta|$ below 2.5. We then apply a set of baseline cuts

$$N_{\text{jets}}(p_T > 50 \text{ GeV}, |\eta| < 3.0) \geq 4, \quad \cancel{E}_T > 100 \text{ GeV} \quad (5.4)$$

For the HL-LHC (HE-LHC), we then search for events where the first two jets have $p_T > 200$ (600) GeV and the third and fourth jets have $p_T > 80$ (80) GeV. Furthermore, we ask that at least two jets are b-tagged. To discriminate signal events from QCD dijet events, we reject events with $S_T < 0.1$ where S_T is the the transverse sphericity. We also reject events with $\Delta\phi(j, \cancel{E}_T) < \pi/18$ where $\Delta\phi(j, \cancel{E}_T)$ is the transverse angle between \cancel{E}_T and the closest jet, to reduce enhancement of \cancel{E}_T due to mismeasurement of jet energies. In addition, we reduce background further by requiring $p_T(j_4)/H_T > 0.1$. After these baseline cuts, further cuts on $p_T(j_1)$ and $\cancel{E}_T/\sqrt{H_T}$ are optimized at each signal point to maximize the significance, which is calculated in the same fashion as above. For the HL-LHC (HE-LHC), we vary $p_T(j_1)$ in steps of 0.1 (0.1) TeV from 0.2 (0.4) up to 1 (1.6) TeV and $\cancel{E}_T/\sqrt{H_T}$ in steps of 1 (1) $\text{GeV}^{1/2}$ from 10 (10) up to 27 (27) $\text{GeV}^{1/2}$.

We show exclusion and discovery contours in Figure 21 (right panel), indicating where the significance reaches 2σ and 5σ , respectively. For a massless LSP, a gluino of approximately 2.3 TeV can be discovered by the HL-LHC with 3 ab^{-1} of integrated luminosity. At 27 TeV with 15 ab^{-1} of integrated luminosity, we find that the exclusion (discovery) reach is roughly 5.7 (4.8) TeV. The latter result is somewhat weaker than that of [215], with respect to which we find larger $b\bar{b}Z$ and $t\bar{t}$ backgrounds, though comparable to the reach in the direct gluino decay simplified model of the previous subsection. In both cases, the HE-LHC represents a significant gain over the HL-LHC in our ability to probe gluinos. A 100 TeV collider with 3 ab^{-1} of integrated luminosity would be able to discover gluinos up to 6.4 TeV decaying as $\tilde{g} \rightarrow t\bar{t}\tilde{\chi}^0$, again assuming a massless LSP [221].

5.3 STOPS

The stop is arguably the most sought-after SUSY state because of its unique role in cancelling the quadratic sensitivity to the new physics scale in the Higgs boson mass corrections from top quarks [219]. In addition, if the soft scalar masses are unified at some high scale, the stops are often the lightest accessible squarks. We thus study the reach of future colliders in probing stops. Because of its color and spin quantum numbers, the stop has a lower production cross section than the gluino. Including NLO + NLL QCD corrections [220], for a stop mass of 1.5 TeV it is

$$0.4 \text{ fb at } 14 \text{ TeV and } 9.2 \text{ fb at } 27 \text{ TeV.}$$

As in the previous section, the 27 TeV NLO + NLL K-factor has been estimated from the 33 TeV cross section and the rate is enhanced by a factor of 23 from 14 TeV to 27 TeV. We restrict ourselves to the case where $\tilde{t} \rightarrow t + \tilde{\chi}^0$ with 100% branching fraction. Owing to the different possible decay modes of the tops, there are several possible final states, involving b -jets and missing energy with either 0, 1 or 2 leptons. Because of the $\approx 20\%$ leptonic branching fraction of the W boson produced in each top decay, the final states with more leptons are more rare despite being cleaner to search for experimentally due to lower backgrounds. Guided by existing limits [230, 231, 232], we choose to estimate the reach of an all-hadronic stop search with similar methodology to [233]. Our final state of interest is thus six jets and missing energy, including two b -tagged jets, and with two triplets of jets each forming tops. The background from SM processes in this state is dominated by $t\bar{t}$ and $t\bar{t}Z$ production, with smaller contributions from $t\bar{t}W$ and $V + \text{jets}$ which we neglect. We generate signal and background events using the same pipeline as for the gluino search above.

To extract the signal, we begin by imposing the baseline cuts as in Eq. (5.1). We once again reject events with leptons by requiring that signal events contain no electrons (muons) with p_T above 20 (10) GeV and $|\eta|$ below 2.5 (2.4). We further require the leading two (next four) jets to have $p_T > 80$ (35) GeV and $|\eta| < 2.5$, with at least two b -tagged jets. Next, we require a minimum angular separation between the three leading jets and the \cancel{E}_T

$m(\tilde{t}, \tilde{\chi}^0)$	(500, 300)	(1500, 300)	Background
Generator-level cuts	662	0.40	$2.92 \cdot 10^5$
Lepton veto	473	0.31	$1.44 \cdot 10^5$
Jet $p_T > (80, 80, 35, 35, 35, 35)$ GeV	34.2	0.07	$3.14 \cdot 10^3$
2 b -jets	17.3	0.05	$1.69 \cdot 10^3$
$\Delta\phi(j_{1,2,3}, \cancel{E}_T) > 0.2\pi$	10.1	0.04	843
Top reconstruction	4.7	0.01	301
$m_T(b) > 300$ GeV	0.09	–	0.61
$\cancel{E}_T > 300$ GeV	0.03	–	0.43
$m_T(b) > 400$ GeV	–	0.005	0.15
$\cancel{E}_T > 800$ GeV	–	0.002	0.002

Table 4: Cut flow for the two stop benchmark points in Eq. (5.5) at HL-LHC. At each step, the cross section remaining after the indicated cut is shown in fb. The baseline cuts are identical for both points.

of $\Delta\phi(j, \cancel{E}_T) > 0.2\pi$. We then reconstruct hadronic top quarks as follows [234]. The two closest jets in $\Delta R = \sqrt{\Delta\phi^2 + \Delta\eta^2}$ are considered as a W candidate from the top decay, and the next-closest jet to the W candidate is combined to form a top candidate. Then, the same technique is applied to the remaining jets in the event, to extract the second top. If the mass of either top candidate is outside the region [80, 270] GeV, the event is rejected. Following the preceding selections, we optimize further cuts on \cancel{E}_T over the interval [300, 1000] ([300, 2500]) GeV, and the bottom transverse mass m_T^b over the interval [200, 600] ([200, 1500]) GeV, where the latter is constructed using the b -jet with the least angular separation from the \cancel{E}_T .

To present the qualitative features of our analyses, we once again choose two benchmark points, with stop and LSP masses

$$m(\tilde{t}, \tilde{\chi}^0) = (500 \text{ GeV}, 300 \text{ GeV}) \text{ and } (1500 \text{ GeV}, 300 \text{ GeV}). \quad (5.5)$$

Again, the first point represents the nearly-degenerate (compressed) mass spectrum—a challenging scenario for collider searches. The second set has a standard light LSP, yielding large missing energy. Table 4 shows the cut flows for two benchmark stop scenarios. Once again, the more compressed point benefits from looser cuts. Figure 22 then shows the kinematic distributions after applying all cuts except for the optimized cut on \cancel{E}_T for these benchmarks, demonstrating that at the expense of allowing more background, we achieve better significance for more compressed stops by retaining events with low \cancel{E}_T . It is primarily due to the optimization of our cuts that we are able to achieve greater sensitivity than the ATLAS study, which varied the \cancel{E}_T and $m_T(b)$ cuts simultaneously with the stop mass.

The results are shown in Figure 23, demonstrating that for a massless LSP, a stop of approximately 1.5 TeV can be probed by the HL-LHC with 3 ab^{-1} of integrated luminosity. At 27 TeV with 15 ab^{-1} of integrated luminosity, the exclusion (discovery) reach is roughly 2.7 (2.3) TeV. Unlike the gluino case, a direct comparison with an even higher potential collider is more difficult because of the challenges in reconstructing boosted top quarks. However, discovery of 5.5 TeV stops may be achieved at a 100 TeV collider with 3 ab^{-1} of data using new top tagging techniques [235], or even 8 TeV stops with 30 ab^{-1} of data [236].

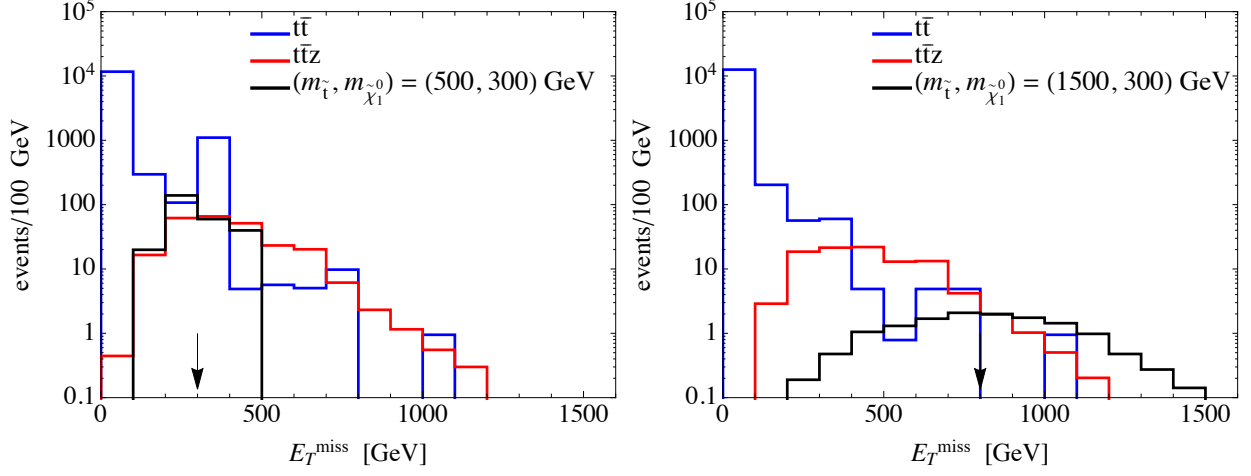


Figure 22: The \cancel{E}_T distribution after all cuts except for that on the \cancel{E}_T are applied, at HL-LHC. In the left/right panel, the signal corresponds to the benchmark points in Eq. (5.5). The arrows indicate the final cuts on \cancel{E}_T for the chosen signal regions.

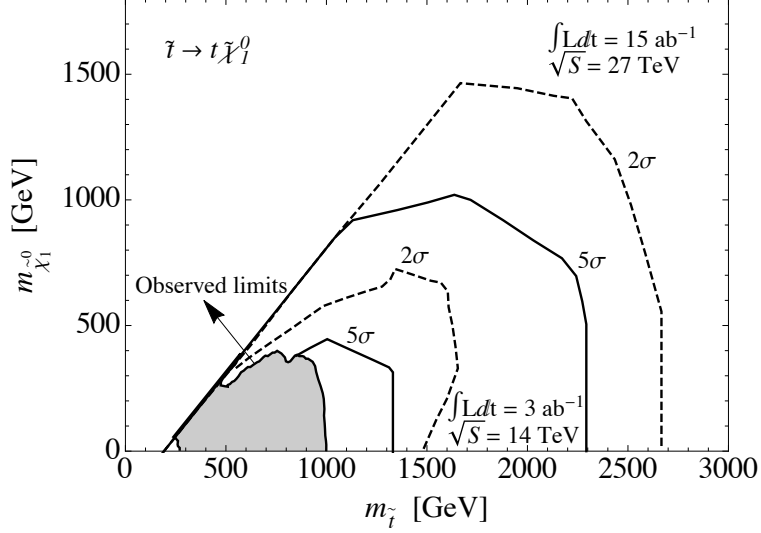


Figure 23: The expected reach of LHC upgrades in probing stops decaying through $\tilde{t} \rightarrow t\tilde{\chi}_1^0$ in the stop-LSP mass plane. The plot shows the stop mass reach at 14 (27) TeV with 3 ab^{-1} (15 ab^{-1}) of data. The shaded region indicates the current observed limits from the LHC.

5.4 DISCUSSION AND CONCLUSIONS

In this work, we have evaluated the reach of the high-luminosity and high-energy upgrades of the LHC in searching for signals of strongly produced supersymmetry. Using simplified models based on production of gluinos and stops, two of the new particles most closely tied to the tuning of the electroweak scale in supersymmetry, we have adapted the existing experimental analyses, optimizing cuts to maximize the sensitivity to both conventional and compressed mass spectra. For gluinos, we find that the HL-LHC and HE-LHC have discovery reach up to masses of 2.8 and 5.2 TeV, respectively. Similarly, our study shows that the HL-LHC and HE-LHC can discover stops with masses up to 1.3 and 2.3 TeV.

Our results for HL-LHC are slightly better than those in existing experimental projections. The main reason for the improvement is that we have adjusted two cuts in each of our analyses to aid in discerning signal from background, which is expected to yield better reach than applying a fixed set of cuts for all potential super-partner masses, or even than performing a one-dimensional optimization. Conversely, it is possible that changing more cuts or even more sophisticated search strategies could improve the results that we have found. As an example, a recent ATLAS search for the same gluino simplified model as we have considered excluded gluinos at 2.0 TeV with 36 fb^{-1} of integrated luminosity. This analysis used a combination of an m_{eff} -based search as we have performed but with additional cuts, as well as signal regions constructed using the recursive jigsaw reconstruction technique. Extrapolating this gluino exclusion up to the HE-LHC by scaling the gluon parton distribution function would yield an expected exclusion of over 7 TeV, suggesting that further refinements could be made to our search. Nevertheless, our results provide a useful estimate of the practical reach that an upgraded LHC could achieve in searching for stops and gluinos. Our procedure should serve as useful guidance for future analyses.

Finally, we comment that while we have considered only simplified models with two particles, in a more complicated scenario it would be more involved to determine the reach of a future collider. For instance, intermediate electroweak gauginos between the strongly produced particle and the LSP would give final states with leptons, which we have not considered, and a variety of different cascade decays would be possible depending on the

super-partner mass splittings and mixings.

As the LHC continues to acquire more data, it is important to assess the sensitivity of its potential successors to BSM theories. Here, we have studied the reach of the high luminosity and high energy upgrades of the LHC in probing gluinos and stops in supersymmetry. Further work is warranted to continue the exploration of the ability of these machines and beyond to explore new physics at the energy frontier.

6.0 CONCLUSIONS

We study the neutrino portal dark matter which explains non-baryonic dark matter and the neutrino masses at the same time and explores their connection. We also calculate the sensitivities of the High Luminosity (HL) and High Energy (HE) upgrades of the Large Hadron Collider (LHC) to strong supersymmetry signals.

In Ref [41], we have investigated a simple model of neutrino portal DM, in which the RHNs simultaneously generate light neutrino masses via the Type-I seesaw mechanism and mediate interactions of DM with the SM. The model is quite minimal and contains a dark sector composed of a fermion χ (the DM candidate) and scalar ϕ , along with the RHN N . Given the generic expectation of tiny neutrino Yukawa couplings, testing this model with direct detection or accelerator experiments is likely to be challenging. However, it is possible in this model that DM efficiently annihilates to RHNs, which allows for a number of indirect probes of this scenario. We have carried out an extensive characterization of the indirect detection phenomenology of the neutrino portal DM scenario. Restricting to an experimentally and theoretically viable mass range, $1 \text{ GeV} \lesssim m_N < m_\chi \lesssim 10 \text{ TeV}$, we have derived the constraints on the $\chi\chi \rightarrow NN$ annihilation cross section from *Planck* CMB measurements, *Fermi* gamma-ray observations from the Galactic Center and from dSphs, and AMS-02 antiproton observations. This model can also provide a DM interpretation of the *Fermi* Galactic Center gamma ray excess as discussed. We have verified that the predicted spectrum of gamma rays is compatible with the observed excess for RHN and DM masses in the 20 – 60 GeV range and annihilation rates close to the thermal value. However, we have also shown that this interpretation faces some tension with the existing constraints from *Fermi* dSphs and AMS-02 antiprotons (subject of course to various astrophysical uncertainties).

In Ref. [151], We have presented a general analysis of thermal relic DM that annihilates

directly to SM neutrinos through the neutrino portal. This possibility is very well motivated theoretically but has been relatively less well studied than other scenarios involving vector or scalar mediators. Indeed, directly annihilating to light neutrinos can allow for thermal relic dark matter below roughly 10 – 50 GeV without spoiling CMB measurements. The model is simple and economical, adding just three new states, fermions N and χ and a scalar ϕ , with masses from about 10 MeV to $\mathcal{O}(100 \text{ GeV})$. It allows for a very simple cosmological history, with the DM number density being set either by annihilation to light neutrinos or by an initial asymmetry, with annihilation reducing the number density to the measured level. The relatively large dark matter-light neutrino coupling needed for annihilation requires that the sterile neutrino mediator N be (pseudo-)Dirac. We discussed the impact of radiative corrections to the scalar mass, identifying regions of parameter space that do not require fine-tuning. We pointed out an interesting feature of this scenario: the fact that the heavy (mostly N) neutrino decays primarily invisibly into the dark sector, allowing for relatively larger active-sterile mixing angles. We discussed and updated limits on the sterile neutrino in this scenario where it decays invisibly. The direct detection signature of this model was examined and we find that it sets an upper limit on the DM mass of around 10 GeV in the simplest scenario. The impact on the small scale structure of DM, which could signal strong interactions between light neutrinos and DM, was also presented. We identified several new measurements or analyses that can be done to probe large regions of viable parameter space in this setup. First, we discussed the possibility that the heavy, invisibly decaying neutrino required for this scenario can affect the kinematics of charged leptons in Drell-Yan W^\pm production at the LHC. The sizable active-sterile mixing angle needed as well as the large number of W bosons produced at the LHC could allow for unconstrained regions of viable parameter space to be probed by such a measurement. In our simple mock analysis, we only considered e^+ and μ^+ transverse momenta above 30 GeV as in the ATLAS measurement of the W mass. Secondly, we discussed the sensitivity of three-body decays of kaons into the dark sector to this scenario. One virtue of this search is that it scales on the parameters of the model in the same way as the DM annihilation cross section and can therefore probe the parameter space without having to assume particular values of some parameters.

In Ref. [200], we have evaluated the reach of the high-luminosity and high-energy up-

grades of the LHC in searching for signals of strongly produced supersymmetry. Using simplified models based on production of gluinos and stops, two of the new particles most closely tied to the tuning of the electroweak scale in supersymmetry, we have adapted the existing experimental analyses, optimizing cuts to maximize the sensitivity to both conventional and compressed mass spectra. For gluinos, we find that the HL-LHC and HE-LHC have discovery reach up to masses of 2.8 and 5.2 TeV, respectively. Similarly, our study shows that the HL-LHC and HE-LHC can discover stops with masses up to 1.3 and 2.3 TeV. Our results for HL-LHC are slightly better than those in existing experimental projections. The main reason for the improvement is that we have adjusted two cuts in each of our analyses to aid in discerning signal from background, which is expected to yield better reach than applying a fixed set of cuts for all potential super-partner masses, or even than performing a one-dimensional optimization. Conversely, it is possible that changing more cuts or even more sophisticated search strategies could improve the results that we have found. Overall, our procedure should serve as useful guidance for future analyses.

APPENDIX A

BOOSTED SPECTRUM FOR MASSLESS PARTICLES

A.1 BOOSTING THE SPECTRUM OF A MASSLESS PARTICLE

If the spectrum of a massless particle is monoenergetic in frame O with energy E_0 , then the energy spectrum can be shown as

$$f(E) = \delta(E - E_0), \quad \int_0^\infty dE f(E) = 1. \quad (\text{A.1})$$

Now we want to apply a boost, $\boldsymbol{\beta}$, to go to another frame, O' , and find the energy spectrum in that frame. We use our freedom to choose particle direction to be along z axis and boost velocity to lie in $x - z$ plane. Therefore:

$$p^\mu = (E, 0, 0, E), \quad \boldsymbol{\beta} = (\beta \sin \theta, 0, \beta \cos \theta). \quad (\text{A.2})$$

The corresponding Lorentz transformation from O to O' is given by

$$\Lambda = \begin{pmatrix} \gamma & -\gamma\beta s_\theta & 0 & -\gamma\beta c_\theta \\ -\gamma\beta s_\theta & 1 - (\gamma - 1)s_\theta^2 & 0 & (\gamma - 1)s_\theta c_\theta \\ 0 & 0 & 1 & 0 \\ -\gamma\beta c_\theta & (\gamma - 1)s_\theta c_\theta & 0 & 1 - (\gamma - 1)c_\theta^2 \end{pmatrix} \quad (\text{A.3})$$

thus, the energy in O' , E' , is related to energy in O , E , as

$$E' = \gamma(1 - \beta \cos \theta)E. \quad (\text{A.4})$$

In order to obtain the energy spectrum in O' , we need to average over $\cos\theta$ to preserve the isotropicity of original spectrum in O . This means that

$$1 = \int_0^\infty dE f(E) = \int_0^\infty dE' \int_{-1}^1 \frac{d\cos\theta}{2} \frac{1}{\gamma(1-\beta\cos\theta)} \delta\left[\frac{1}{\gamma(1-\beta\cos\theta)} - E_0\right] \quad (\text{A.5})$$

The integral over $\cos\theta$ can be done by using the properties of delta function:

$$\int dx g(x) \delta[h(x)] = \int dx g(x) \sum_i \frac{\delta(x-x_i)}{|h'(x_i)|} = \sum_i \frac{g(x_i)}{|h'(x_i)|} \quad (\text{A.6})$$

where x_i 's are those x 's for which

$$h(x_i) = 0. \quad (\text{A.7})$$

In this case:

$$h(c_\theta) = \frac{E'}{\gamma(1-\beta c_\theta)} - E_0, \quad h'(c_\theta) = \frac{\beta E'}{\gamma(1-\beta c_\theta)^2}, \quad g(c_\theta) = \frac{1}{2} \frac{1}{\gamma(1-\beta c_\theta)} \quad (\text{A.8})$$

and c_{θ_0} is the angle that makes $f(c_\theta)$ zero:

$$h(c_{\theta_0}) = \frac{E'}{\gamma(1-\beta c_{\theta_0})} - E_0 = 0, \quad c_{\theta_0} = \frac{\gamma E_0 - E'}{\beta \gamma E_0}. \quad (\text{A.9})$$

Therefore, we have

$$\frac{g(c_{\theta_0})}{|h'(c_{\theta_0})|} = \frac{E_0/2}{\beta \gamma E_0^2} = \frac{1}{2\beta \gamma E_0}. \quad (\text{A.10})$$

The new spectrum can be obtained from

$$1 = \int_0^\infty \frac{dE'}{2\beta \gamma E_0} \theta[E' - \gamma(1-\beta)E_0] \theta[\gamma(1+\beta)E_0 - E'] \equiv \int_0^\infty dE' f(E') \quad (\text{A.11})$$

A.1.1 Generalization to a Continuous Energy Spectrum

We know the boosted monoenergetic spectrum is related to the original spectrum as

$$\begin{aligned}
 1 &= \int_0^\infty dE \delta(E - E_0) \xrightarrow{\text{boost}} \\
 1 &= \int_0^\infty \frac{dE'}{2\beta\gamma E_0} \theta[E' - \gamma(1 - \beta)E_0] \theta[\gamma(1 + \beta)E_0 - E']. \quad (\text{A.12})
 \end{aligned}$$

A general spectrum can be boosted accordingly by using the sifting property of delta function:

$$1 = \int_0^\infty dE f(E) = \int_0^\infty dE \int_0^\infty dE_0 \delta(E - E_0) f(E_0) = \int_0^\infty dE_0 f(E_0) \int_0^\infty dE \delta(E - E_0) \quad (\text{A.13})$$

$$\begin{aligned}
 \xrightarrow{\text{boost}} 1 &= \int_0^\infty dE_0 f(E_0) \int_0^\infty \frac{dE'}{2\beta\gamma E_0} \theta[E' - \gamma(1 - \beta)E_0] \theta[\gamma(1 + \beta)E_0 - E'] \\
 &= \int_0^\infty dE' \int_0^\infty \frac{dE_0}{2\beta\gamma E_0} f(E_0) \theta[E' - \gamma(1 - \beta)E_0] \theta[\gamma(1 + \beta)E_0 - E']. \quad (\text{A.14})
 \end{aligned}$$

Two step functions give us the range of E_0 for a fixed value of E' as:

$$\frac{E'}{\gamma(1 + \beta)} < E_0 < \frac{E'}{\gamma(1 - \beta)} \xrightarrow{\gamma^2(1 - \beta^2) = 1} \gamma(1 - \beta)E' < E_0 < \gamma(1 + \beta)E'. \quad (\text{A.15})$$

We can apply the limits of integration to rewrite the boosted spectrum

$$1 = \int_0^\infty dE f(E) = \int_0^\infty dE' \int_{\gamma(1 - \beta)E'}^{\gamma(1 + \beta)E'} \frac{dE_0}{2\beta\gamma E_0} f(E_0) \equiv \int_0^\infty dE' f(E'). \quad (\text{A.16})$$

Therefore

$$f(E') = \int_{\gamma(1 - \beta)E'}^{\gamma(1 + \beta)E'} \frac{dE}{2\beta\gamma E} f(E). \quad (\text{A.17})$$

APPENDIX B

BOOSTED SPECTRUM FOR MASSIVE PARTICLES

B.1 BOOSTING THE SPECTRUM OF A MASSIVE PARTICLE

If the spectrum of a massive particle with mass m is monoenergetic in frame O with energy E_0 , then the energy spectrum can be shown as

$$f(E) = \delta(E - E_0), \quad \int_m^\infty dE f(E) = 1. \quad (\text{B.1})$$

Now we want to apply a boost, β , to go to another frame, O' , and find the energy spectrum in that frame. We use our freedom to choose particle direction to be along z axis and boost velocity to lie in $x - z$ plane. Therefore:

$$p^\mu = (E, 0, 0, \sqrt{E^2 - m^2}), \quad \beta = (\beta \sin \theta, 0, \beta \cos \theta). \quad (\text{B.2})$$

The corresponding Lorentz transformation from O to O' is given by

$$\Lambda = \begin{pmatrix} \gamma & -\gamma\beta s_\theta & 0 & -\gamma\beta c_\theta \\ -\gamma\beta s_\theta & 1 - (\gamma - 1)s_\theta^2 & 0 & (\gamma - 1)s_\theta c_\theta \\ 0 & 0 & 1 & 0 \\ -\gamma\beta c_\theta & (\gamma - 1)s_\theta c_\theta & 0 & 1 - (\gamma - 1)c_\theta^2 \end{pmatrix}. \quad (\text{B.3})$$

Thus, the energy in O' , E' , is related to energy in O , E , as

$$E' = \gamma(E - \beta \cos\theta \sqrt{E^2 - m^2}). \quad (\text{B.4})$$

Or equivalently

$$E = \frac{E' + \beta c_\theta \sqrt{E'^2 + \gamma^2 m^2 (\beta^2 c_\theta^2 - 1)}}{\gamma(1 - \beta^2 c_\theta^2)}, \quad (\text{B.5})$$

$$dE = \frac{1}{\gamma(1 - \beta^2 c_\theta^2)} \left[1 + \frac{\beta c_\theta E'}{\sqrt{E'^2 + \gamma^2 m^2 (\beta^2 c_\theta^2 - 1)}} \right] dE'. \quad (\text{B.6})$$

In order to obtain the energy spectrum in O' , we need to average over $\cos\theta$ to preserve the isotropicity of original spectrum in O . This means that

$$1 = \int_m^\infty dE f(E) = \int_{\gamma m}^\infty dE' \int_{-1}^1 \frac{d\cos\theta}{2} \frac{1}{\gamma(1 - \beta^2 c_\theta^2)} \left[1 + \frac{\beta c_\theta E'}{\sqrt{E'^2 + \gamma^2 m^2 (\beta^2 c_\theta^2 - 1)}} \right] \delta \left[\frac{E' + \beta c_\theta \sqrt{E'^2 + \gamma^2 m^2 (\beta^2 c_\theta^2 - 1)}}{\gamma(1 - \beta^2 c_\theta^2)} - E_0 \right]. \quad (\text{B.7})$$

The integral over $\cos\theta$ can be done by using the properties of delta function:

$$\int dx g(x) \delta[h(x)] = \int dx g(x) \sum_i \frac{\delta(x - x_i)}{|h'(x_i)|} = \sum_i \frac{g(x_i)}{|h'(x_i)|} \quad (\text{B.8})$$

where x_i 's are those x 's for which

$$h(x_i) = 0. \quad (\text{B.9})$$

In this case:

$$h(c_\theta) = \frac{E' + \beta c_\theta \sqrt{E'^2 + \gamma^2 m^2 (\beta^2 c_\theta^2 - 1)}}{\gamma(1 - \beta^2 c_\theta^2)} - E_0, \quad g(c_\theta) = \frac{1}{2\gamma(1 - \beta^2 c_\theta^2)} \left[1 + \frac{\beta c_\theta E'}{\sqrt{E'^2 + \gamma^2 m^2 (\beta^2 c_\theta^2 - 1)}} \right] \quad (\text{B.10})$$

and c_{θ_0} is the angle that makes $h(c_\theta)$ zero:

$$c_{\theta_0}^2 = \frac{(\beta^2 \gamma^2 m^2 - \beta^2 E'^2 + 2\gamma \beta^2 E' E_0 - 2\gamma^2 \beta^2 E_0^2) \pm \sqrt{(\beta^2 \gamma^2 m^2 - \beta^2 E'^2 + 2\gamma \beta^2 E' E_0 - 2\gamma^2 \beta^2 E_0^2)^2 - 4(\beta^4 \gamma^2 m^2 - \beta^4 \gamma^2 E_0^2)(-E^2 + 2\gamma E E_0 - \gamma^2 E_0^2)}}{2(\beta^4 \gamma^2 m^2 - \beta^4 \gamma^2 E_0^2)}. \quad (\text{B.11})$$

After simplification we have

$$c_{\theta_0}^2 = \begin{cases} \frac{2\gamma^2(E^2 - m^2)}{2\beta^2\gamma^2(E^2 - m^2)} = \frac{1}{\beta^2}, & + \\ \frac{2(\gamma E_0 - E')^2}{2\beta^2\gamma^2(E^2 - m^2)} = \frac{(\gamma E_0 - E')^2}{\beta^2\gamma^2(E^2 - m^2)}, & - \end{cases}$$

There are four solutions, we choose that solution which is in agreement with massless case,

$c_{\theta_0} = \frac{\gamma E_0 - E'}{\beta \gamma E_0}$. Therefore,

$$c_{\theta_0} = \frac{\gamma E_0 - E'}{\beta \gamma \sqrt{E_0^2 - m^2}}, \quad (\text{B.12})$$

and we have

$$\frac{g(c_{\theta_0})}{|h'(c_{\theta_0})|} = \frac{E'^2 \sqrt{E_0^2 - m^2} - \gamma E' E_0 \sqrt{E_0^2 - m^2} + \gamma \sqrt{E_0^2 - m^2} \sqrt{(\gamma m^2 - E' E_0)^2}}{2\beta \gamma (E_0^2 - m^2) (E'^2 - \gamma^2 m^2)}. \quad (\text{B.13})$$

Because of square root of perfect squared expression, we have

$$\frac{g(c_{\theta_0})}{|h'(c_{\theta_0})|} = \begin{cases} \frac{\sqrt{E_0^2 - m^2}(E'^2 - \gamma E' E_0 + \gamma^2 m^2 - \gamma E' E_0)}{2\beta\gamma(E_0^2 - m^2)(E'^2 - \gamma^2 m^2)} = \frac{(E'^2 - 2\gamma E' E_0 + \gamma^2 m^2)}{2\beta\gamma\sqrt{E_0^2 - m^2}(E'^2 - \gamma^2 m^2)}, & + \\ \frac{\sqrt{E_0^2 - m^2}(E'^2 - \gamma E' E_0 - \gamma^2 m^2 + \gamma E' E_0)}{2\beta\gamma(E_0^2 - m^2)(E'^2 - \gamma^2 m^2)} = \frac{1}{2\beta\gamma\sqrt{E_0^2 - m^2}}, & - \end{cases}$$

Again, we choose that solution which is in agreement with massless case, $\frac{g(c_{\theta_0})}{|h'(c_{\theta_0})|} = \frac{1}{2\beta\gamma E_0}$.

Therefore

$$\frac{g(c_{\theta_0})}{|h'(c_{\theta_0})|} = \frac{1}{2\beta\gamma\sqrt{E_0^2 - m^2}}. \quad (\text{B.14})$$

The new spectrum can be obtained from

$$1 = \int_{\gamma m}^{\infty} \frac{dE'}{2\beta\gamma\sqrt{E_0^2 - m^2}} \theta[E' - \gamma(E_0 - \beta\sqrt{E_0^2 - m^2})] \theta[\gamma(E_0 + \beta\sqrt{E_0^2 - m^2}) - E'] \equiv \int_{\gamma m}^{\infty} dE' f(E'). \quad (\text{B.15})$$

B.1.1 Generalization to a Continious Energy Spectrum

We know the boosted monoenergetic spectrum is related to the original spectrum as

$$1 = \int_m^{\infty} dE \delta(E - E_0) \xrightarrow{\text{boost}} 1 = \int_{\gamma m}^{\infty} \frac{dE'}{2\beta\gamma\sqrt{E_0^2 - m^2}} \theta[E' - \gamma(E_0 - \beta\sqrt{E_0^2 - m^2})] \theta[\gamma(E_0 + \beta\sqrt{E_0^2 - m^2}) - E'] . \quad (\text{B.16})$$

A general spectrum can be boosted accordingly by using the sifting property of delta function:

$$1 = \int_m^{\infty} dE f(E) = \int_m^{\infty} dE \int_m^{\infty} dE_0 \delta(E - E_0) f(E_0) = \int_m^{\infty} dE_0 f(E_0) \int_m^{\infty} dE \delta(E - E_0) \quad (\text{B.17})$$

$\xrightarrow{\text{boost}}$

$$\begin{aligned}
1 &= \int_m^\infty dE_0 f(E_0) \int_{\gamma m}^\infty \frac{dE'}{2\beta\gamma\sqrt{E_0^2 - m^2}} \theta[E' - \gamma(E_0 - \beta\sqrt{E_0^2 - m^2})] \\
&\times \theta[\gamma(E_0 + \beta\sqrt{E_0^2 - m^2}) - E'] \\
&= \int_{\gamma m}^\infty dE' \int_m^\infty \frac{dE_0}{2\beta\gamma\sqrt{E_0^2 - m^2}} f(E_0) \theta[E' - \gamma(E_0 - \beta\sqrt{E_0^2 - m^2})] \\
&\times \theta[\gamma(E_0 + \beta\sqrt{E_0^2 - m^2}) - E']
\end{aligned} \tag{B.18}$$

Two step functions give us the range of E_0 for a fixed value of E' as:

$$\begin{aligned}
\gamma(E_0 - \beta\sqrt{E_0^2 - m^2}) < E' &\xrightarrow[c_\theta=1]{\text{Eq. (B.5)}} E_0 < \frac{E' + \beta\sqrt{E'^2 + \gamma^2 m^2(\beta^2 - 1)}}{\gamma(1 - \beta^2)} \\
&\xrightarrow{\gamma^2(1-\beta^2)=1} E_0 < \gamma(E' + \beta\sqrt{E'^2 - m^2}),
\end{aligned} \tag{B.19}$$

$$\begin{aligned}
E' < \gamma(E_0 + \beta\sqrt{E_0^2 - m^2}) &\xrightarrow[c_\theta=-1]{\text{Eq. (B.5)}} E_0 > \frac{E' - \beta\sqrt{E'^2 + \gamma^2 m^2(\beta^2 - 1)}}{\gamma(1 - \beta^2)} \\
&\xrightarrow{\gamma^2(1-\beta^2)=1} E_0 > \gamma(E' - \beta\sqrt{E'^2 - m^2}).
\end{aligned} \tag{B.20}$$

Altogether

$$\gamma(E' - \beta\sqrt{E'^2 - m^2}) < E_0 < \gamma(E' + \beta\sqrt{E'^2 - m^2}). \tag{B.21}$$

We can apply the limits of integration to rewrite the boosted spectrum

$$\begin{aligned}
1 &= \int_m^\infty dE f(E) = \int_{\gamma m}^\infty dE' \int_{\gamma(E' - \beta\sqrt{E'^2 - m^2})}^{\gamma(E' + \beta\sqrt{E'^2 - m^2})} \frac{dE_0}{2\beta\gamma\sqrt{E_0^2 - m^2}} f(E_0) \\
&\equiv \int_{\gamma m}^\infty dE' f(E').
\end{aligned} \tag{B.22}$$

Therefore

$$f(E') = \int_{\gamma(E'-\beta\sqrt{E'^2-m^2})}^{\gamma(E'+\beta\sqrt{E'^2-m^2})} \frac{dE}{2\beta\gamma\sqrt{E^2-m^2}} f(E), \quad (\text{B.23})$$

which in the massless limit returns the correct result

$$\begin{aligned} \lim_{m \rightarrow 0} f(E')_{\text{massive}} &= \lim_{m \rightarrow 0} \int_{\gamma(E'-\beta\sqrt{E'^2-m^2})}^{\gamma(E'+\beta\sqrt{E'^2-m^2})} \frac{dE}{2\beta\gamma\sqrt{E^2-m^2}} f(E) \\ &= \int_{\gamma(1-\beta)E'}^{\gamma(1+\beta)E'} \frac{dE}{2\beta\gamma E} f(E) \xrightarrow{\text{Eq. (A.17)}} f(E')_{\text{massless}}. \end{aligned} \quad (\text{B.24})$$

BIBLIOGRAPHY

- [1] H. K. Dreiner, H. E. Haber and S. P. Martin, Phys. Rept. **494**, 1 (2010) doi:10.1016/j.physrep.2010.05.002 [arXiv:0812.1594 [hep-ph]].
- [2] Y. Fukuda *et al.* [Super-Kamiokande Collaboration], Phys. Rev. Lett. **81**, 1562 (1998) doi:10.1103/PhysRevLett.81.1562 [hep-ex/9807003]; Y. Fukuda *et al.* [Super-Kamiokande Collaboration], Phys. Rev. Lett. **82**, 2644 (1999) doi:10.1103/PhysRevLett.82.2644 [hep-ex/9812014]; S. Fukuda *et al.* [Super-Kamiokande Collaboration], Phys. Rev. Lett. **85**, 3999 (2000) doi:10.1103/PhysRevLett.85.3999 [hep-ex/0009001].
- [3] Q. R. Ahmad *et al.* [SNO Collaboration], Phys. Rev. Lett. **87**, 071301 (2001) doi:10.1103/PhysRevLett.87.071301 [nucl-ex/0106015]; Q. R. Ahmad *et al.* [SNO Collaboration], Phys. Rev. Lett. **89**, 011301 (2002) doi:10.1103/PhysRevLett.89.011301 [nucl-ex/0204008]; Q. R. Ahmad *et al.* [SNO Collaboration], Phys. Rev. Lett. **89**, 011302 (2002) doi:10.1103/PhysRevLett.89.011302 [nucl-ex/0204009].
- [4] K. Eguchi *et al.* [KamLAND Collaboration], Phys. Rev. Lett. **90**, 021802 (2003) doi:10.1103/PhysRevLett.90.021802 [hep-ex/0212021].
- [5] B. T. Cleveland, T. Daily, R. Davis, Jr., J. R. Distel, K. Lande, C. K. Lee, P. S. Wildenhain and J. Ullman, Astrophys. J. **496**, 505 (1998). doi:10.1086/305343
- [6] S. Fukuda *et al.* [Super-Kamiokande Collaboration], Phys. Rev. Lett. **86**, 5651 (2001) doi:10.1103/PhysRevLett.86.5651 [hep-ex/0103032].
- [7] W. W. M. Allison *et al.* [Soudan-2 Collaboration], Phys. Lett. B **449**, 137 (1999) doi:10.1016/S0370-2693(99)00056-8 [hep-ex/9901024].
- [8] P. Minkowski, Phys. Lett. **B67**, 421 (1977); T. Yanagida, in *Proc. of the Workshop on Grand Unified Theory and Baryon Number of the Universe*, KEK, Japan, 1979; M. Gell-Mann, P. Ramond and R. Slansky in *Sanibel Symposium*, February 1979, CALT-68-709 [retroprint arXiv:hep-ph/9809459], and in *Supergravity*, eds. D. Freedman *et al.* (North Holland, Amsterdam, 1979); S. L. Glashow in *Quarks and Leptons, Cargese*, eds. M. Levy *et al.* (Plenum, 1980, New York), p. 707; R. N. Mohapatra and G. Senjanovic, Phys. Rev. Lett. **44**, 912 (1980); J. Schechter and J. W. F. Valle, Phys. Rev. D **22**, 2227 (1980).

- [9] R. Haag, J. T. Lopuszanski and M. Sohnius, Nucl. Phys. B **88**, 257 (1975). doi:10.1016/0550-3213(75)90279-5
- [10] S. R. Coleman and J. Mandula, Phys. Rev. **159**, 1251 (1967). doi:10.1103/PhysRev.159.1251
- [11] P. Fayet, Phys. Lett. **64B**, 159 (1976). doi:10.1016/0370-2693(76)90319-1
- [12] P. Fayet, Phys. Lett. **69B**, 489 (1977). doi:10.1016/0370-2693(77)90852-8; P. Fayet, Phys. Lett. **84B**, 416 (1979). doi:10.1016/0370-2693(79)91229-2
- [13] G. R. Farrar and P. Fayet, Phys. Lett. **76B**, 575 (1978). doi:10.1016/0370-2693(78)90858-4
- [14] J. C. Pati and A. Salam, Phys. Rev. D **10**, 275 (1974) Erratum: [Phys. Rev. D **11**, 703 (1975)]. doi:10.1103/PhysRevD.10.275, 10.1103/PhysRevD.11.703.2
- [15] H. Georgi and S. L. Glashow, Phys. Rev. Lett. **32**, 438 (1974). doi:10.1103/PhysRevLett.32.438
- [16] H. Georgi, H. R. Quinn and S. Weinberg, Phys. Rev. Lett. **33**, 451 (1974). doi:10.1103/PhysRevLett.33.451
- [17] S. Dimopoulos, S. Raby and F. Wilczek, Phys. Rev. D **24**, 1681 (1981). doi:10.1103/PhysRevD.24.1681
- [18] J. R. Ellis, S. Kelley and D. V. Nanopoulos, Phys. Lett. B **249**, 441 (1990). doi:10.1016/0370-2693(90)91013-2
- [19] P. Langacker and M. x. Luo, Phys. Rev. D **44**, 817 (1991). doi:10.1103/PhysRevD.44.817
- [20] V. A. Rubakov and D. S. Gorbunov, doi:10.1142/10447
- [21] V. C. Rubin and W. K. Ford, Jr., Astrophys. J. **159**, 379 (1970). doi:10.1086/150317
- [22] V. C. Rubin, N. Thonnard and W. K. Ford, Jr., Astrophys. J. **238**, 471 (1980). doi:10.1086/158003
- [23] M. Markevitch *et al.*, Astrophys. J. **606**, 819 (2004) doi:10.1086/383178 [astro-ph/0309303].
- [24] D. Clowe, M. Bradac, A. H. Gonzalez, M. Markevitch, S. W. Randall, C. Jones and D. Zaritsky, Astrophys. J. **648**, L109 (2006) doi:10.1086/508162 [astro-ph/0608407].
- [25] N. Aghanim *et al.* [Planck Collaboration], arXiv:1807.06209 [astro-ph.CO].
- [26] S. D. M. White, C. S. Frenk and M. Davis, Astrophys. J. **274**, L1 (1983). doi:10.1086/161425

- [27] S. Tremaine and J. E. Gunn, Phys. Rev. Lett. **42**, 407 (1979). doi:10.1103/PhysRevLett.42.407
- [28] M. Drewes *et al.*, JCAP **1701**, no. 01, 025 (2017) doi:10.1088/1475-7516/2017/01/025 [arXiv:1602.04816 [hep-ph]].
- [29] T. Appelquist, H. C. Cheng and B. A. Dobrescu, Phys. Rev. D **64**, 035002 (2001) doi:10.1103/PhysRevD.64.035002 [hep-ph/0012100].
- [30] G. Servant and T. M. P. Tait, Nucl. Phys. B **650**, 391 (2003) doi:10.1016/S0550-3213(02)01012-X [hep-ph/0206071].
- [31] R. D. Peccei and H. R. Quinn, Phys. Rev. Lett. **38**, 1440 (1977). doi:10.1103/PhysRevLett.38.1440
- [32] S. Weinberg, Phys. Rev. Lett. **40**, 223 (1978). doi:10.1103/PhysRevLett.40.223
- [33] F. Wilczek, Phys. Rev. Lett. **40**, 279 (1978). doi:10.1103/PhysRevLett.40.279
- [34] P. Langacker, Boca Raton, USA: CRC Pr. (2010) 663 p
- [35] P. Svrcek and E. Witten, JHEP **0606**, 051 (2006) doi:10.1088/1126-6708/2006/06/051 [hep-th/0605206].
- [36] M. W. Goodman and E. Witten, Phys. Rev. D **31**, 3059 (1985). doi:10.1103/PhysRevD.31.3059
- [37] M. Tanabashi *et al.* [Particle Data Group], Phys. Rev. D **98**, no. 3, 030001 (2018). doi:10.1103/PhysRevD.98.030001
- [38] J. Engel, S. Pittel and P. Vogel, Int. J. Mod. Phys. E **1**, 1 (1992). doi:10.1142/S0218301392000023
- [39] W. H. Press and D. N. Spergel, Astrophys. J. **296**, 679 (1985). doi:10.1086/163485
- [40] J. Silk, K. A. Olive and M. Srednicki, Phys. Rev. Lett. **55**, 257 (1985). doi:10.1103/PhysRevLett.55.257
- [41] B. Batell, T. Han and B. Shams Es Haghi, Phys. Rev. D **97**, no. 9, 095020 (2018) doi:10.1103/PhysRevD.97.095020 [arXiv:1704.08708 [hep-ph]].
- [42] G. Jungman, M. Kamionkowski and K. Griest, Phys. Rept. **267**, 195 (1996) doi:10.1016/0370-1573(95)00058-5 [hep-ph/9506380].
- [43] L. Bergström, Rept. Prog. Phys. **63**, 793 (2000) doi:10.1088/0034-4885/63/5/2r3 [hep-ph/0002126].
- [44] G. Bertone, D. Hooper and J. Silk, Phys. Rept. **405**, 279 (2005) doi:10.1016/j.physrep.2004.08.031 [hep-ph/0404175].

- [45] J. L. Feng, *Ann. Rev. Astron. Astrophys.* **48**, 495 (2010) doi:10.1146/annurev-astro-082708-101659 [arXiv:1003.0904 [astro-ph.CO]].
- [46] V. Silveira and A. Zee, *Phys. Lett.* **161B**, 136 (1985). doi:10.1016/0370-2693(85)90624-0
- [47] B. Patt and F. Wilczek, hep-ph/0605188.
- [48] P. Galison and A. Manohar, *Phys. Lett.* **136B**, 279 (1984). doi:10.1016/0370-2693(84)91161-4
- [49] B. Holdom, *Phys. Lett.* **166B**, 196 (1986). doi:10.1016/0370-2693(86)91377-8
- [50] J. McDonald, *Phys. Rev. D* **50**, 3637 (1994) doi:10.1103/PhysRevD.50.3637 [hep-ph/0702143 [HEP-PH]].
- [51] C. P. Burgess, M. Pospelov and T. ter Veldhuis, *Nucl. Phys. B* **619**, 709 (2001) doi:10.1016/S0550-3213(01)00513-2 [hep-ph/0011335].
- [52] K. Assamagan *et al.*, arXiv:1604.05324 [hep-ph].
- [53] M. Pospelov, A. Ritz and M. B. Voloshin, *Phys. Lett. B* **662**, 53 (2008) doi:10.1016/j.physletb.2008.02.052 [arXiv:0711.4866 [hep-ph]].
- [54] N. Arkani-Hamed, D. P. Finkbeiner, T. R. Slatyer and N. Weiner, *Phys. Rev. D* **79**, 015014 (2009) doi:10.1103/PhysRevD.79.015014 [arXiv:0810.0713 [hep-ph]].
- [55] J. Alexander *et al.*, arXiv:1608.08632 [hep-ph].
- [56] Y. L. Tang and S. h. Zhu, arXiv:1609.07841 [hep-ph].
- [57] Y. L. Tang and S. h. Zhu, *JHEP* **1603**, 043 (2016) doi:10.1007/JHEP03(2016)043 [arXiv:1512.02899 [hep-ph]].
- [58] M. Ajello *et al.* [Fermi-LAT Collaboration], *Astrophys. J.* **819**, no. 1, 44 (2016) doi:10.3847/0004-637X/819/1/44 [arXiv:1511.02938 [astro-ph.HE]].
- [59] L. Goodenough and D. Hooper, arXiv:0910.2998 [hep-ph].
- [60] D. Hooper and L. Goodenough, *Phys. Lett. B* **697**, 412 (2011) doi:10.1016/j.physletb.2011.02.029 [arXiv:1010.2752 [hep-ph]].
- [61] T. Daylan, D. P. Finkbeiner, D. Hooper, T. Linden, S. K. N. Portillo, N. L. Rodd and T. R. Slatyer, *Phys. Dark Univ.* **12**, 1 (2016) doi:10.1016/j.dark.2015.12.005 [arXiv:1402.6703 [astro-ph.HE]].
- [62] F. Calore, I. Cholis and C. Weniger, *JCAP* **1503**, 038 (2015) doi:10.1088/1475-7516/2015/03/038 [arXiv:1409.0042 [astro-ph.CO]].
- [63] M. D. Campos, F. S. Queiroz, C. E. Yaguna and C. Weniger, arXiv:1702.06145 [hep-ph].

- [64] A. Falkowski, J. Juknevich and J. Shelton, arXiv:0908.1790 [hep-ph].
- [65] Z. Kang and T. Li, JHEP **1102**, 035 (2011) doi:10.1007/JHEP02(2011)035 [arXiv:1008.1621 [hep-ph]].
- [66] A. Falkowski, J. T. Ruderman and T. Volansky, JHEP **1105**, 106 (2011) doi:10.1007/JHEP05(2011)106 [arXiv:1101.4936 [hep-ph]].
- [67] J. F. Cherry, A. Friedland and I. M. Shoemaker, arXiv:1411.1071 [hep-ph].
- [68] V. Gonzalez Macias and J. Wudka, JHEP **1507**, 161 (2015) doi:10.1007/JHEP07(2015)161 [arXiv:1506.03825 [hep-ph]].
- [69] V. Gonzalez-Macias, J. I. Illana and J. Wudka, JHEP **1605**, 171 (2016) doi:10.1007/JHEP05(2016)171 [arXiv:1601.05051 [hep-ph]].
- [70] M. Escudero, N. Rius and V. Sanz, arXiv:1606.01258 [hep-ph].
- [71] M. Escudero, N. Rius and V. Sanz, arXiv:1607.02373 [hep-ph].
- [72] R. Allahverdi, Y. Gao, B. Knockel and S. Shalgar, arXiv:1612.03110 [hep-ph].
- [73] B. Bertoni, S. Ipek, D. McKeen and A. E. Nelson, JHEP **1504**, 170 (2015) doi:10.1007/JHEP04(2015)170 [arXiv:1412.3113 [hep-ph]].
- [74] A. Ibarra, S. Lopez-Gehler, E. Molinaro and M. Pato, Phys. Rev. D **94**, no. 10, 103003 (2016) doi:10.1103/PhysRevD.94.103003 [arXiv:1604.01899 [hep-ph]].
- [75] G. Steigman, B. Dasgupta and J. F. Beacom, Phys. Rev. D **86**, 023506 (2012) doi:10.1103/PhysRevD.86.023506 [arXiv:1204.3622 [hep-ph]].
- [76] K. Griest and M. Kamionkowski, Phys. Rev. Lett. **64**, 615 (1990). doi:10.1103/PhysRevLett.64.615
- [77] A. Boyarsky, O. Ruchayskiy and M. Shaposhnikov, Ann. Rev. Nucl. Part. Sci. **59**, 191 (2009) doi:10.1146/annurev.nucl.010909.083654 [arXiv:0901.0011 [hep-ph]].
- [78] O. Ruchayskiy and A. Ivashko, JCAP **1210**, 014 (2012) doi:10.1088/1475-7516/2012/10/014 [arXiv:1202.2841 [hep-ph]].
- [79] P. Bandyopadhyay, E. J. Chun and J. C. Park, JHEP **1106**, 129 (2011) doi:10.1007/JHEP06(2011)129 [arXiv:1105.1652 [hep-ph]].
- [80] J. Alwall *et al.*, JHEP **1407**, 079 (2014) doi:10.1007/JHEP07(2014)079 [arXiv:1405.0301 [hep-ph]].
- [81] D. Alva, T. Han and R. Ruiz, JHEP **1502**, 072 (2015) doi:10.1007/JHEP02(2015)072 [arXiv:1411.7305 [hep-ph]].

- [82] C. Degrande, O. Mattelaer, R. Ruiz and J. Turner, Phys. Rev. D **94**, no. 5, 053002 (2016) doi:10.1103/PhysRevD.94.053002 [arXiv:1602.06957 [hep-ph]].
- [83] T. Sjostrand, S. Mrenna and P. Z. Skands, Comput. Phys. Commun. **178**, 852 (2008) doi:10.1016/j.cpc.2008.01.036 [arXiv:0710.3820 [hep-ph]].
- [84] J. Mardon, Y. Nomura, D. Stolarski and J. Thaler, JCAP **0905**, 016 (2009) doi:10.1088/1475-7516/2009/05/016 [arXiv:0901.2926 [hep-ph]].
- [85] P. Agrawal, B. Batell, P. J. Fox and R. Harnik, JCAP **1505**, 011 (2015) doi:10.1088/1475-7516/2015/05/011 [arXiv:1411.2592 [hep-ph]].
- [86] G. Elor, N. L. Rodd and T. R. Slatyer, Phys. Rev. D **91**, 103531 (2015) doi:10.1103/PhysRevD.91.103531 [arXiv:1503.01773 [hep-ph]].
- [87] G. Elor, N. L. Rodd, T. R. Slatyer and W. Xue, JCAP **1606**, no. 06, 024 (2016) doi:10.1088/1475-7516/2016/06/024 [arXiv:1511.08787 [hep-ph]].
- [88] G. Hinshaw *et al.* [WMAP Collaboration], Astrophys. J. Suppl. **208**, 19 (2013) doi:10.1088/0067-0049/208/2/19 [arXiv:1212.5226 [astro-ph.CO]].
- [89] K. T. Story *et al.*, Astrophys. J. **779**, 86 (2013) doi:10.1088/0004-637X/779/1/86 [arXiv:1210.7231 [astro-ph.CO]].
- [90] Z. Hou *et al.*, Astrophys. J. **782**, 74 (2014) doi:10.1088/0004-637X/782/2/74 [arXiv:1212.6267 [astro-ph.CO]].
- [91] J. L. Sievers *et al.* [Atacama Cosmology Telescope Collaboration], JCAP **1310**, 060 (2013) doi:10.1088/1475-7516/2013/10/060 [arXiv:1301.0824 [astro-ph.CO]].
- [92] P. A. R. Ade *et al.* [Planck Collaboration], Astron. Astrophys. **594**, A13 (2016) doi:10.1051/0004-6361/201525830 [arXiv:1502.01589 [astro-ph.CO]].
- [93] N. Padmanabhan and D. P. Finkbeiner, Phys. Rev. D **72**, 023508 (2005) doi:10.1103/PhysRevD.72.023508 [astro-ph/0503486].
- [94] L. Zhang, X. L. Chen, Y. A. Lei and Z. G. Si, Phys. Rev. D **74**, 103519 (2006) doi:10.1103/PhysRevD.74.103519 [astro-ph/0603425].
- [95] S. Galli, F. Iocco, G. Bertone and A. Melchiorri, Phys. Rev. D **80**, 023505 (2009) doi:10.1103/PhysRevD.80.023505 [arXiv:0905.0003 [astro-ph.CO]].
- [96] T. R. Slatyer, N. Padmanabhan and D. P. Finkbeiner, Phys. Rev. D **80**, 043526 (2009) doi:10.1103/PhysRevD.80.043526 [arXiv:0906.1197 [astro-ph.CO]].
- [97] T. Kanzaki, M. Kawasaki and K. Nakayama, Prog. Theor. Phys. **123**, 853 (2010) doi:10.1143/PTP.123.853 [arXiv:0907.3985 [astro-ph.CO]].

- [98] J. Hisano, M. Kawasaki, K. Kohri, T. Moroi, K. Nakayama and T. Sekiguchi, Phys. Rev. D **83**, 123511 (2011) doi:10.1103/PhysRevD.83.123511 [arXiv:1102.4658 [hep-ph]].
- [99] G. Hutsi, J. Chluba, A. Hektor and M. Raidal, Astron. Astrophys. **535**, A26 (2011) doi:10.1051/0004-6361/201116914 [arXiv:1103.2766 [astro-ph.CO]].
- [100] S. Galli, F. Iocco, G. Bertone and A. Melchiorri, Phys. Rev. D **84**, 027302 (2011) doi:10.1103/PhysRevD.84.027302 [arXiv:1106.1528 [astro-ph.CO]].
- [101] D. P. Finkbeiner, S. Galli, T. Lin and T. R. Slatyer, Phys. Rev. D **85**, 043522 (2012) doi:10.1103/PhysRevD.85.043522 [arXiv:1109.6322 [astro-ph.CO]].
- [102] T. R. Slatyer, Phys. Rev. D **87**, no. 12, 123513 (2013) doi:10.1103/PhysRevD.87.123513 [arXiv:1211.0283 [astro-ph.CO]].
- [103] S. Galli, T. R. Slatyer, M. Valdes and F. Iocco, Phys. Rev. D **88**, 063502 (2013) doi:10.1103/PhysRevD.88.063502 [arXiv:1306.0563 [astro-ph.CO]].
- [104] L. Lopez-Honorez, O. Mena, S. Palomares-Ruiz and A. C. Vincent, JCAP **1307**, 046 (2013) doi:10.1088/1475-7516/2013/07/046 [arXiv:1303.5094 [astro-ph.CO]].
- [105] M. S. Madhavacheril, N. Sehgal and T. R. Slatyer, Phys. Rev. D **89**, 103508 (2014) doi:10.1103/PhysRevD.89.103508 [arXiv:1310.3815 [astro-ph.CO]].
- [106] T. R. Slatyer, Phys. Rev. D **93**, no. 2, 023527 (2016) doi:10.1103/PhysRevD.93.023527 [arXiv:1506.03811 [hep-ph]].
- [107] T. R. Slatyer, Phys. Rev. D **93**, no. 2, 023521 (2016) doi:10.1103/PhysRevD.93.023521 [arXiv:1506.03812 [astro-ph.CO]].
- [108] J. F. Navarro, C. S. Frenk and S. D. M. White, Astrophys. J. **462**, 563 (1996) doi:10.1086/177173 [astro-ph/9508025].
- [109] J. F. Navarro, C. S. Frenk and S. D. M. White, Astrophys. J. **490**, 493 (1997) doi:10.1086/304888 [astro-ph/9611107].
- [110] J. Einasto Trudy. 1965. Inst.Astrofiz.Alma-Ata.,5,87.
- [111] J. F. Navarro *et al.*, Mon. Not. Roy. Astron. Soc. **402**, 21 (2010) doi:10.1111/j.1365-2966.2009.15878.x [arXiv:0810.1522 [astro-ph]].
- [112] V. Springel *et al.*, Mon. Not. Roy. Astron. Soc. **391**, 1685 (2008) doi:10.1111/j.1365-2966.2008.14066.x [arXiv:0809.0898 [astro-ph]].
- [113] G. R. Blumenthal, S. M. Faber, R. Flores and J. R. Primack, Astrophys. J. **301**, 27 (1986). doi:10.1086/163867
- [114] B. S. Ryden and J. E. Gunn, Astrophys. J. **318**, 15 (1987). doi:10.1086/165349

- [115] O. Y. Gnedin, A. V. Kravtsov, A. A. Klypin and D. Nagai, *Astrophys. J.* **616**, 16 (2004) doi:10.1086/424914 [astro-ph/0406247].
- [116] O. Y. Gnedin, D. Ceverino, N. Y. Gnedin, A. A. Klypin, A. V. Kravtsov, R. Levine, D. Nagai and G. Yepes, arXiv:1108.5736 [astro-ph.CO].
- [117] F. Governato *et al.*, *Mon. Not. Roy. Astron. Soc.* **422**, 1231 (2012) doi:10.1111/j.1365-2966.2012.20696.x [arXiv:1202.0554 [astro-ph.CO]].
- [118] F. Iocco, M. Pato, G. Bertone and P. Jetzer, *JCAP* **1111**, 029 (2011) doi:10.1088/1475-7516/2011/11/029 [arXiv:1107.5810 [astro-ph.GA]].
- [119] S. K. Lee, M. Lisanti and B. R. Safdi, *JCAP* **1505**, no. 05, 056 (2015) doi:10.1088/1475-7516/2015/05/056 [arXiv:1412.6099 [astro-ph.CO]].
- [120] R. Bartels, S. Krishnamurthy and C. Weniger, *Phys. Rev. Lett.* **116**, no. 5, 051102 (2016) doi:10.1103/PhysRevLett.116.051102 [arXiv:1506.05104 [astro-ph.HE]].
- [121] S. K. Lee, M. Lisanti, B. R. Safdi, T. R. Slatyer and W. Xue, *Phys. Rev. Lett.* **116**, no. 5, 051103 (2016) doi:10.1103/PhysRevLett.116.051103 [arXiv:1506.05124 [astro-ph.HE]].
- [122] S. D. McDermott, P. J. Fox, I. Cholis and S. K. Lee, *JCAP* **1607**, no. 07, 045 (2016) doi:10.1088/1475-7516/2016/07/045 [arXiv:1512.00012 [astro-ph.HE]].
- [123] S. Horiuchi, M. Kaplinghat and A. Kwa, *JCAP* **1611**, no. 11, 053 (2016) doi:10.1088/1475-7516/2016/11/053 [arXiv:1604.01402 [astro-ph.HE]].
- [124] D. Hooper, C. Kelso and F. S. Queiroz, *Astropart. Phys.* **46**, 55 (2013) doi:10.1016/j.astropartphys.2013.04.007 [arXiv:1209.3015 [astro-ph.HE]].
- [125] M. Ackermann *et al.* [Fermi-LAT Collaboration], *Phys. Rev. Lett.* **115**, no. 23, 231301 (2015) doi:10.1103/PhysRevLett.115.231301 [arXiv:1503.02641 [astro-ph.HE]].
- [126] M. Aguilar *et al.* [AMS Collaboration], *Phys. Rev. Lett.* **117**, no. 9, 091103 (2016). doi:10.1103/PhysRevLett.117.091103
- [127] M. Boudaud, M. Cirelli, G. Giesen and P. Salati, *JCAP* **1505**, no. 05, 013 (2015) doi:10.1088/1475-7516/2015/05/013 [arXiv:1412.5696 [astro-ph.HE]].
- [128] F. Donato, *Nucl. Phys. Proc. Suppl.* **138**, 303 (2005). doi:10.1016/j.nuclphysbps.2004.11.068
- [129] M. Cirelli *et al.*, *JCAP* **1103**, 051 (2011) Erratum: [*JCAP* **1210**, E01 (2012)] doi:10.1088/1475-7516/2012/10/E01, 10.1088/1475-7516/2011/03/051 [arXiv:1012.4515 [hep-ph]].
- [130] M. Aguilar *et al.* [AMS Collaboration], *Phys. Rev. Lett.* **114**, 171103 (2015). doi:10.1103/PhysRevLett.114.171103

- [131] G. Giesen, M. Boudaud, Y. Giacomolini, V. Poulin, M. Cirelli, P. Salati and P. D. Serpico, JCAP **1509**, no. 09, 023 (2015) doi:10.1088/1475-7516/2015/09/023, 10.1088/1475-7516/2015/9/023 [arXiv:1504.04276 [astro-ph.HE]].
- [132] M. Aguilar *et al.* [AMS Collaboration], Phys. Rev. Lett. **113**, 121102 (2014). doi:10.1103/PhysRevLett.113.121102
- [133] O. Adriani *et al.* [PAMELA Collaboration], Phys. Rev. Lett. **111**, 081102 (2013) doi:10.1103/PhysRevLett.111.081102 [arXiv:1308.0133 [astro-ph.HE]].
- [134] M. G. Aartsen *et al.* [IceCube Collaboration], arXiv:1612.05949 [astro-ph.HE].
- [135] E. Charles *et al.* [Fermi-LAT Collaboration], Phys. Rept. **636**, 1 (2016) doi:10.1016/j.physrep.2016.05.001 [arXiv:1605.02016 [astro-ph.HE]].
- [136] T. Abbott *et al.* [DES Collaboration], astro-ph/0510346.
- [137] D. G. York *et al.* [SDSS Collaboration], Astron. J. **120**, 1579 (2000) doi:10.1086/301513 [astro-ph/0006396].
- [138] Z. Ivezić *et al.* [LSST Collaboration], arXiv:0805.2366 [astro-ph].
- [139] H. Abdallah *et al.* [HESS Collaboration], Phys. Rev. Lett. **117**, no. 11, 111301 (2016) doi:10.1103/PhysRevLett.117.111301 [arXiv:1607.08142 [astro-ph.HE]].
- [140] A. W. Smith *et al.*, arXiv:1304.6367 [astro-ph.HE].
- [141] J. Aleksić *et al.*, JCAP **1402**, 008 (2014) doi:10.1088/1475-7516/2014/02/008 [arXiv:1312.1535 [hep-ph]].
- [142] M. Doro *et al.* [CTA Consortium], Astropart. Phys. **43**, 189 (2013) doi:10.1016/j.astropartphys.2012.08.002 [arXiv:1208.5356 [astro-ph.IM]].
- [143] A. U. Abeysekara *et al.* [HAWC Collaboration], Phys. Rev. D **90**, no. 12, 122002 (2014) doi:10.1103/PhysRevD.90.122002 [arXiv:1405.1730 [astro-ph.HE]].
- [144] E. Moulin [CTA Consortium],
- [145] H. Silverwood, C. Weniger, P. Scott and G. Bertone, JCAP **1503**, no. 03, 055 (2015) doi:10.1088/1475-7516/2015/03/055 [arXiv:1408.4131 [astro-ph.HE]].
- [146] K. Bernlöhr *et al.*, Astropart. Phys. **43**, 171 (2013) doi:10.1016/j.astropartphys.2012.10.002 [arXiv:1210.3503 [astro-ph.IM]].
- [147] R. N. Mohapatra, Phys. Rev. Lett. **56**, 561 (1986). doi:10.1103/PhysRevLett.56.561
- [148] A. Atre, T. Han, S. Pascoli and B. Zhang, JHEP **0905**, 030 (2009) doi:10.1088/1126-6708/2009/05/030 [arXiv:0901.3589 [hep-ph]].

- [149] F. F. Deppisch, P. S. Bhupal Dev and A. Pilaftsis, *New J. Phys.* **17**, no. 7, 075019 (2015) doi:10.1088/1367-2630/17/7/075019 [arXiv:1502.06541 [hep-ph]].
- [150] E. Izaguirre and B. Shuve, *Phys. Rev. D* **91**, no. 9, 093010 (2015) doi:10.1103/PhysRevD.91.093010 [arXiv:1504.02470 [hep-ph]].
- [151] B. Batell, T. Han, D. McKeen and B. Shams Es Haghi, *Phys. Rev. D* **97**, no. 7, 075016 (2018) doi:10.1103/PhysRevD.97.075016 [arXiv:1709.07001 [hep-ph]].
- [152] C. Boehm and P. Fayet, *Nucl. Phys. B* **683**, 219 (2004) doi:10.1016/j.nuclphysb.2004.01.015 [hep-ph/0305261].
- [153] C. Boehm, P. Fayet and J. Silk, *Phys. Rev. D* **69**, 101302 (2004) doi:10.1103/PhysRevD.69.101302 [hep-ph/0311143].
- [154] L. B. Okun, *Sov. Phys. JETP* **56**, 502 (1982) [*Zh. Eksp. Teor. Fiz.* **83**, 892 (1982)].
- [155] A. Berlin, D. Hooper and G. Krnjaic, *Phys. Rev. D* **94**, no. 9, 095019 (2016) doi:10.1103/PhysRevD.94.095019 [arXiv:1609.02555 [hep-ph]].
- [156] G. Krnjaic, *Phys. Rev. D* **94**, no. 7, 073009 (2016) doi:10.1103/PhysRevD.94.073009 [arXiv:1512.04119 [hep-ph]]; Y. L. Tang and S. h. Zhu, *JHEP* **1603**, 043 (2016) doi:10.1007/JHEP03(2016)043 [arXiv:1512.02899 [hep-ph]]; Y. L. Tang and S. h. Zhu, *JHEP* **1701**, 025 (2017) doi:10.1007/JHEP01(2017)025 [arXiv:1609.07841 [hep-ph]]; M. Escudero, N. Rius and V. Sanz, *JHEP* **1702**, 045 (2017) doi:10.1007/JHEP02(2017)045 [arXiv:1606.01258 [hep-ph]]; M. Escudero, N. Rius and V. Sanz, *Eur. Phys. J. C* **77**, no. 6, 397 (2017) doi:10.1140/epjc/s10052-017-4963-x [arXiv:1607.02373 [hep-ph]]; R. Allahverdi, Y. Gao, B. Knockel and S. Shalgar, *Phys. Rev. D* **95**, no. 7, 075001 (2017) doi:10.1103/PhysRevD.95.075001 [arXiv:1612.03110 [hep-ph]]; M. D. Campos, F. S. Queiroz, C. E. Yaguna and C. Weniger, *JCAP* **1707**, no. 07, 016 (2017) doi:10.1088/1475-7516/2017/07/016 [arXiv:1702.06145 [hep-ph]].
- [157] L. M. Krauss and F. Wilczek, *Phys. Rev. Lett.* **62**, 1221 (1989). doi:10.1103/PhysRevLett.62.1221
- [158] B. Pontecorvo, *Sov. Phys. JETP* **26**, 984 (1968) [*Zh. Eksp. Teor. Fiz.* **53**, 1717 (1967)]; B. Pontecorvo, *Sov. Phys. JETP* **6**, 429 (1957) [*Zh. Eksp. Teor. Fiz.* **33**, 549 (1957)]; Z. Maki, M. Nakagawa and S. Sakata, *Prog. Theor. Phys.* **28**, 870 (1962). doi:10.1143/PTP.28.870.
- [159] R. N. Mohapatra and J. W. F. Valle, *Phys. Rev. D* **34**, 1642 (1986). doi:10.1103/PhysRevD.34.1642
- [160] M. Malinsky, J. C. Romao and J. W. F. Valle, *Phys. Rev. Lett.* **95**, 161801 (2005) doi:10.1103/PhysRevLett.95.161801 [hep-ph/0506296].
- [161] E. Izaguirre, G. Krnjaic, P. Schuster and N. Toro, *Phys. Rev. Lett.* **115**, no. 25, 251301 (2015) doi:10.1103/PhysRevLett.115.251301 [arXiv:1505.00011 [hep-ph]].

- [162] P. A. R. Ade *et al.* [Planck Collaboration], *Astron. Astrophys.* **571**, A16 (2014) doi:10.1051/0004-6361/201321591 [arXiv:1303.5076 [astro-ph.CO]].
- [163] P. D. Serpico and G. G. Raffelt, *Phys. Rev. D* **70**, 043526 (2004) doi:10.1103/PhysRevD.70.043526 [astro-ph/0403417]; C. Boehm, M. J. Dolan and C. McCabe, *JCAP* **1308**, 041 (2013) doi:10.1088/1475-7516/2013/08/041 [arXiv:1303.6270 [hep-ph]]; K. M. Nollett and G. Steigman, *Phys. Rev. D* **91**, no. 8, 083505 (2015) doi:10.1103/PhysRevD.91.083505 [arXiv:1411.6005 [astro-ph.CO]].
- [164] F. Iocco, G. Mangano, G. Miele, O. Pisanti and P. D. Serpico, *Phys. Rept.* **472**, 1 (2009) doi:10.1016/j.physrep.2009.02.002 [arXiv:0809.0631 [astro-ph]].
- [165] A. Das, P. Konar and S. Majhi, *JHEP* **1606**, 019 (2016) doi:10.1007/JHEP06(2016)019 [arXiv:1604.00608 [hep-ph]].
- [166] A. de Gouvêa and A. Kobach, *Phys. Rev. D* **93**, no. 3, 033005 (2016) doi:10.1103/PhysRevD.93.033005 [arXiv:1511.00683 [hep-ph]].
- [167] V. Tishchenko *et al.* [MuLan Collaboration], *Phys. Rev. D* **87**, no. 5, 052003 (2013) doi:10.1103/PhysRevD.87.052003 [arXiv:1211.0960 [hep-ex]].
- [168] C. Patrignani *et al.* [Particle Data Group], *Chin. Phys. C* **40**, no. 10, 100001 (2016). doi:10.1088/1674-1137/40/10/100001
- [169] R. Bayes *et al.* [TWIST Collaboration], arXiv:1010.4998 [hep-ex].
- [170] S. N. Gninenko, *Phys. Rev. D* **83**, 015015 (2011) doi:10.1103/PhysRevD.83.015015 [arXiv:1009.5536 [hep-ph]].
- [171] K. Belous *et al.* [Belle Collaboration], *Phys. Rev. Lett.* **112**, no. 3, 031801 (2014) doi:10.1103/PhysRevLett.112.031801 [arXiv:1310.8503 [hep-ex]].
- [172] A. Pich, *Prog. Part. Nucl. Phys.* **75**, 41 (2014) doi:10.1016/j.pnpnp.2013.11.002 [arXiv:1310.7922 [hep-ph]].
- [173] R. Barate *et al.* [ALEPH Collaboration], *Eur. Phys. J. C* **2**, 395 (1998). doi:10.1007/s100520050149
- [174] D. I. Britton *et al.*, *Phys. Rev. D* **46**, R885 (1992). doi:10.1103/PhysRevD.46.R885; M. Aoki *et al.* [PIENU Collaboration], *Phys. Rev. D* **84**, 052002 (2011) doi:10.1103/PhysRevD.84.052002 [arXiv:1106.4055 [hep-ex]]; S. Ito *et al.*, *Hyperfine Interact.* **238**, no. 1, 1 (2017). doi:10.1007/s10751-016-1375-5.
- [175] T. Yamazaki *et al.*, *Conf. Proc. C* **840719**, 262 (1984).
- [176] C. S. Park *et al.* [Belle Collaboration], *Phys. Rev. D* **94**, no. 1, 012003 (2016) doi:10.1103/PhysRevD.94.012003 [arXiv:1605.04430 [hep-ex]].

- [177] R. Abela, M. Daum, G. H. Eaton, R. Frosch, B. Jost, P. R. Kettle and E. Steiner, Phys. Lett. **105B**, 263 (1981) Erratum: [Phys. Lett. **106B**, 513 (1981)]. doi:10.1016/0370-2693(81)90884-4
- [178] R. S. Hayano *et al.*, Phys. Rev. Lett. **49**, 1305 (1982). doi:10.1103/PhysRevLett.49.1305; A. V. Artamonov *et al.* [E949 Collaboration], Phys. Rev. D **91**, no. 5, 052001 (2015) Erratum: [Phys. Rev. D **91**, no. 5, 059903 (2015)] doi:10.1103/PhysRevD.91.059903, 10.1103/PhysRevD.91.052001 [arXiv:1411.3963 [hep-ex]]; C. Lazzeroni *et al.* [NA62 Collaboration], Phys. Lett. B **772**, 712 (2017) doi:10.1016/j.physletb.2017.07.055 [arXiv:1705.07510 [hep-ex]].
- [179] D. I. Britton *et al.*, Phys. Rev. Lett. **68**, 3000 (1992). doi:10.1103/PhysRevLett.68.3000; G. Czapek *et al.*, Phys. Rev. Lett. **70**, 17 (1993). doi:10.1103/PhysRevLett.70.17; W. J. Marciano and A. Sirlin, Phys. Rev. Lett. **71**, 3629 (1993). doi:10.1103/PhysRevLett.71.3629
- [180] A. V. Artamonov *et al.* [E949 Collaboration], Phys. Rev. D **91**, no. 5, 052001 (2015) Erratum: [Phys. Rev. D **91**, no. 5, 059903 (2015)] doi:10.1103/PhysRevD.91.059903, 10.1103/PhysRevD.91.052001 [arXiv:1411.3963 [hep-ex]].
- [181] C. Lazzeroni *et al.* [NA62 Collaboration], Phys. Lett. B **772**, 712 (2017) doi:10.1016/j.physletb.2017.07.055 [arXiv:1705.07510 [hep-ex]].
- [182] E. Cortina Gil *et al.* [NA62 Collaboration], JINST **12**, no. 05, P05025 (2017) doi:10.1088/1748-0221/12/05/P05025 [arXiv:1703.08501 [physics.ins-det]].
- [183] K. Abe *et al.* [Super-Kamiokande Collaboration], Phys. Rev. D **91**, 052019 (2015) doi:10.1103/PhysRevD.91.052019 [arXiv:1410.2008 [hep-ex]].
- [184] V. Khachatryan *et al.* [CMS Collaboration], JHEP **1702**, 135 (2017) doi:10.1007/JHEP02(2017)135 [arXiv:1610.09218 [hep-ex]].
- [185] M. E. Peskin, arXiv:1312.4974 [hep-ph].
- [186] M. Aaboud *et al.* [ATLAS Collaboration], Eur. Phys. J. C **78**, no. 2, 110 (2018) Erratum: [Eur. Phys. J. C **78**, no. 11, 898 (2018)] doi:10.1140/epjc/s10052-018-6354-3, 10.1140/epjc/s10052-017-5475-4 [arXiv:1701.07240 [hep-ex]].
- [187] J. de Favereau *et al.* [DELPHES 3 Collaboration], JHEP **1402**, 057 (2014) doi:10.1007/JHEP02(2014)057 [arXiv:1307.6346 [hep-ex]].
- [188] E. Aprile *et al.* [XENON Collaboration], Phys. Rev. Lett. **119**, no. 18, 181301 (2017) doi:10.1103/PhysRevLett.119.181301 [arXiv:1705.06655 [astro-ph.CO]].
- [189] X. Cui *et al.* [PandaX-II Collaboration], Phys. Rev. Lett. **119**, no. 18, 181302 (2017) doi:10.1103/PhysRevLett.119.181302 [arXiv:1708.06917 [astro-ph.CO]].

- [190] R. Agnese *et al.* [SuperCDMS Collaboration], Phys. Rev. D **95**, no. 8, 082002 (2017) doi:10.1103/PhysRevD.95.082002 [arXiv:1610.00006 [physics.ins-det]].
- [191] F. Ruppin, J. Billard, E. Figueroa-Feliciano and L. Strigari, Phys. Rev. D **90**, no. 8, 083510 (2014) doi:10.1103/PhysRevD.90.083510 [arXiv:1408.3581 [hep-ph]].
- [192] M. Battaglieri *et al.*, arXiv:1707.04591 [hep-ph].
- [193] A. A. Klypin, A. V. Kravtsov, O. Valenzuela and F. Prada, Astrophys. J. **522**, 82 (1999) doi:10.1086/307643 [astro-ph/9901240]; B. Moore, T. R. Quinn, F. Governato, J. Stadel and G. Lake, Mon. Not. Roy. Astron. Soc. **310**, 1147 (1999) doi:10.1046/j.1365-8711.1999.03039.x [astro-ph/9903164];
- [194] C. Boehm, P. Fayet and R. Schaeffer, Phys. Lett. B **518**, 8 (2001) doi:10.1016/S0370-2693(01)01060-7 [astro-ph/0012504].
- [195] C. Boehm, A. Riazuelo, S. H. Hansen and R. Schaeffer, Phys. Rev. D **66**, 083505 (2002) doi:10.1103/PhysRevD.66.083505 [astro-ph/0112522];
- [196] A. M. Green, S. Hofmann and D. J. Schwarz, JCAP **0508**, 003 (2005) doi:10.1088/1475-7516/2005/08/003 [astro-ph/0503387]; A. Loeb and M. Zaldarriaga, Phys. Rev. D **71**, 103520 (2005) doi:10.1103/PhysRevD.71.103520 [astro-ph/0504112].
- [197] L. E. Strigari, J. S. Bullock, M. Kaplinghat, J. D. Simon, M. Geha, B. Willman and M. G. Walker, Nature **454**, 1096 (2008) doi:10.1038/nature07222 [arXiv:0808.3772 [astro-ph]]; P. Jethwa, D. Erkal and V. Belokurov, Mon. Not. Roy. Astron. Soc. **473**, no. 2, 2060 (2018) doi:10.1093/mnras/stx2330 [arXiv:1612.07834 [astro-ph.GA]].
- [198] M. Viel, G. D. Becker, J. S. Bolton and M. G. Haehnelt, Phys. Rev. D **88**, 043502 (2013) doi:10.1103/PhysRevD.88.043502 [arXiv:1306.2314 [astro-ph.CO]].
- [199] S. Vegetti, D. J. Lagattuta, J. P. McKean, M. W. Auger, C. D. Fassnacht and L. V. E. Koopmans, Nature **481**, 341 (2012) doi:10.1038/nature10669 [arXiv:1201.3643 [astro-ph.CO]].
- [200] T. Han, A. Ismail and B. Shams Es Haghi, arXiv:1902.05109 [hep-ph].
- [201] J. L. Feng, Ann. Rev. Nucl. Part. Sci. **63**, 351 (2013) doi:10.1146/annurev-nucl-102010-130447 [arXiv:1302.6587 [hep-ph]].
- [202] G. Apollinari, I. Béjar Alonso, O. Brüning, M. Lamont and L. Rossi, doi:10.5170/CERN-2015-005
- [203] A. Abada *et al.* [FCC Collaboration], CERN-ACC-2018-0059.
- [204] M. Cahill-Rowley, J. L. Hewett, A. Ismail and T. G. Rizzo, Phys. Rev. D **91**, no. 5, 055002 (2015) doi:10.1103/PhysRevD.91.055002 [arXiv:1407.4130 [hep-ph]].

- [205] J. Alwall, M. P. Le, M. Lisanti and J. G. Wacker, Phys. Rev. D **79**, 015005 (2009) doi:10.1103/PhysRevD.79.015005 [arXiv:0809.3264 [hep-ph]].
- [206] J. Alwall, P. Schuster and N. Toro, Phys. Rev. D **79**, 075020 (2009) doi:10.1103/PhysRevD.79.075020 [arXiv:0810.3921 [hep-ph]].
- [207] H. Baer, X. Tata and J. Woodside, Phys. Rev. D **42**, 1568 (1990). doi:10.1103/PhysRevD.42.1568
- [208] H. Baer, J. Sender and X. Tata, Phys. Rev. D **50**, 4517 (1994) doi:10.1103/PhysRevD.50.4517 [hep-ph/9404342].
- [209] Y. Gershtein *et al.*, arXiv:1311.0299 [hep-ex].
- [210] M. Ahmad *et al.*, IHEP-CEPC-DR-2015-01, IHEP-TH-2015-01, IHEP-EP-2015-01.
- [211] N. Arkani-Hamed, T. Han, M. Mangano and L. T. Wang, Phys. Rept. **652**, 1 (2016) doi:10.1016/j.physrep.2016.07.004 [arXiv:1511.06495 [hep-ph]].
- [212] T. Golling *et al.*, CERN Yellow Rep. , no. 3, 441 (2017) doi:10.23731/CYRM-2017-003.441 [arXiv:1606.00947 [hep-ph]].
- [213] H. Baer, V. Barger, J. S. Gainer, H. Serce and X. Tata, Phys. Rev. D **96**, no. 11, 115008 (2017) doi:10.1103/PhysRevD.96.115008 [arXiv:1708.09054 [hep-ph]].
- [214] A. Aboubrahim and P. Nath, Phys. Rev. D **98**, no. 1, 015009 (2018) doi:10.1103/PhysRevD.98.015009 [arXiv:1804.08642 [hep-ph]].
- [215] H. Baer, V. Barger, J. S. Gainer, D. Sengupta, H. Serce and X. Tata, Phys. Rev. D **98**, no. 7, 075010 (2018) doi:10.1103/PhysRevD.98.075010 [arXiv:1808.04844 [hep-ph]].
- [216] Search for Supersymmetry at the high luminosity LHC with the ATLAS experiment, Tech. Rep. ATL-PHYS-PUB-2014-010, CERN, Geneva (Jul 2014). URL <http://cds.cern.ch/record/1735031>
- [217] M. Aaboud *et al.* [ATLAS Collaboration], Eur. Phys. J. C **76**, no. 7, 392 (2016) doi:10.1140/epjc/s10052-016-4184-8 [arXiv:1605.03814 [hep-ex]].
- [218] X. Cid Vidal *et al.*, arXiv:1812.07831 [hep-ph].
- [219] N. Craig, arXiv:1309.0528 [hep-ph].
- [220] C. Borschensky, M. Krämer, A. Kulesza, M. Mangano, S. Padhi, T. Plehn and X. Portell, Eur. Phys. J. C **74**, no. 12, 3174 (2014) doi:10.1140/epjc/s10052-014-3174-y [arXiv:1407.5066 [hep-ph]].
- [221] T. Cohen, T. Golling, M. Hance, A. Henrichs, K. Howe, J. Loyal, S. Padhi and J. G. Wacker, JHEP **1404**, 117 (2014) doi:10.1007/JHEP04(2014)117 [arXiv:1311.6480 [hep-ph]].

- [222] M. Aaboud *et al.* [ATLAS Collaboration], Phys. Rev. D **97**, no. 11, 112001 (2018) doi:10.1103/PhysRevD.97.112001 [arXiv:1712.02332 [hep-ex]].
- [223] A. M. Sirunyan *et al.* [CMS Collaboration], Eur. Phys. J. C **77**, no. 9, 578 (2017) doi:10.1140/epjc/s10052-017-5079-z [arXiv:1704.07323 [hep-ex]].
- [224] M. Aaboud *et al.* [ATLAS Collaboration], JHEP **1709**, 084 (2017) doi:10.1007/JHEP09(2017)084 [arXiv:1706.03731 [hep-ex]].
- [225] J. Alwall *et al.*, JHEP **1407**, 079 (2014) doi:10.1007/JHEP07(2014)079 [arXiv:1405.0301 [hep-ph]].
- [226] T. Sjöstrand *et al.*, Comput. Phys. Commun. **191**, 159 (2015) doi:10.1016/j.cpc.2015.01.024 [arXiv:1410.3012 [hep-ph]].
- [227] M. L. Mangano, M. Moretti, F. Piccinini and M. Treccani, JHEP **0701**, 013 (2007) doi:10.1088/1126-6708/2007/01/013 [hep-ph/0611129].
- [228] M. Cacciari, G. P. Salam and G. Soyez, Eur. Phys. J. C **72**, 1896 (2012) doi:10.1140/epjc/s10052-012-1896-2 [arXiv:1111.6097 [hep-ph]].
- [229] M. Cacciari, G. P. Salam and G. Soyez, JHEP **0804**, 063 (2008) doi:10.1088/1126-6708/2008/04/063 [arXiv:0802.1189 [hep-ph]].
- [230] M. Aaboud *et al.* [ATLAS Collaboration], JHEP **1712**, 085 (2017) doi:10.1007/JHEP12(2017)085 [arXiv:1709.04183 [hep-ex]].
- [231] A. M. Sirunyan *et al.* [CMS Collaboration], Phys. Rev. D **97**, no. 3, 032009 (2018) doi:10.1103/PhysRevD.97.032009 [arXiv:1711.00752 [hep-ex]].
- [232] M. Aaboud *et al.* [ATLAS Collaboration], JHEP **1806**, 108 (2018) doi:10.1007/JHEP06(2018)108 [arXiv:1711.11520 [hep-ex]].
- [233] ProspectsforbenchmarkSupersymmetrysearchesatthehighluminosity LHC with the ATLAS Detector, Tech. Rep. ATL-PHYS-PUB-2013-011, CERN, Geneva (Sep 2013). URL <http://cds.cern.ch/record/1604505>
- [234] G. Aad *et al.* [ATLAS Collaboration], Phys. Rev. Lett. **109**, 211803 (2012) doi:10.1103/PhysRevLett.109.211803 [arXiv:1208.2590 [hep-ex]].
- [235] T. Cohen, R. T. D'Agnolo, M. Hance, H. K. Lou and J. G. Wacker, JHEP **1411**, 021 (2014) doi:10.1007/JHEP11(2014)021 [arXiv:1406.4512 [hep-ph]].
- [236] A. Abada *et al.* [FCC Collaboration], CERN-ACC-2018-0056.